UNIVERSITY OF CALIFORNIA SAN DIEGO

Low Power Analog Techniques for Wearable Biosensors

A Dissertation submitted in partial satisfaction of the requirements for the degree
Doctor of Philosophy

in

Electrical Engineering (Electronic Circuits and Systems)

by

Somayeh Imani

Committee in charge:

Professor Patrick P. Mercier, Chair
Professor Peter Asbeck
Professor Gert Cauwenberghs
Professor Drew Hall
Professor Joseph Wang

2020

The Dissertation of Somayeh Imani is approved, and it is acceptable in quality and form for publication on microfilm and electronically:

_____

_____

_____

_____

_____

Chair

University of California San Diego

2020

TABLE OF CONTENTS

LIST OF FIGURES

ACKNOWLEDGEMENTS

First and foremost, I would like to thank my PhD advisor, Dr. Patrick Mercier for the continuous support of my PhD study and research, for his patience, motivation, and immense knowledge.

I would also like to express my sincere gratitude to our research collaborator and the committee member Dr. Joseph Wang for his guidance throughout my PhD study.

I would like to acknowledge my committee members Dr. Peter Asbeck, Dr. Gert Cauwenberghs, and Dr. Drew Hall for their supervision and advice.

I was fortunate to have wonderful friends and co-workers in EEMS group and Wang's Lab. I would like to thank all of them and also other supportive friends from San Diego, and all around the world. Finally, I greatly appreciate the continuous compassion and support of my parents and my lovely sisters.

Somayeh Imani

March 15th, 2020

The material in this dissertation is mostly based on the following published papers. Chapter 2 is based on and mostly a reprint of the following publications:

- Imani, Somayeh; Bandodkar, Amay; Kim, Jayoung; Wang, Joseph; Mercier, Patrick P., "Wearable Chemical Sensors: Challenges and Opportunities", International Symposium on Circuits and Systems, 2016.

- Kim, Jayoung[1]; Imani, Somayeh[1]; de Araujo, William R.[1]; Warchall, Julian; Valdés-Ramírez, Gabriela; Paixão, Thiago RLC; Mercier, Patrick P.; Wang, Joseph. "Wearable salivary uric acid mouthguard biosensor with integrated wireless electronics.", Biosensors and Bioelectronics, vol.74, 2015 ([1]: equally contributed).

- Bandodkar, Amay J[1]; Imani, Somayeh[1]; Nuñez-flores, Rogelio[1]; Kumar, Rajan; Wang, Chiyi; Mohan, A M Vinu; Wang, Joseph; Mercier, Patrick P, "Re-usable electrochemical glucose sensors integrated into a smartphone platform", Biosensors and Bioelectronics Journal, vol. 101, 2018 ([1]: equally contributed).

The dissertation author was the primary investigator and author of these papers.

Chapter 3 is based on and mostly a reprint of the following publication:

- Kim, Jayoung[1]; Jeerapan, Itthipon[1]; Imani, Somayeh[1]; Cho, Thomas N.; Bandodkar, Amay J.; Cinti, Stefano; Mercier, Patrick P.; Wang, Joseph. "Noninva-

sive alcohol monitoring using a wearable tattoo-based iontophoretic-biosensing system.", ACS Sensors, vol.1, 2016 ([1]: equally contributed).

The dissertation author was the primary investigator and author of this paper.

Chapter 4 is based on and mostly a reprint of the following publications:

- Imani, Somayeh[1]; Bandodkar, Amay J.[1]; Muhan, AM Vinu; Kumar, Rajan; Yu, Shengfei; Wang, Joseph; Mercier, Patrick P., "A Wearable - Chemical Electrophysiological Hybrid Biosensing System for Real-Time Health and Fitness Monitoring", Nature Communications, vol. 7, May 2016. ([1]: equally contributed).

- Kim, Jayoung; Sempionatto, Juliane R.; Imani, Somayeh; Hartel, Martin C.; Barfidokht, Abbas; Tang, Guangda; Campbell, Alan S; Mercier, Patrick P.; Wang, Joseph, "Simultaneous Monitoring of Sweat and Interstitial Fluid Using a Single Wearable Biosensor Platform," Advanced Science, Vol. 5, 2018.

The dissertation author was the primary investigator and author of these papers.

Chapter 5 is based on and mostly a reprint of the following publications:

- Jia, Wenzhao; Wang, Xuan; Imani, Somayeh; Bandodkar, Amay J; Ramírez, Julian; Mercier, Patrick P; Wang, Joseph, "Wearable textiles biofuel cells for powering electronics," Journal of Materials Chemistry A, Vol. 2, 2014.

- Bandodkar, Amay. J; You, Jung-Min; Kim, Nam-Heon; Gu, Yue; Kumar, Rajan; Mohan, AM Vinu; Kurniawan, Jonas; Imani, Somayeh; Nakagawa, Tatsuo; Parish, Brianna; Parthasarathy, Mukunth; Mercier, Patrick P; Xu, Sheng; Wang, Joseph, "Soft, stretchable, high power density electronic skin-based biofuel cells for scavenging energy from human sweat," Energy and Environmental Science, Vol. 10, pp. 1581-1589, 2017.

- Fazli Yeknami, Ali; Wang, Xiaoyang; Imani, Somayeh; Nikoofard, Ali; Jeerapan, Itthipon; Wang, Joseph; Mercier, Patrick P, "A 0.3V Biofuel-Cell-Powered Glucose/Lactate Biosensing System Employing a 180nW 64dB SNR Passive $\Delta\Sigma$ ADC and a 920MHz Wireless Transmitter," in Proc. IEEE International Solid-State Circuits Conference (ISSCC), Feb. 2018.

- Fazli Yeknami, Ali; Wang, Xiaoyang; Jeerapan, Itthipon; Imani, Somayeh; Nikoofard, Ali; Wang, Joseph; Mercier, Patrick P, "A 0.3V Biofuel-Cell-Powered Glucose/Lactate Biosensing System," IEEE Journal of Solid-State Circuits, vol. 53, no. 11, Nov. 2018.

The dissertation author was the primary investigator and author of these papers.

VITA

2006	Bachelor Degree in Electrical Engineering, Amirkabir University of Technology.
2009	Masters of Science in Electrical Engineering, Amirkabir University of Technology.
2013	Masters of Science in Electrical Engineering, The University of New Mexico.
2013-2020	Graduate Student Researcher, University of California San Diego, La Jolla, CA, US.
2020	Doctor of Philosophy in Electrical Engineering (Electronic Circuits and Systems), University of California San Diego.

ABSTRACT OF THE DISSERTATION

Low Power Analog Techniques for Wearable Biosensors

by

Somayeh Imani

Doctor of Philosophy in Electrical Engineering (Electronic Circuits and Systems)

University of California San Diego, 2020

Professor Patrick P. Mercier, Chair

Wearable biosensors show considerable promise in monitoring and assessing the real-time performance of athletes, the health status of patients, or the general well-being of interested users. Despite this promising status, wearables still face many challenges related to power consumption, device flexibilities, and sensor-circuit interface. For instance, in many current wearable devices, the user needs to replace/recharge the battery every day, which is inconvenient and ultimately limits the adoption of this technology. On the other hand, most wearables today focus on monitoring physical parameters (e.g.,

activity, respiration rate, etc.), or electrophysiology (e.g., ECG, EEG, etc.). In order to augment the richness of collected data, the next-generation of wearables will also be capable of monitoring underlying chemical homeostatis of the user, for example through measurement of glucose in interstitial fluid, lactate in saliva, or electrolytes in sweat.

This thesis discusses the challenges of the next generation of wearable biosensors, and introduces some new biosensing systems and low-power instrumentation circuits for their implementation. These wearable systems have been implemented in different novel platforms including mouthguard, cell phone, and variable types of flexible temporary tattoos.

The energy harvesting from other energy sources, such as sweat from the body, has been also considered as a viable means of powering the next generation of wearable devices. In this thesis, we investigated a few examples of this approach including an implementation of a fully self-powered biosensor system.

Chapter 1

Introduction

Wearable devices are receiving more and more attentions owing to their affordability, novel applications and convenient form factors. The market for wearable sensors is expected to grow at a Compound Annual Growth Rate (CAGR) of 19.15% from 2019 to 2025 to reach $31.96 billion by 2025. most wearable devices today only measure physical or electrophysiological parameters such as motion, pressure, temperature, ECG, or EEG [1]. While these parameters may be useful for monitoring general well-being and a few specific diseases, acquiring a more comprehensive picture of underlying physiology via additional wearable sensors will provide significant value to a much wider range of users. Nowadays, wearable devices that are embedded in textiles or directly mounted on the human skin are trending in the field. These improvements necessitate us moving forward to investigate flexible and light instrumentation circuits as well as energy sources. This thesis shows some of the efforts towards the next genera-

tion of these wearable devices. On the other hands, the battery life time of the wearable sensor device is of the tremendous importance.

In many current wearable devices, the user needs to replace/recharge the battery every day, which is inconvenient and ultimately limits the adoption of this technology. In order to extend the battery lifetime, two main approaches are considered. In one approach we have sought to overcome this specific barrier by designing low-power circuits that consume significantly less energy. Chapter 2, 3 and 4 present some devices which are developing ultra low power circuits for biosensor characterization to reduce the power consumption of the novel wearable devices. In another approach, energy harvesting from the body fluid has been investigated. In this approach, we demonstrated some energy harvesting system which are extracting the power from body fluids such as sweat from the body, which is a viable means of powering the next generation of wearable devices. Chapter 5 presents a few examples of these energy harvesting and self-powered biosensors.

Chapter 2

Characterization of Electrochemical Wearable Sensors

Measurement of chemicals can provide important additional insight into a user's overall health status. However, body chemistries are typically measured via lab- or point-of-care (PoC)-based in-vitro testing of blood samples extracted via needles or finger-prick sensors. Such approaches are invasive, inconvenient, and do not support continuous, realtime monitoring. For this reason, there has been tremendous recent activity in the area of wearable chemical sensors, which support continuous, real-time, and non-invasive monitoring of chemical constituents in interstitial fluid, sweat, saliva, tears, urine, and other bodily fluids [2]. These measurements can be made using optical, impedimetric, or electrochemical biosensors [2]. While there has been significant progress in optical and resistive biosensor designs, they still generally suffer from suboptimal selectivity, poor sensitivity, and environmental interference. On the other hand, electrochemical transducers have been shown to be robust, low-power and portable, highly

sensitive and selective. Thus, electrochemical biosensors have been utilized in a number of different wearable devices (Fig2.1), and are the focus of this paper, which will describe state-of-the art biosensor fabrication techniques, instrumentation electronic design, integration/data challenges, and will conclude with the design of a representative saliva sensing system.

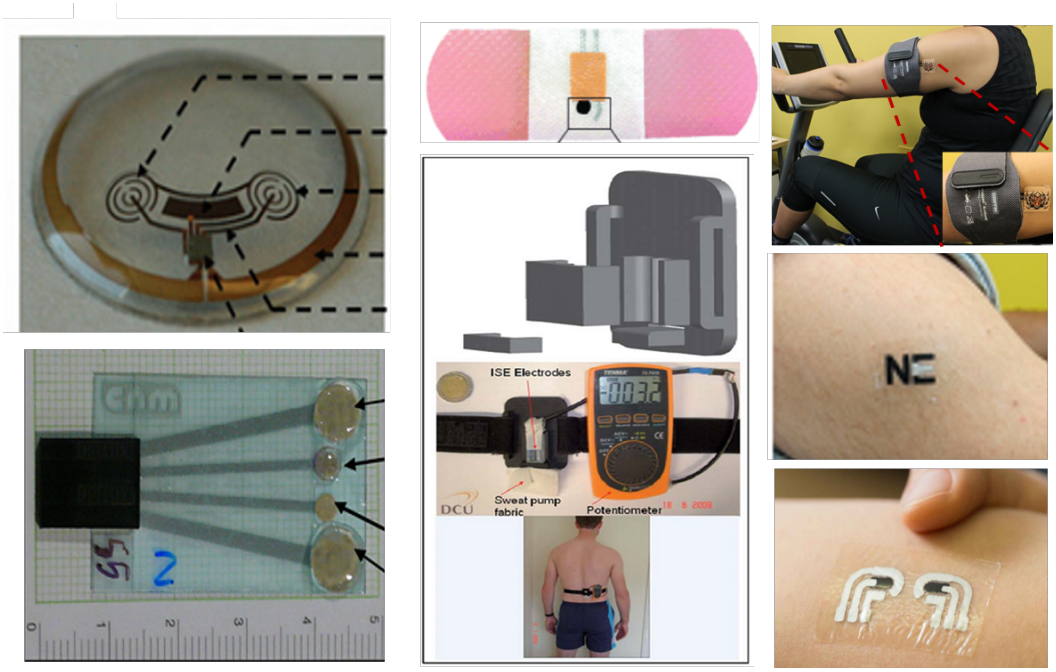

Figure 2.1: Images of plastic-based, textile-based, and tattoo-based sensors
plastic-based (A) tears glucose lens (B) sweat Cl- sensor; textile-based (C) bandage pH (D) sodium sensor, and tattoo-based (E) sodium (F) lactate and (G) glucose non-invasive sensor([3] and refs therein).

Electrochemical transducers are devices that generate electrical signals that are directly proportional to the concentration of the desired chemical analyte. The most popular electrochemical biosensors utilize either potentiometric, amperometric, or electrochemical impedance spectroscopy (EIS) techniques, which measure voltages, cur-

rents, and impedances, respectively. Selectivity towards a particular chemical analyte is achieved by functionalizing the transducer with specific chemicals and biological receptors, for example, ionophores, enzymes, antibodies, etc. Potentiometric biosensors are often used in wearable systems to sense physiologically-relevant electrolytes via measurement of the open-circuit voltage between a working electrode (WE) and a reference electrode (RE), where the WE is functionalized with an ion-specific ionophore. The measured voltage is proportional to the electrolyte concentration. Measurement of chemicals, such as metabolites, is commonly acquired via amperometry, which measures the current between a WE and RE electrode after the WE is functionalized with an enzyme that catalyzes the specific reaction of the metabolite substrate (Fig2.2).

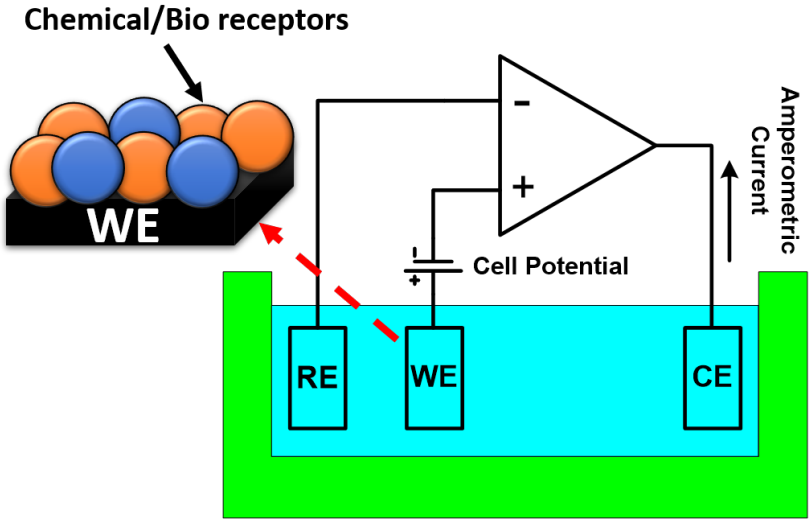

Figure 2.2: Measurement set-up for an electrochemical amperometric system; working electrode has been functionalized for sensing specific analyte.

The measured current due to redox reaction of the product is proportional to the underlying metabolite concentration. In such applications, the resistance of the reference electrode may lead to significant IR voltage drops, potentially disrupting the accuracy of the applied voltage. Thus, similar to a 4-wire current measurement as utilized by highprecision power supplies, a third electrode, a counter electrode (CE), if often added to measure the current. There are many variants of controlled-potential techniques, where the applied reference potential is either kept constant, stepped or swept in a linear manner (e.g., as in cyclic voltammetry). Finally, EIS sensors operate by applying a voltage or current across two or more electrodes, and measuring the impedance across a specific frequency range, which may reveal information about underlying chemical concentrations [4].

Several lithographic and printing technologies have been employed to fabricate wearable electrochemical biosensors. Since lithography is expensive and time consuming, and since many wearable chemical biosensors are envisioned to operate in high-volume disposable applications, most wearable chemical biosensors are instead fabricated via screen printing. Wearable chemical sensors achieve the best performance when they are in tight contact with underlying tissue, and thus it is important to fabricate such sensors not on conventional rigid and brittle substrates like silicon or glass, but instead on flexible or even stretchable substrates that easily comply with the smooth,

curvilinear features of human anatomy. Fortunately, printing enables easy fabrication of chemical biosensors on a wide range of such substrates, including plastics, textiles, tattoo paper, and stretchable elastomers.

Taking advantage of these attributes, a wide range of wearable electrochemical sensors, biofuel cells, and alkaline batteries have been demonstrated [3]. In order to achieve low-cost, high-precision devices, the tattoo sensors can be fabricated using inexpensive screen printing processes as this technique relies on printing inks on surfaces using a squeegee and a low-cost stencil as a mask. We have demonstrated that such printed tattoo devices can withstand repeated mechanical deformations commonly experienced by the human body with minimal effect on their chemical response. Relying on the tattoo platform, non-invasive electrochemical sensors have been fabricated that can continuously monitor pH, Na+ (Fig2.1E), NH4+, lactate (Fig2.1F), heavy metals in human sweat, and glucose levels (Fig2.1G) in interstitial fluid. By incorporating elastomeric binders and self-healing agent loaded microcapsules, Wang's lab further demonstrated all-printed electrochemical devices that can endure strains as high as 100 $\%$ [5] and self-heal [6] after scratching. There are, however, still significant challenges in the fabrication of these devices. For example, the stability of biomolecular receptors requires improvement, via stabilizers, specially engineered biomolecules or by identifying new immobilization routes. Surface fouling in complex fluids requires the use of

suitable protective (permselective) coatings. In addition, most prior art has not considered the challenges of integrating rigid electronic devices with flexible chemical sensors, which is necessary when building practical systems.

Wearable chemical biosensors are not useful in isolation – active electronics are necessary to bias the biosensor, amplify and digitize the output, calibrate the sensor, then transmit or process the data. All of this interaction requires power, which must also be incorporated into the wearable chemical sensor. A block diagram of a representative system is shown in Fig2.3.

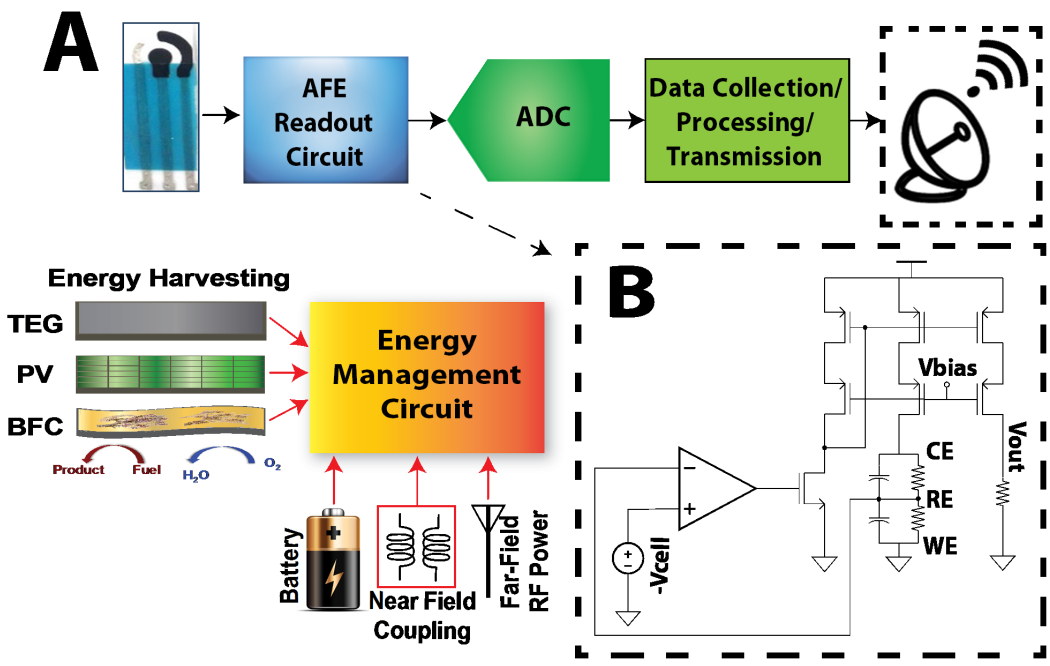

Figure 2.3: A wearable chemical sensing system: (A) Front end circuitry block diagram. (B) An example potentiostat circuit implementation.

Fabricated biosensors directly connect to front-end circuits that serve to bias/drive

the biosensor and/or amplify the output signal. Potentiometric biosensors have the simplest front-ends: high-input impedance amplifiers are typically used to buffer the open-circuit potentiometric signal to an ADC. Amperometric biosensors require slightly more complexity to bias the 2- or 3- electrode biosensor and read out current. This is typically performed by a circuit called a potentiostat, which utilizes a collection of active circuits to bias the biosensor at a specific voltage, and uses a current-mirror or transimpedance amplifier to read out current. An example circuit implementation is shown in Fig2.3B. Potentiostats can be used in constant-potential amperometry by applying a fixed reference voltage to the input of the potentiostat, while more advanced forms of amperometry and EIS can be achieved by modulating the reference voltage. Potentiostats used in wearable applications must support high performance, in the form of large dynamic range (100s of fA to 10s of μA) and low-noise, in addition to achieving low-power operation. There are many designs suitable to do current read-out: transimpedance amplifiers, current conveyors, capacitor charging architectures, or current mirror read-out circuits (the latter is illustrated in Fig2.3B). Many prior-art potentiostat designs are targeted towards bench-top or point-of-care(PoC) use, and utilize transimpedance amplifier structures along with sigma-delta ADCs to achieve fA sensitivity levels at 0.1-10 mW power levels. The next-generation of wearables will need to reduce the power of both analog front-ends in order to extend the operational lifetime of wearable devices.

There are two primary ways users can interact with wearable chemical sensors: 1) build a far-field wireless telemetry module right into the wearable itself, or 2) wirelessly interrogate the wearable with a far- or near-field reader device. Using far-field telemetry such as Bluetooth is generally the ideal use-case, as in this manner, data can be continuously relayed from the sensor to a local gateway such as a smartphone or smartwatch, which can then relay the data to the user or the cloud. However, doing so generally requires substantial power, and thus such devices must incorporate large batteries, energy harvesters, or both. On the other hand, wireless interrogation techniques such as RFID or near-field communication (NFC) can also provide power to the wearable, thereby eliminating the need to include energy storage/harvesting devices. However, the interrogation device must either support high power for far-field interrogation and remote powering, or must be placed very near the wearable in order to provide sufficient power. Far-field interrogation often requires prohibitively large power for a smartphone gateway scenario (path loss around the human body can easily approach 70dB), and active placement of a device (e.g., a smartphone) directly over top the wearable is inconvenient and often precludes continuous measurement. Thus, unless a high-power or proximal reader is present, it is generally preferred to employ far-field communications.

Far-field radios employing WiFi, ANT+, and Bluetooth transceivers have been

used in many wearable devices. However, none of these radios satisfy the peak power requirements of most small wearable systems. For instance, WiFi, ANT+, Bluetooth, and Bluetooth Low-Energy (BLE) support increasingly low power, yet the peak power constraints of all such radios is generally at least 15mW, which exceeds the peak power ratings of many small batteries. While BLE radios can approach sub-mW power on average, the peak power requirements necessitate inclusion of batteries that may be larger than appropriate for many wearable applications. For this reason, next-generation wearable systems will require new radios with significantly reduced peak power constraints to enable increasingly miniaturized anatomic integration.

It is typically necessary to fully encapsulate the entire electronic system, including the battery, in a biocompatible insulator (e.g., Parylene-C, titanium, sapphire, etc.) to avoid liquid damage. Encapsulation necessitates a wireless re-charging circuit to ensure the longevity of the sensing electronics. The interface between the electronics and the disposable sensor is an active area of research. Wirelessly-interrogated devices do not suffer from peak power constraints, since communications typically occur via low-power back-scattering instead of high-powered active transmissions. By additionally delivering wireless power to the wearable device, batteries are not required [7]. For these reasons, wirelessly-interrogated devices can be smaller than active transmission devices. However, the requirement of a proximal power source limits the utility of such

devices in many practical scenarios. While the entire electronic module can be easily sealed, the biosensor-electronics interface remains a challenge. Since the response of electrochemical biosensors can have sample-to-sample variation and non-ideal specificity, most sensors require calibration after fabrication in various representative solutions; this can become prohibitively expensive, especially when biosensors are used in complex fluids with many potential interferers. Thus, calibration and data processing via chemometric and other statistical approaches are required to enable next-generation wearable chemical sensors to be both low-cost and reliable. Since such statistical approaches require complex computation, cloud or fog-based computing may become necessary, though some in-sensor pre-processing may help reduce wireless data rates and overall system energy consumption. Alternatively, if appropriate training data can be pre-loaded onto the platform, it may be possible to implement simple multi-variate analysis locally, thereby enabling direct display of post-calibration results to the user without any energy-expensive communications at all. In addition, there are significant challenges in analyzing the large amounts of data that will be generated by such sensors, with the ultimate goal of identifying important correlations between measurements and healthcare outcomes. Since many of such measurements have not been made on freely behaving humans, it is expected that there will be many ripe opportunities for big data analytics here.

In this chapter, we will present two examples for implementation of novel electrochemical biosystems. First, a wearable salivary Uric Acid mouthguard biosensor with integrated wireless electronics will be described [8]. Then, re-usable electrochemical glucose sensors integrated into a smartphone platform will be introduced in details [9].

2.1 Wearable Salivary Uric Acid Mouthguard Biosensor with Integrated Wireless Electronics

Utilizing electrochemical sensors in wearables can provide information to track health and activity of the users. However, there were very few previous works accomplished to implement electronic circuits for developing electrochemical wearable systems. The electrochemical biosensors provide an attractive means to analyze the content of a biological sample due to the direct conversion of a biological event to an electronic signal; therefore, they especially as wearable devices, are of great importance for furthering health monitoring endeavors. However, wearable electronics have so far been limited by their power management; for a very small wearable device, the heart of the system is the power management. A wearable device can lose its appeal if it must be recharged multiple times a day or has a heavy battery pack. Achieving multi-day run

times and keeping the device small and light requires ultra-low power-optimized power management to efficiently convert the battery's limited energy to usable power by the loads. Moreover, due to the restrictions of wearable devices, it is necessary to design novel low power instrumentational circuitries while we are introducing new systems and form factors for different wearable applications such as health and activity fields.

While the majority of existing wearable technologies focus on monitoring physical parameters (e.g., motion, respiration rate, etc.) or electrophysiology (e.g., ECG, EMG, etc.), there is tremendous interest in developing wearable sensors for important chemical markers relevant to health or fitness [2,10,11]. Saliva is a great diagnostic fluid providing an alternative to direct blood analysis via the permeation of blood constituents without any skin-piercing for blood sampling. Early work in electrochemical salivary sensors was demonstrated by Graf in the 1960s, measuring pH and fluoride ion levels on a partial denture [12, 13]. Several efforts have more recently developed salivary sensors based on screen-printing techniques that take advantage of scalable low-cost fabrication. For example, Diamond's group has developed disposable potentiometric pH sensor strips [14], and Wang's group has demonstrated a wearable salivary lactate sensor using a mouthguard platform [15]. Despite these recent advances, the realization of wearable biosensors for real-time monitoring of chemical markers is limited by the small number of demonstrated target analytes and the lack of integrated wireless data

transmission in measurement platforms. While it was predicted that the wireless wearable chemo-sensors for personal health/wellness was slated to expand rapidly [16], challenges such as power consumption and size of wireless sensor systems remain. Mannoor et al reported a novel graphene-based wireless resistometric sensor for continuous monitoring of bacteria on a silk dental tattoo platform [17]; however, this platform does not measure salivary metabolites and requires a large active device to be held in close proximity to the sensor, which is inconvenient for continuous real-time readout. In another work, a radio-frequency identification (RFID) wireless sensor tag with potentiometric input has been introduced [18]. The tag, which is too large for integration in typical anatomically-sized platforms, is powered by a 3V battery, and a larger reader device still needs to be positioned in close proximity to the tag for successful data readout. A similar system has been recently developed by Wang's group [19] to implement a smart bandage, though the drawbacks of short-range communication and bulky monitoring devices remain. The size of the wireless system can potentially be decreased by transitioning from near-field or RFID-like approaches, which require a large proximal reader device, to far-field radios that communicate with small receivers that can potentially be placed far away. Wireless monitoring of blood glucose and lactic acid level in fish has been reported by Endo et al [20] and Hibi et al. [21], respectively. These designs utilized a 3102BP Pinnacle Technology wireless potentiostat operating at 916.5MHz,

which transmits sensed data to a proprietary receiver (3100RX, Pinnacle Technology Inc.). On the other hand, more common communication links, such as Bluetooth, do not require specific reader/receiver designs; therefore, a broad range of receivers can be employed. For example, a Bluetooth-enabled system for real time monitoring of physical parameters was proposed by Depari et al [22]. The system consists of a commercial Bluetooth earphone along with a PPG sensor, tissue impedance sensor, and interface circuits. In another work, a portable smart-phone based impedance TNT monitoring system has been reported [23]. These examples employed Bluetooth 2.0 and Hands-Free Profile(HFP) commercial based systems and have opportunities to reduce power consumption and size. In this work, we have demonstrated an instrumented mouthguard capable of non-invasively monitoring salivary uric acid (SUA) levels. The enzyme (uricase)-modified screen printed electrode system has been integrated onto a mouthguard platform along with anatomically-miniaturized instrumentation electronics featuring a potentiostat, microcontroller, and a Bluetooth Low Energy (BLE) transceiver. Unlike RFID-based biosensing systems, which require large proximal power sources, the developed platform enables real-time wireless transmission of the sensed information to standard smartphones, laptops, and other consumer electronics for on-demand processing, diagnostics, or storage. The mouthguard biosensor system offers high sensitivity, selectivity, and stability towards uric acid detection in human saliva, covering

the concentration ranges for both healthy people and hyperuricemia patients. The new wireless mouthguard biosensor system is able to monitor SUA level in real-time and continuous fashion, and can be readily expanded to an array of sensors for different analytes to enable an attractive wearable monitoring system for diverse health and fitness applications.

The implemented wireless amperometric circuit, paired with a Bluetooth low energy (BLE) communication system-on-chip(SoC) for miniaturized and low-power operation, is fully integrated into a novel salivary metabolite mouthguard biosensor for continuous and real-time amperometric monitoring. The mouthguard enzyme electrode is applied for the detection of uric acid (UA), which is the end product of purine metabolism in the human body. An abnormal concentration of UA is a biomarker for various diseases, including hyperuricemia, gout, lesch-Nyhan syndrome, and renal syndrome [24]. In addition, higher UA levels implicate a higher future risk of type 2 diabetes and its severity and complications [25]. UA can also be an indicator of physical stress induced reactive oxygen species (ROS), acting as a free radical scavenger [26]. While blood UA (BUA) measurements require invasive blood collection, salivary uric acid (SUA) measurements could be carried out non-invasively and in a continuous real-time manner. Shibasaki et al. [27] and Soukup et al. [28] have found a good correlation of UA blood and saliva levels, demonstrating that this metabolite can be monitored

in saliva in a non-invasive way without need for blood sampling. The new mouthguard biosensor has been fabricated using a well-established screen-printing technology on a flexible PET (polyethylene terephthalate) substrate. Chemical modification of the printed working electrode Prussian-blue transducer has been made by crosslinking the uricase enzyme and electropolymerizing o-phenylenediamine. The performance of the new mouthguard biosensor has been evaluated through UA measurements in artificial saliva and undiluted human saliva. The feasibility of the new mouthguard biosensor system for clinical use has been tested by monitoring a hyperuricemia patient under medication treatment. Finally, the sensor has been integrated with a wireless amperometric circuitry to realize a comfortable wearable device (Fig2.4A). The resulting integrated mouthguard biosensor offered real-time uric-acid measurements along with wireless data transmission. A BLE chipset has been adopted to enable wireless connectivity to a smartwatch, smartphone, tablet, portable media player, laptop or any other BLE-enabled device. In the following sections, we will describe the design of the integrated mouthguard biosensor coupled with a miniaturized printed circuit board for wireless data collection and its attractive performance in the continuous monitoring of salivary UA.

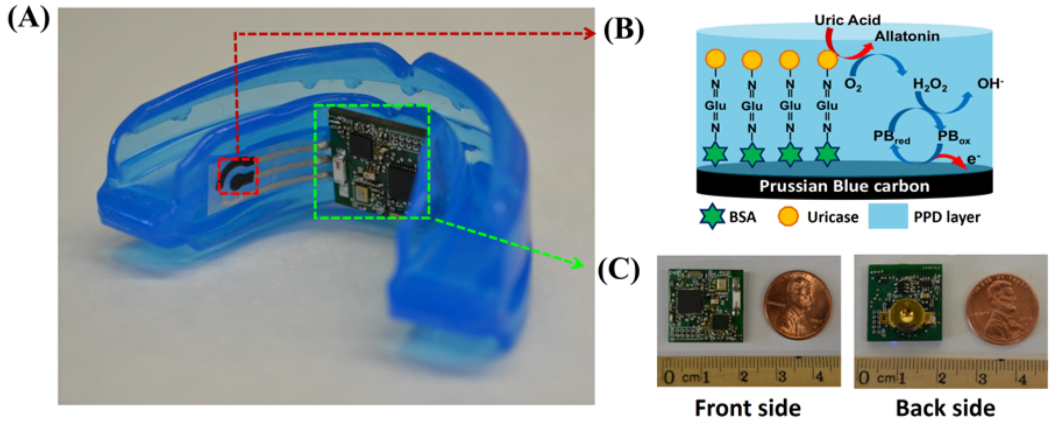

Figure 2.4: (A) Photograph of the mouthguard biosensor integrated with wireless amperometric circuit board (B) Reagent layer of the working electrode containing uricase for SUA biosensor (C) Photograph of the wireless amperometric circuit board: front (left) and back(right) side.

2.1.1 Design, Fabrication, Assembly, and Characterization of Integrated Wireless Mouthguard

Unlike near-field communication(NFC) chipsets that can only communicate over a distance of a few centimeters, a Bluetooth Low Energy(BLE) chipset was adopted in this work to enable wireless connectivity to a smartwatch, smartphone, or laptop over the distance of several meters, enabling unobtrusive, real-time monitoring. Specifically, the design employed a Texas Instrument(TI) CC2541 BLE System-on-Chip for communication and processing. An LMP91000 Analog Front End(AFE), programmable through an I2C interface driven by the CC2541, was used as the on-board potentiostat. The fabricated printed circuit board assembly(PCBA), shown in Fig2.4C, measured 1.8cmx1.9cm. A Johanson Technology 2.45GHz chip antenna(2450AT42A100)

and impedance matched balun (2450BM15A0002) were employed for wireless transmission. Two 396/397 watch batteries(2x1.55V, 33mAh each) in series were utilized as a power source, regulated for the electronics via a TPS61220 boost converter and an LM4120 low-dropout voltage regulator. The board consumed, on average, 7mA from a 3V supply during "active mode" (21mW). In order to maximize the battery life, a 0.6mW "sleep mode" was engaged during extended periods of time when measurements were not being taken. In this mode, the LMP91000 entered a "deep sleep" state while the CC2541 was placed in power mode 1 (with a 4μs wake-up time). A third mode, "stand-by," was used when there was a moderate delay between data transmissions. In this mode, the LMP91000 remained in the potentiostat configuration, while the CC2541 was placed in "power mode 1," resulting in a total power consumption of 0.7mW.

The CC2541 firmware was configured to support calibration, stability and application specific use-case scenarios. To extract calibration curves, chronoamperometric measurements were performed once every three minutes, with current levels transmitted every 0.5seconds for 6seconds. The following two minute interval was reserved for sample preparation and incubation. The same scenario was repeated with a 10minute period for study of the stability of the sensor.

Continuous data transmission with millisecond sampling rates is not required in all application use-cases, and thus the CC2541 firmware was also configured to support

duty-cycled measurements. For example, the board was programmed to enable measurement once every few minutes. In this mode, the potentiostat is periodically activated for a period of 60seconds, or until the current measurement settles. After settling, the current is sampled and transmitted over the wireless link and the concentration is recovered at the receiver based on calibration data. After transmission, the board enters the "sleep mode" for a pre-configured amount of time. Exploiting low-power sleep modes with deeply duty-cycled operation extends the estimated battery life from 12hours to 5days.

After testing the performance of the mouthguard biosensor in artificial saliva and real human saliva, the wireless electronics board was integrated into the mouthguard platform. Stainless steel wires connected to the screen-printed electrode on PET substrate were soldered to the fabricated PCB, and the electronics board together with the printed electrode was assembled into the mouthguard using medical adhesive (Loctite) as shown in Fig2.4A. To test its operation, 100μl of artificial saliva was placed on the electrode and the same experimental condition as previous experiments was applied (video data). Chronoamperometric measurements of integrated mouthguard biosensor were carried out by applying -0.3V (vs. Ag/AgCl) for 1minute following 1minute of incubation in the sample drop (artificial saliva). The measurement results were sent by Bluetooth wireless data transmission and were displayed on a laptop screen with a custom-made graphical interface. Data communication between the integrated mouth-

guard sensor and Android smart phones has also been verified using the Texas Instrument BLE Monitor application. For calibration curve extraction, an LED indicator turned on every 3minutes indicating the time to spike UA to measure the next concentration point. Every time the indicator turned on, a 1minute long incubation was taken after spiking UA and then the current response was measured for another 1minute. Stability was also examined in 300μM UA in artificial saliva at 10minute intervals over 4hours of operation. The sensor was kept in artificial saliva between successive measurements.

2.1.2 Results and Discussion

The implementation of wearable biosensors for real-time monitoring of saliva has been hindered by the lack of low power far-field wireless transmission circuits. To realize a wearable sensor, a miniaturized Bluetooth-enabled amperometric circuit board was implemented and integrated into a mouthguard biosensor (as shown in Fig2.4A) and its performance was evaluated in artificial saliva in terms of sensitivity and stability. Following the optimized experimental conditions determined with a lab-scale potentiostat, the custom-made board was set to apply the detection potential of -0.3 V for 60 s for each measurement. The current response was sampled every 0.5 s (a frequency of 2 Hz) and transmitted in real time via Bluetooth 4.0 to a laptop or desktop screen with graphical interface, shown in Fig2.5.

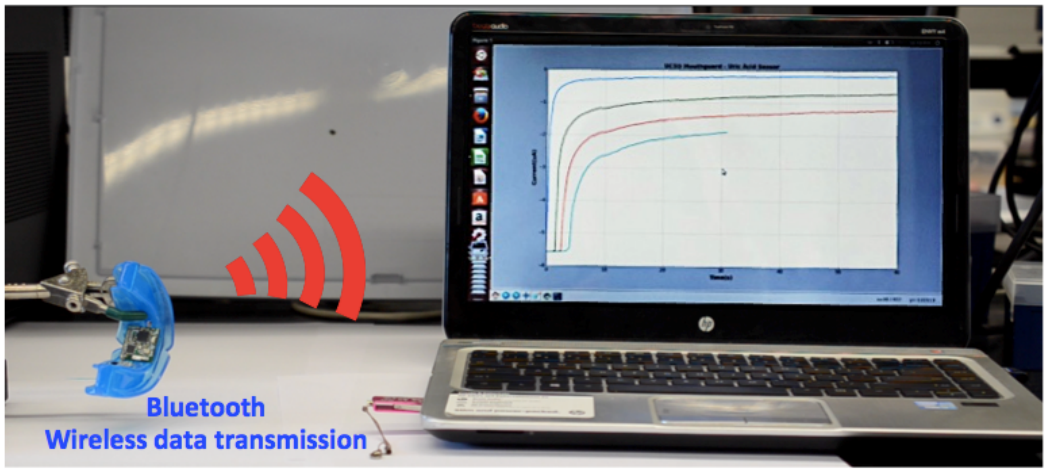

Figure 2.5: Real-time monitoring of electrochemical current response of the integrated mouthguard biosensor with wireless data transmission to graphical interface on laptop via Bluetooth

Fig2.6A displays the resulting calibration plot for UA detection in artificial saliva obtained by wireless transmission for different UA concentrations up to 600 mM with 100 mM increments, covering possible physio- logical levels of SUA. The resulting calibration (shown in the inset is highly linear (correlation coefficient R^2=0.998) with a sensitivity of 2.45 mA/mM). The plot produced through wireless transmission shows agreement with the data obtained using a lab-scale potentiostat (CHI).

The stability of our integrated mouthguard biosensor was tested for continuous monitoring applications. As shown in Fig2.6B, the sensor retains its current signal throughout the entire 4 h of operation with measurements carried out at 10 min intervals (RSD: 3.13%). This test provides evidence for the practicality of the wireless wearable mouthguard biosensor towards for relevant health-care monitoring applications.

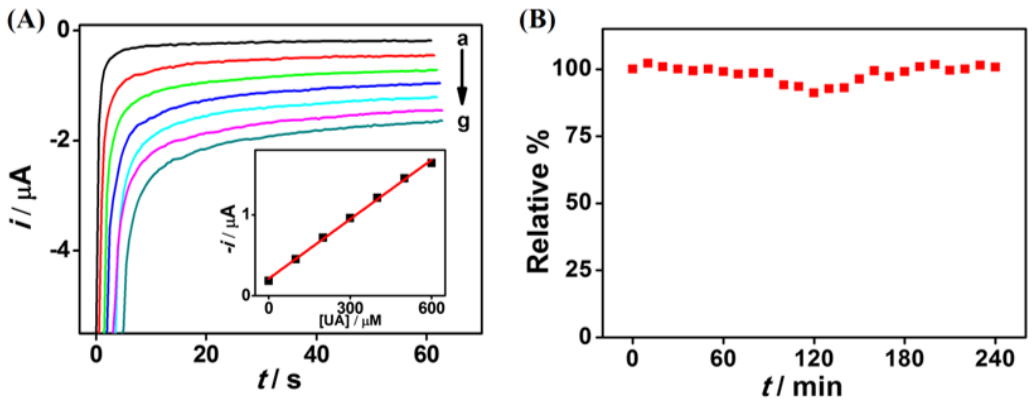

Figure 2.6: Electrochemical measurement results from the wireless integrated mouthguard biosensor in artificial saliva
(A) Chronoamperograms obtained for increasing uric acid concentration with 100 μM increments up to 600 μM (a - g). The resulting calibration plot is shown in the inset.
(B) Stability of the electrochemical response to 300 μM uric acid over a 4 h operation with 10 min intervals.

2.1.3 Conclusions

The new wearable mouthguard biosensor has been coupled with a miniaturized printed circuit board for wireless data collection. The biosensor displays attractive electrochemical performance with high selectivity, sensitivity and stability. Future efforts will focus on a critical assessment of potential toxicity and biocompatibility issues essential for the realization of real-time 'in mouth' testing on humans. The new mouthguard sensor platform can be readily expanded to a multiple salivary analytes in connection to a sensor array, along with further miniaturization of the circuit board and wireless transceiver for diverse fitness and biomedical daily-life applications.

2.2 Re-usable electrochemical glucose sensors integrated into a smartphone platform

Diabetes mellitus is a serious global disease that affected nearly 8.8 $\%$ (415 million) of adults worldwide in 2015 [29], with projections to nearly 522 million by 2030 [30]. The financial effect of this disease is immense, with most countries spending between 5 and 20$\%$ of total healthcare expenditure on diabetes and related health issues [31]. Unfortunately, there is no cure, and as a result, diabetic patients must carefully manage their disease via periodic measurement of blood glucose levels. Consequently, invasive, minimally invasive [32], and non-invasive [33] glucose monitoring approaches have been a research topic for decades. In an ideal world, monitoring should be accomplished non-invasively; while there has been recent progress towards such an approach [34], challenges remain towards successful commercialization. Thus, most diabetic patients monitor their glucose levels by periodically extracting a small amount of blood by pricking a fingertip with a lancet, and transferring extracted blood to a glucose-sensitive test strip that is read via a handheld electrochemical glucometer. This method is both accurate, due to excellent selectivity and sensitivity of the functionalized test strips alongside electrochemical detection, and low-cost, since test strips can be economically screen printed at scale. However, as glucose levels need to be measured regularly, di-

abetic patients must carry the device and the test strips with them throughout the day. This adds additional responsibility onto the patient, and forgetting to carry the glucometer can potentially lead to sub-optimal diabetes control, and in some cases even more serious health issues [35]. Thus, efforts should be made to facilitate more convenient monitoring of blood glucose levels in order to help improve healthcare outcomes. With billions of smartphones around the globe, these devices have become an inseparable part of daily life and thus, integrating a blood glucose meter within a smartphone would help reduce the chances of a diabetic patient forgetting to carry their glucometer with them. In addition, the ability to autonomously store, process, and send blood glucose reading from the phone to a care provider or cloud service via the built-in wireless functionality is an attractive additional benefit. As a result, there have been several recent reports on integrating glucose measurement functionality into a smartphone-compatible platform [36–38]. However, many such approaches rely on colorimetric glucose detection, which unfortunately lacks in sufficient accuracy to support therapeutic intervention (e.g., administration of insulin injections). Instead, electrochemical glucose detection, which is sufficiently accurate to be employed in existing commercial glucometers, has also been proposed for integration with smartphone platforms (Dario ® Blood Glucose Monitoring System User Guide, 2014). However, all prior-art requires separate dongles or test strips [39], which is not a fully-integrated solution, and thus does not

achieve the desired level of increase in convenience. To make a non-negligible difference in use case, eliminating the need for patients to carry a separate glucometer device, whether implemented as a dongle or an altogether separate device, is necessary. The key challenge to integrate electrochemical glucose sensors into smartphone platforms is convenient re-usability: such sensors operate by measuring the output of electrochemical reactions catalyzed by glucose-specific enzymes via functionalized electrodes, and, unfortunately, such functionalization is destroyed after only a few uses due to gradual leaching of sensor reagents. Hence, most prior-art solutions rely on screen-printing functionalized electrodes on paper strips that are inserted into the glucometer device (or smartphone dongle), and disposed of afterwards. In this work, we present the design of a glucose sensing system that features integration of electrochemical electrodes directly onto the smartphone platform, eliminating the need for a separate glucometer dongle, while still leveraging the electronics and processing capabilities of the smartphone. Instead of functionalizing the permanently-attached electrodes during manufacturing for single-use applications, enzymes are applied to the electrodes on-demand by the end user via a stylus containing magnetic enzyme-loaded carbon composite pellets, enabling re-use of the electrodes. In order to demonstrate this concept, a custom smartphone case was built that comprised the permanent bare (without enzyme) three-electrode biosensor, a Bluetooth Low-Energy (BLE)-based wireless transceiver and potentiostat, and a

stylus slot, all shown in Fig2.7A. The case snugly fits around the phone, adding negligible weight and size. Testing is accomplished by opening a custom-built application, dispensing a magnetic enzyme pellet onto the magnetic sensor surface as shown in Fig2.7B, and dropping a blood sample onto the sensor; within a few seconds, the blood glucose concentration is measured via the integrated potentiostat (Fig2.7C), and the results are displayed on the screen of the smartphone. Finally, the employed pellet is discarded and the sensor surface cleansed to reobtain a bare transducer surface for the next test with a fresh enzyme pellet, all with negligible test-to-test contamination. The following sections discuss the design rationale for the phone case and stylus, enzyme pellets, wireless potentiostat circuits, smartphone application, and the seamless integration of these to realize a practical standalone smartphone-based glucose sensor.

2.2.1 Materials and methods

The overarching goal of this work is to integrate glucose sensing functionality into a smartphone without requiring an external electronic dongle. While reusable glucose sensors are in principal possible to integrated into a phone, their long-term use is extremely limited due to gradual leaching of sensor reagents leading to erratic responses and carryover effect from previous tests. In this work, we address this challenge through the development of a two-part glucose sensor. The first part comprises a permanently-

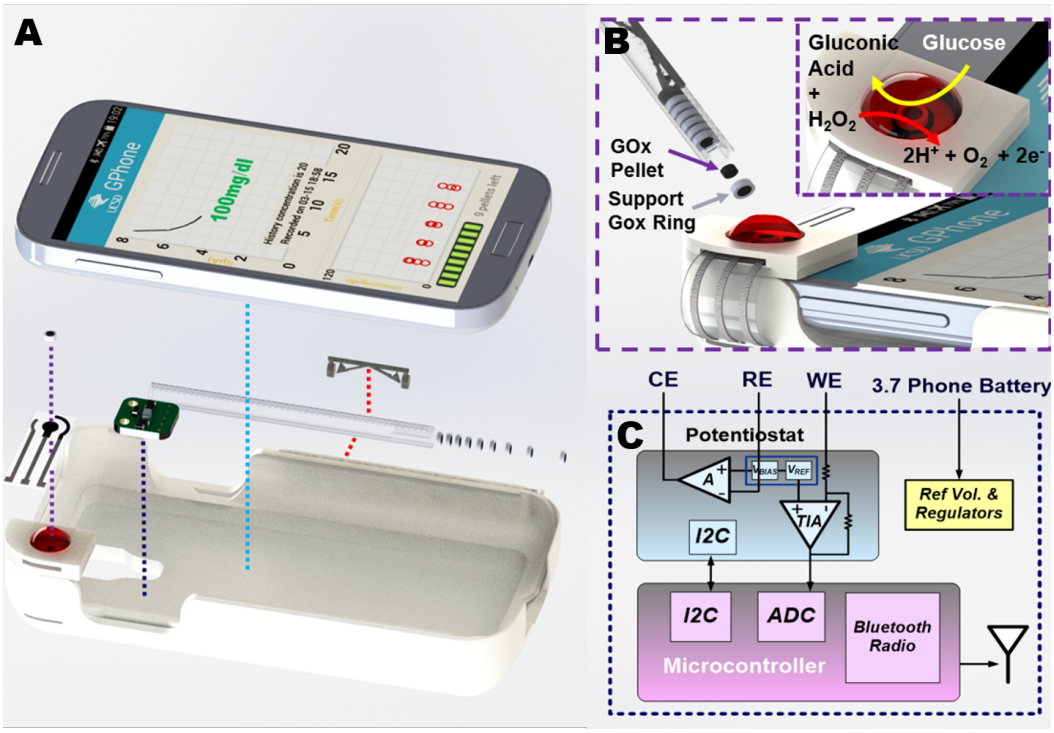

Figure 2.7: (A) Exploded view of the smartphone-based glucose sensing system (B) Dispensing carbon composite pellets loaded with GOx onto the bare carbon working electrode (C) Block diagram of the electronic readout circuits.

installed passive sensor strip consisting of a conventional three electrode electrochemical measurement system, though in this case with the working electrode being carbon with no permanent functionalization. The second part involves a biocatalytic pellet that imparts selectivity towards glucose on top of the working electrode. The pellet, which is a small, solid, and circularly packed disc, contains the active sensor components such as glucose oxidase and rhodium within a carbon composite. A functional glucose sensor is realized when the replaceable pellet is applied to the permanent passive sensor strip. After each test, the enzyme-loaded pellet is replaced with a fresh active layer for the next test. By doing so, major issues relating to leaching and carryover effect are obviated.

Ideally, the un-functionalized electrochemical electrodes, electronic instrumentation, and stylus would all be integrated directly into the housing of a smartphone. However, this requires intimate coordination with the smartphone manufacturing process; instead, a custom-designed phone case was developed to more easily demonstrate the proposed concept. The phone case was designed using CAD software (Solidworks®, Dassault Systemes Solidworks Corp., France), and fabricated using an Acrylonitrile-Butadiene-Styrene based 3D printer (Mojo Desktop Printer, Stratasys, Eden Prairie, Minnesota) for prototyping purposes. The case could also be adopted to more affordable injection molding that is commonly used for smartphone accessories commercialized at scale. The case was carefully designed to include dedicated housing for the permanently-installed passive sensor strip, BLE electronics, and the pellet dispensing stylus. The slot where the sensor strip is located has a housing for a neodymium magnet (diameter = 2 mm; height = 1 mm) to facilitate reliable placement of magnetic pellets in the same location for each test. The phone case also has a pair of cylindrical magnets (diameter = 1 mm; height = 0.5 mm) affixed to its side wall for holding the stylus.

A custom-built 3D printed stylus has been designed to reproducibly dispense enzymatic pellets on top of the working electrode. Three different pellet compositions (P1–P3) were tested for maximizing sensor stability under ambient conditions. All three compositions include magnetic materials to facilitate a simple and reliable pellet place-

ment procedure. Each composition was firmly packed in a hollow cylindrical tube to form the active portion of the working electrode, while an external Ag/AgCl electrode and platinum wire was utilized as the reference and counter electrode, respectively. For benchtop testing and characterization, a stainless-steel wire was inserted into the cylindrical electrodes at one end to serve as an electrical contact while the other end of the cylinder defined the active area of the electrode.

A Texas Instruments LMP91000 Analog Front End (AFE) was used as a potentiostat to drive the electrochemical biosensor to 0.4 V, and read out the corresponding current (i.e., constant-potential amperometry). The output of the LMP91000 can, in principal, be directly digitized by analog-to-digital converters readily available internal to most smartphones. However, in this implementation we did not have access to smartphone internals, and thus instead we developed a custom printed circuit board (PCB) featuring a Texas Instruments CC2541 BLE System-on-Chip for sensor digitization, processing, and communication of sensed data to the smartphone. A block diagram of the PCB is shown in Fig2.7C, which occupied 1.8 cm $\times$ 1.9 cm. The CC2541 was loaded with firmware that set configuration registers on the LMP91000 via I2C. A Johanson Technology 2.45 GHz antenna (2450AT42A100) and impedance matched balun (24550BM15A0002) were employed for wireless transmission. The PCB was powered directly from the battery of the smartphone, with on-board low-drop out regulators

LP5907 and LM4120 respectively providing the main DC voltage supply and the reference voltage for the instrumentation circuitry.

To provide the user with a friendly interface, an Android-based smartphone application was designed to display blood glucose concentration in real time. The application also has the ability to log measurements. The application launches with a welcome page with application name: GPhone Glucose Meter. It starts a background thread that scans supported BLE devices and automatically establishes a connection. Upon achieving a successful connection, the welcome page is hidden and the application starts to communicate with the BLE device. If no wireless connection could be obtained, a message is displayed to inform the user. The communication rules between the application and the BLE device is based on Universally Unique Identifier (UUID), which enables every object in a distributed system to be distinguishable from the others without the help of a central controller. In this way, the application only needs to know the UUIDs that it should write commands to and read data from. The application calculates the value of the current with a group of high and low digits (byte) data. As communication begins, another thread that holds the UI display is started. There is also a handler and a timer inside this thread. The handler listens to three messages:

(1) A current value is received Plot a data point (Message ID = 0x123)

(2) 5 s since last current value received (Message ID = 0x124)

(3) 28 s since last current value received (Message ID = 0x125)

The background thread sends a calculated current value in a message with ID 0x123 to this handler. The timer increases a counter after each second. The handler resets the counter so that the counter saves the number of seconds since last current value was received. The layout of the UI is shown in Fig2.7A and consists of three blocks. The upper part plots the current value versus time since a round of measurement started. It visualizes how the current lands in a stable value at the end of a 20-s measurement. After one round of measurement finishes and the counter reaches 5, the timer sends a message with ID 0x124 to the handler. Then, the handler renders the glucose concentration in the plot area. Based on the measured current value at time t=10 s, the resulting glucose concentration is indicated in the upper or lower part in the plot area to avoid overlapping with the curve. The glucose concentration text has different colors in different range according to the following values (units in mg/dL):

* $C \leq 60$ or $C > 125$: Red(Danger)

* $110 < C \leq 125$ or $60 < C \leq 70$: Orange(Warning)

* $70 < C \leq 110$: Green(Safe)

When the counter reaches 28, the timer sends a message with ID 0x125 to the handler. The handler records the glucose concentration result in a log file. The logged results are shown in the lower part of the interface, where each result is represented

as a white circle. The maximum value on the Y axis of the history graph changes automatically so that all the data points can fit within. When the user touches a white circle, a pop up window reveals the corresponding concentration value and time of the record. The canvas is colored red, orange, and green according to the definitions in the table above so that each data point sits in the region with its corresponding color. This part visualizes the distribution of glucose concentration over time. Finally, the bar at the bottom shows the remaining number of pellets in the dispenser.

2.2.2 Results and discussion

In our previous work, we explored a similar 2-part glucose sensing approach where the user draws the active sensor layer onto a sensor strip using a roller pen filled with enzymatic ink [40]. However, there are certain limitations to the aqueous-mediabased enzymatic ink approach. For example, evaporation of aqueous media, long-term stability of enzyme and other reagents, and reproducibility in applying a fixed amount of active sensor material to the sensor strip are all serious limitations. In the present work, we overcome these shortcomings by developing a silicon oil-based solid enzymatic pellet system. Such a system has several attractive attributes: the enzyme stability is much higher in a hydrophobic environment than in aqueous media; each pellet has a fixed quantity of active sensor reagents and hence the pellet approach has

better sensor response reproducibility than the previously explored enzymatic ink route; evaporation, which is a major problem for ink-based system, is not an issue for the pellets. Three different routes for pellet preparation were explored to obtain the optimal configuration.

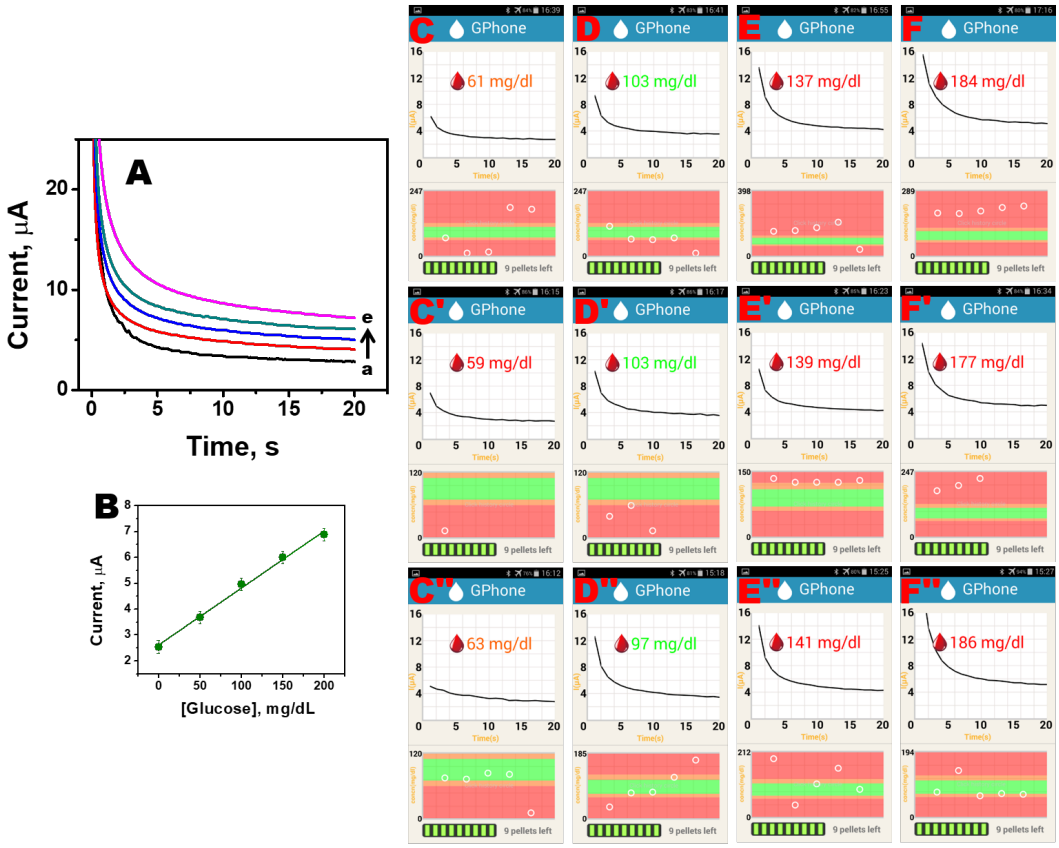

Figure 2.8: Sensor reproducibility study. (A) Chronoamperograms for different glucose concentrations. (B) Calibration plot of the study (R.S.D.$\leq$ 2.5%). (C-F) Screenshot plots of the Android Application software for different concentrations (60, 100, 140 or 180 mg/dl).

Sensor reproducibility is an important parameter for practical applications. In the present reusable sensor system, factors such as homogeneity of the composition, reproducible packing of the composition within each pellet casing, repeatable release

and attachment of the pellet from the stylus to the unfunctionalized working electrode, and its removal after each test without leaving any residue behind on the electrode will affect sensor reproducibility. The effect of these parameters was initially tested by performing reproducibility studies for pellets using a benchtop electrochemical analyzer (CH Instruments, Model 630C) as shown in Fig2.8A and B. In this study, a fresh pellet was dispensed onto an unfunctionalized three electrode system and data was recorded for different glucose concentrations. Thereafter, the pellet was discarded and a fresh one was dispensed on top of the unfunctionalized working electrode and the test was repeated for 6 different pellets. Fig2.8A illustrates the typical chronoamperometric plots obtained for a pellet in physiologically relevant glucose concentrations, while, the calibration plot for this study appears in Fig2.8B (n = 6; R.S.D$\leq$ 2.5$\%$). Thereafter, the complete system was tested for reproducibility wherein the ease and repeatability of dispensing a pellet onto the unfunctionalized working electrode affixed to the phone case, wireless data transmission from the sensor to the phone, and accuracy of the application software to display the test result was analyzed. In this study, a smartphone with an Andriod OS was placed in the phone case. A fresh pellet was dispensed from the stylus onto the sensor strip housed in the phone case and then the custom-built application software was loaded. Thereafter, a solution of known glucose concentration (60, 100, 140 or 180 mg/dl) was dropped onto the sensor strip. The glucose concentration was then

recorded by the application software. The "used" pellet was discarded after the glucose concentration was displayed on the phone screen. These steps were repeated multiple times for different concentrations. Fig2.8C–F illustrates the phone screenshots for this study. Data plotted in Fig2.8 highlight the reproducibility of system.

2.2.3 Conclusions

In this work we have demonstrated a reusable smartphone based glucose meter consisting of a custom-built smartphone case that includes a permanent bare sensor strip and a stylus for housing and dispensing enzymatic pellets directly onto the sensor strip. The case also has a slot for attaching a custom-built Bluetooth electronic module for data acquisition and transmission. A user-friendly Andriod based application software has also been developed for clear display of glucose level. The user performs a glucose test by loading the software on their phone, followed by dispensing a pellet from the stylus onto the sensor strip and introducing the sample. The pellet and the sample are discarded after the test is over to reobtain a fresh sensor surface for the next test. Such a reusable system overcomes the challenges faced by previously reported reusable sensors, such as gradual enzyme leaching, enzyme degradation, and hysteresis effect. Future work will focus on further optimizing the system by analyzing the sensor performance at different ambient temperatures, studying the effects of varying sample volumes, testing for the

effects of common electroactive species that can potentially affect the sensor response, and characterizing and optimizing the reversible magnetic bonding of the pellets to the sensor surface.

This chapter is based on and mostly a reprint of the following publications:

- Imani, Somayeh; Bandodkar, Amay; Kim, Jayoung; Wang, Joseph; Mercier, Patrick P., "Wearable Chemical Sensors: Challenges and Opportunities", International Symposium on Circuits and Systems, 2016.

- Kim, Jayoung[1]; Imani, Somayeh[1]; de Araujo, William R.[1]; Warchall, Julian; Valdés-Ramírez, Gabriela; Paixão, Thiago RLC; Mercier, Patrick P.; Wang, Joseph. "Wearable salivary uric acid mouthguard biosensor with integrated wireless electronics.", Biosensors and Bioelectronics, vol.74, 2015 ([1]: equally contributed).

- Bandodkar, Amay J[1]; Imani, Somayeh[1]; Nuñez-flores, Rogelio[1]; Kumar, Rajan; Wang, Chiyi; Mohan, A M Vinu; Wang, Joseph; Mercier, Patrick P, "Re-usable electrochemical glucose sensors integrated into a smartphone platform", Biosensors and Bioelectronics Journal, vol. 101, 2018 ([1]: equally contributed).

The dissertation author was the primary investigator and author of these papers.

Chapter 3

Non-Invasive Characterization of Electrochemical Wearable Sensors

In this chapter, we demonstrate a wearable tattoobased alcohol biosensing system for noninvasive alcohol monitoring in induced sweat. The skin-worn alcohol monitoring platform integrates an iontophoretic-biosensing temporary tattoo system along with flexible wireless electronics. The wearable prototype enables the transdermal delivery of the pilocarpine drug to induce sweat via iontophoresis and amperometric detection of ethanol in the generated sweat using the alcohol-oxidase enzyme and the Prussian Blue electrode transducer. The new skin-compliant biosensor displays a highly selective and sensitive response to ethanol. On-body results with human subjects show distinct differences in the current response before and after alcohol consumption, reflecting the increase of ethanol levels. The skin-worn alcohol sensor is coupled with a flexible electronics board, which controls the iontophoresis/amperometry operation and transmits data wirelessly in real time via Bluetooth communication. The new wireless epidermal

iontophoretic-biosensing system offers considerable promise for noninvasive monitoring of alcohol consumption in practical settings [41] and can be readily expanded toward the monitoring of additional analytes.

Unsafe levels of alcohol consumption can lead to vehicle crashes, violence, and the degenerated health of heavy drinkers. Such alcohol-related incidents and health concerns continue to rise rapidly across the globe, leading to considerable socioeconomic costs. Accordingly, there are tremendous needs for an accurate easy-to-use alcohol measuring device for use by law enforcement personnel, service/hospitality industry, or individual drinkers to provide a convenient means to monitor alcohol consumption. Although different methods have been used for determining alcohol consumption, including direct measurements of urine, blood, saliva, breath, or sweat, or verbal/interview measures, Blood Alcohol Concentration (BAC) is the most commonly used indicator of alcohol intoxication. Unfortunately, blood samples cannot currently be obtained without penetrating skin, typically via a lancet pricking a finger or earlobe, which can be painful and inconvenient, and demands user compliance. Such blood sampling methods limit the general use of alcohol monitoring devices to the most extreme cases (e.g., law enforcement), rather than as a general-purpose tool that can monitor a user's alcohol levels and warn or prevent what could amount to a catastrophe. Accordingly, there are considerable demands for developing an alternative approach for measuring BAC

indirectly in a noninvasive and real-time manner. Currently, breathalyzers are the most commonly used devices to indirectly estimate BAC, and operate by measuring breath alcohol concentration (BrAC). BrAC instruments calculate BAC by following Henry's law, but may compromise accuracy since the results can be easily affected by humidity, temperature, and individual traits [42, 43]. BrAC can also generate false alarms due to alcohol vapor associated with consumer products (e.g., mouthwash and breath freshener), and environmental factors (e.g., paint fume, varnish, and chemicals) [44]. BAC can also be estimated by measuring transdermal alcohol concentration (TAC), because a person's perspiration can contain traces of alcohol after alcohol consumption [45]. Two wearable transdermal alcohol sensor devices (SCRAM, Giner WrisTAS) have been developed for detecting local ethanol vapor concentration in insensible perspiration over the skin, which is not secreted by sweat glands [46, 47]. However, these devices suffer from long time delays ($0.5-2$h) compared to BAC estimated by breathalyzers. [46] Therefore, the development of a new prototype to monitor BAC noninvasively in real time is highly desired.

Recent work [48] has combined iontophoresis and biosensing processes for measuring alcohol level in induced sweat (sensible sweat) based on the established correlation between the two fluids during alcohol consumption. Such an operation showed that the maximum ethanol level in both fluids, blood Here we demonstrate a wearable

temporary-tattoo biosensing system capable of real-time noninvasive alcohol monitoring via integration of printed and flexible iontophoretic-sensing electrodes with wireless electronics (Fig3.1). Our study is built upon recently developed noninvasive wearable chemical sensors for monitoring chemical markers in sweat toward health or fitness applications.

In the following sections we describe an integrated tattoo-based wearable system for effective noninvasive ethanol monitoring based on coupling sweat-inducing iontophoresis and amperometric enzymatic biosensing (Fig3.1A), along with a flexible

supporting electronic readout module featuring wireless telemetry (Fig3.1B). The new skin-worn low-cost noninvasive alcohol monitoring device enables real-time alcohol measurements in induced sweat and obviates the need for lengthy and costly procedures. This represents the first example of integrating a drug-loaded iontophoretic operation and electrochemical amperometric biosensing of metabolite on a wearable tattoo platform, in general, and for tattoo-based flexible epidermal alcohol sensor system, in particular. The new wearable epidermal alcohol sensor system uses constant-current iontophoresis for inducing sweat by delivering the drug pilocarpine across the skin, followed by amperometric biosensing of the sweat ethanol (Fig3.1C). The latter relies on an alcohol-oxidase (AOx) enzymatic electrode along with a printed Prussian Blue (PB) electrode transducer. All the electrodes were fabricated by a screen-printing

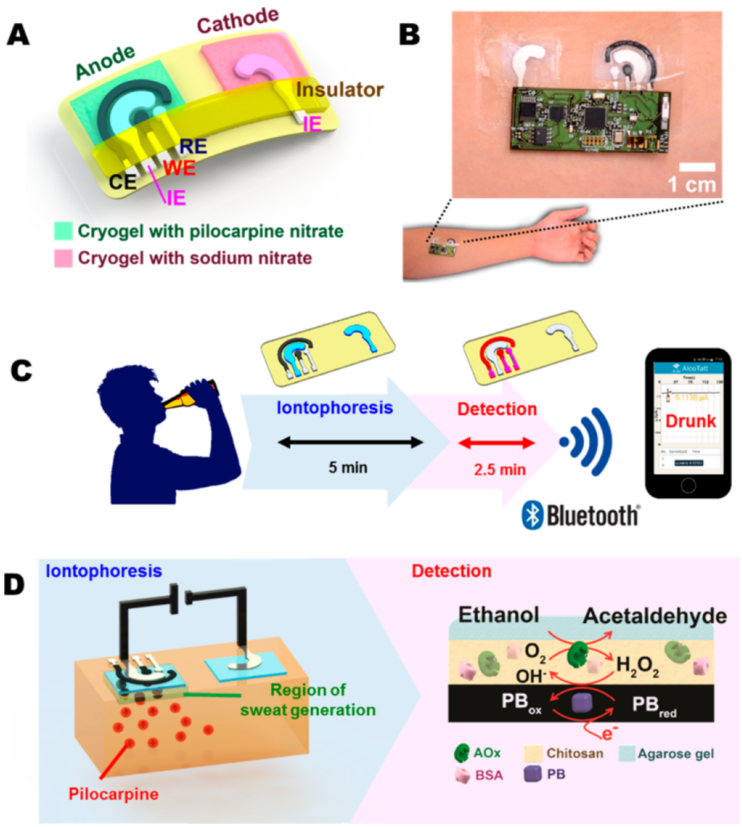

Figure 3.1: Tattoo-based transdermal alcohol sensor.
(A) Schematic diagram of an iontophoretic-sensing tattoo device, containing the iontophoretic electrodes (IEs; anode and cathode) and the three sensing electrodes. (B) Photograph of an alcohol iontophoretic-sensing tattoo device with integrated flexible electronics applied to a human subject. (C) Schematic diagram of a wireless operation of the iontophoretic-sensing tattoo device (D) Schematic diagram of constituents in the iontophoretic system (left) and of the reagent layer and processes involved in the amperometric sensing of ethanol on the working electrode (right).

technique on the wearable temporary-tattoo paper to offer cost-effective mass production along with convenient placement and removal from the skin. For realization of real-time alcohol monitoring with the wearable sensor, the tattoo alcohol sensor was integrated with flexible printed electronic circuitry (Fig3.1B), which controls the entire iontophoretic-sensing operation wirelessly and transmits the data to laptop or mobile

devices via Bluetooth communication (Fig3.1C). Both the skin-worn sensor and electronic board are flexible and compatible with the nonplanarity of the epidermis and offer resistance to mechanical stress from the wearer's movement.

The performance of the developed sensor was evaluated first in a buffer medium for its sensitivity, selectivity, and potential cross talk between the iontophoretic and sensing operations. Subsequently, the on-body iontophoresis operation was optimized on the human skin and the epidermal sensor was tested with human subjects under ingestion of alcoholic beverages. The on-body results (including corresponding control experiments) indicate that the new wearable epidermal alcohol sensor system holds considerable promise for reliable decentralized noninvasive alcohol monitoring in diverse practical settings toward saving lives and supporting the criminal justice system.

The epidermal evaluation on human subjects was conducted in strict compliance following a protocol approved by the institutional review board (IRB) at the University of California, San Diego. A total of nine healthy volunteers were recruited for on-body evaluation of the developed sensor before and after consumption of alcoholic beverages. In all experiments, the tattoo biosensors were placed on the subjects' arms, and ethanol sweat measurement was performed using the iontophoresis-amperometry operation to obtain the current response at BAC 0.000% ("before drinking"). During the iontophoresis process, a constant current of 0.6 mA (0.2 mA/cm^2) was applied for 5 min through

a cryogel layer between the two iontophoresis (i.e., anode and cathode) electrodes to deliver pilocarpine and induce sweat. The applied current density and duration were optimized and selected using on-body test as a trade-off between efficient sweat generation and the subject's compliant. For example, high currents that result in efficient pilocarpine drug delivery, also lead to skin burning/irritation. The applied time (5 min) was also selected based on the on-body results; 5 min is minimum duration to induce sweat and detect the alcohol sweat current signal. This was evaluated by multiple subjects (n = 9), since skin permeability varies among individuals. It was followed by a 5 min rest period during which the sweat was generated. Subsequently, the amperometric response of ethanol in sweat (BAC 0.000%) was recorded at an applied potential of -0.2 V (vs Ag/AgCl) for 150 s with a benchtop potentiostat. The subject then consumed an alcoholic beverage (12 oz. of beer or 5 oz. of table wine) for 5 min and waited for 10 min to allow alcohol diffusion in blood. Upon consumption, the alcohol passes through the stomach and gastrointestinal (GI) tract into the bloodstream. Afterward, it diffuses to the surrounding body tissues, including the skin. The iontophoresis/ detection cycle was then repeated to measure the corresponding ethanol sweat concentration. Along with the above on-body iontophoresis-sensing experiments involving alcohol consumption, three different control experiments (without drinking, without enzyme modification, and without iontophoresis) were performed. The sensor response toward

sweat ethanol was confirmed first in comparison with measurements without drinking alcoholic beverages. The selectivity of the sensor toward ethanol was evaluated also by comparison with the response of the enzyme-free electrodes. The effect of iontophoresis was verified by control experiments without the iontophoresis step. These three different control experiments were carried out under otherwise identical conditions, ensuring that the observed response is solely due to increased alcohol level following drinking. Each set of measurement cycles was accompanied by simultaneous BAC measurements using a commercial FDA-approved breathalyzer (Alcovisor Mars Breathalyzer, Hong Kong) to validate the sensor performance. Several additional on-body tests involved estimating the correlation between BAC and the current response of the tattoo sensor with repeated consumption of wine. These involved the same iontophoresis- amperometry experimental procedure using two sets of repeated drinking and measurement. The current response was measured initially before drinking (when BAC is 0.000%) using the iontophoresis-sensing operation. Then, the current response of such operation was recorded following the first and second drinking.

The flexible tattoo-based iontophoretic alcohol monitoring patch must connect to instrumentation electronics to control the iontophoretic and amperometric electrodes and readout data. While initial testing and characterization of the biosensor system have been carried out using benchtop equipment (CH Instruments), such a bulky electrochem-

ical analyzer limits the system-level attractiveness of having a thin temporary-tattoo design. Accordingly, the tattoo sensor was connected directly to a flexible printed circuit board (PCB) containing commercial off-the-shelf (COTS) integrated circuits for instrumentation, control, and telemetry in a thin, wearable form-factor. Specifically, the PCB employs a Texas Instrument (TI) CC2541 Bluetooth Low Energy (BLE) System-on-Chip for communication and processing. Iontophoretic current injection is achieved via a TI LM334 current source, which applies a 0.6 mA current between the iontophoretic cathode and anode electrodes. After 5 min of current injection, the LM334 was disconnected by control signals from the CC2541. Following an additional 5 min, a TI LMP91000 chemical sensing analog front end was enabled, and applied a 0.2 V potential across the amperometric electrodes for constant-potential amperometry experiments. The potential was held for up to 60 s, or until the resulting amperometric current, also read by the LMP91000, stabilized. The resulting current throughout the 60 s experiment was sampled and digitized by an on-board analog-to-digital converter (ADC) on the CC2541, and was transmitted via a Johanson Technology 2.45 GHz chip antenna (2450AT42A100) and impedance matched balun (2450BM15A0002) in a 2-byte format to a Bluetooth 4.0-enabled receiver. The receiver decoded the data and presented the results in a Python-based graphical interface on a desktop or laptop. The flexible PCB was powered by two 396/397 watch batteries (2 $\times$ 1.55 V, 33 mAh each) mounted in

series and conditioned via a TPS61220 boost converter and an LM4120 low-dropout voltage regulator. The PCB prototype, shown in Figure 1B, measured 2 cm $\times$ 5 cm.

A stainless steel sheet was cut in 2 mm $\times$ 10 mm size and attached on connection point of electrodes using conductive silver epoxy adhesive for detachable magnetic connection with magnets soldered on flexible board. The sensor-board assembly is shown in Fig3.1B; on-body evaluation proceeded following the same protocol described in the previous section. The resulting current response was transmitted to a laptop via a Bluetooth 4.0 and was displayed using a custom-made graphical interface.

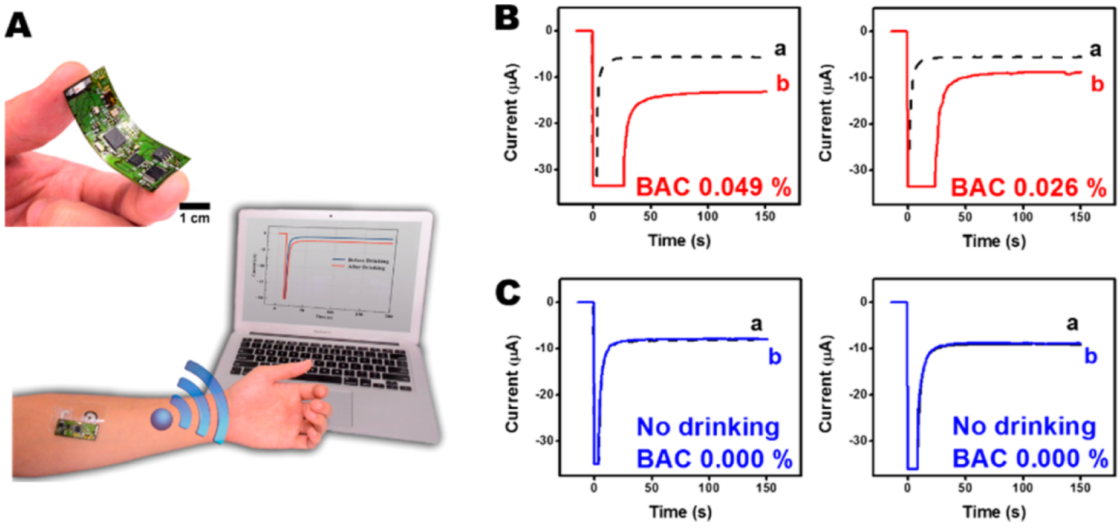

Figure 3.2: (A) Photograph of the wearable device with an integrated flexible electronics and the wireless communication with a laptop computer via Bluetooth; (B) experiment results from two different human subjects, before(plot"a") and after drinking alcohol beverage(plot"b"); (C) control experiments without drinking

A novel aspect of the new wearable alcohol biosensor is the integration of pilocarpineionotphoretic and amperometric detection systems and their coupling onto a single flexible tattoo-based device. Combining both systems and operations into a sin-

gle skin-worn platform requires a specific electrode design. The alcohol tattoo sensor system thus consisted of the iontophoretic electrodes (anode and cathode) and the three amperometric sensing electrodes (WE, RE, and CE) located in the anode compartment (Fig3.1A). The pair of iontophoretic electrodes is responsible for inducing sweat by delivering the pilocarpine drug from the anode compartment. These sweat-generating electrodes are thus positioned in the middle of sensing electrodes. Such a specific electrode layout is essential for an optimal integration of iontophoretic and detection systems and its skin-worn operation.

The practical use of the new wearable alcohol biosensor requires integration with a body-compliant wireless circuit board. As illustrated in Fig3.2A, a flexible and compact printed electronic circuitry has been developed for controlling the iontophoretic and detection processes along with a real-time wireless data transmission via a BLE radio. The performance of the integrated wearable device was evaluated following the same protocol as previous on-body experiments. A BLE-enabled printed circuit board was employed for iontophoresis by applying 0.6 mA current and amperometric measurements at -0.2 V for 150 s. The current response was sampled with a frequency of 1 Hz, and transmitted in real time via Bluetooth 4.0 to laptop/mobile devices and plotted on screen with graphical interface developed using Python. Fig3.2B, and C illustrate the application of the integrated flexible tattoo iontophoresis/sensor-electronic platform

for on-body testing of alcohol consumption using two human subjects. Fig3.2B displays the wirelessly transmitted current response and demonstrates a clear difference in the signals before (a) and after (b) consumption of the alcohol beverage. As illustrated in Fig3.2C, no current response is observed in analogous onbody control experiments without drinking. This performance corresponds to that observed in the on-body data involving the lab-scale potentiostatic analyzer. Overall, Fig3.2B,C demonstrates the practicality of the skin-worn integrated flexible alcohol sensor-electronic wireless system toward noninvasive BAC monitoring.

Chapter 3 is based on and mostly a reprint of the following publication:

- Kim, Jayoung[1]; Jeerapan, Itthipon[1]; Imani, Somayeh[1]; Cho, Thomas N.; Bandodkar, Amay J.; Cinti, Stefano; Mercier, Patrick P.; Wang, Joseph. "Noninvasive alcohol monitoring using a wearable tattoo-based iontophoretic-biosensing system.", ACS Sensors, vol.1, 2016 ([1]: equally contributed).

The dissertation author was the primary investigator and author of this paper.

Chapter 4

Wearable Multi-Measurand biosensing system for real-time health and fitness monitoring

Flexible, wearable sensing devices can yield important information about the underlying physiology of a human subject for applications in real-time health and fitness monitoring. Despite significant progress in the fabrication of flexible biosensors that naturally comply with the epidermis, most designs measure only a small number of physical or electrophysiological parameters, and neglect the rich chemical information available from biomarkers. Here, in this chapter, we introduce two skin-worn wearable hybrid sensing systems that offer simultaneous real-time monitoring of biological parameters.

4.1 A wearable chemical–electrophysiological hybrid biosensing system for real-time health and fitness monitoring

In this section, we present a wearable system that measures, for the first time, a biochemical – lactate, and an electrophysiological signal – electrocardiogram (ECG), for more comprehensive fitness monitoring than from physical or electrophysiological sensors alone [49]. The two sensing modalities, comprising a three-electrode amperometric lactate biosensor and a bipolar ECG sensor, are co-fabricated on a flexible substrate and mounted on the skin. Human experiments reveal that physiochemistry and electrophysiology can be measured simultaneously with negligible cross-talk, enabling a new class of hybrid sensing devices.

Wearable sensors present an exciting opportunity to measure human physiology in a continuous, real-time non-invasive manner. Recent advances in hybrid fabrication techniques have enabled the design of wearable sensing devices in thin, conformal form factors that naturally comply with the smooth curvilinear geometry of human skin [1,50] thereby enabling intimate contact necessary for robust physiological measurements. Development of such epidermal electronic sensors has enabled devices that can monitor respiration rate, heart rate, electrocardiograms (ECGs), blood oxygenation, skin tem-

perature, bodily motion, brain activity, and blood pressure. To date, most systems have targeted only a single measurement at a time, and most such sensors measure only physical and electrophysiological parameters, significantly limiting the monitoring information and diagnostic opportunities. For example, the human body undergoes complex physiological changes during physical activities such as exercise, and monitoring the physiologic effect of physical activity can be important for a wide variety of subjects ranging from athletes to the elderly and patients. Yet current devices that only measure heart rate, motion, and ECG provide an incomplete picture of the complex physiological changes taking place. As a result, further progress in the area of wearable sensors must include new, relevant sensing modalities, and must integrate these different modalities into a single platform for continuous, simultaneous sensing of multiple parameters, relevant to a wide range of conditions, diseases, health, and performance states. Specifically, inclusion of chemical measurements can provide extremely useful insights into the performance level and health status of the individual not available from physical or electrophysiological sensors. While chemical information is currently acquired via clinical labs or Point-of-Care (PoC) devices, such approaches do not support continuous, real-time measurements, limiting their utility to applications where stationary, infrequent tests are sufficient. While recent work, including our own, has demonstrated that chemicals such as electrolytes and metabolites can be measured continuously using

epidermal electronics on the skin, or through non-invasive monitoring of other bodily fluids, these devices measure only a single parameter at once, and are not integrated with other sensing modalities.

Here we introduce a wearable device that can simultaneously measure chemical and electrophysiological parameters in the form factor of a single epidermal patch, thus fusing on-body chemical sensing with the monitoring of vital signs into single wearable platform. The hybrid wearable, termed here as a "Chem-Phys" patch, comprises a screen-printed three-electrode amperometric lactate biosensor and two ECG electrodes, enabling, for the first time, concurrent real-time measurements of lactate and ECG. When used in physical exertion monitoring, ECG measurements can help monitor heart health and function, while sweat lactate can be used to track an individual's performance and exertion level during physical activity. Sweat lactate is an important biomarker for tissue oxygenation and can act also as marker for pressure ischemia. By combining a lactate biosensor and an ECG sensor, the new Chem-Phys hybrid wearable patch represents a powerful platform capable of simultaneously tracking both physicochemical and electrophysiological changes of a human body, thus providing a more comprehensive view of a person's health status than current wearable fitness monitors.

The Chem-Phys hybrid patch has been fabricated by leveraging screen printing technology on a thin, highly flexible polyester sheet that conforms well with the

complex three dimensional morphology of the human skin to provide a low-noise signal. The working electrode of the lactate biosensor is functionalized and coated with a biocompatible biocatalytic layer (Lactate Oxidase-modified Prussian Blue). The three amperometric electrodes are separated from the Ag/AgCl ECG electrodes via a printed hydrophobic layer to maximize sensor stability and signal-to-noise ratio even in the presence of significant perspiration. The Chem-Phys hybrid patch has been judiciously designed to attain a compact form-factor with the three lactate biosensor electrodes in the center, and the two ECG electrodes at each corner. The dimensions of the electrodes and the inter-electrode distances have been optimized based on human trails to acquire a clean ECG signal and lactate response with minimal interference between the two sensors. The two sensors are interfaced to a custom printed circuit board (PCB) featuring a potentiostat, an ECG analog front-end (AFE), and a Bluetooth Low-Energy (BLE) radio for wireless telemetry of the results to a mobile platform, such as a smartphone or laptop. Results presented in the following sections show that lactate and ECG can be measured simultaneously on human subjects, that lactate measurements do not adversely interfere with high-impedance ECG measurements, and that measurements of lactate levels and heart rate acquired from ECG data correlate with each other and with a commercially-available measurement device.

The Chem-Phys hybrid patch was fabricated via screen printing technology while

the wearable electronic board was realized by relying on standard 4-layer PCB fabrication and assembly protocols.

The 4-layer Bluetooth-enabled PCB employed a Texas Instrument (TI) CC2541 BLE System-on-Chip for communication and processing. An ADS1293 analog front end chip was employed for biopotential measurements to record the electrocardiogram (ECG) signals from the fabricated ECG electrodes. An LMP91000 analog front end, programmable through an I2C interface driven by the CC2541, was used as the on-board potentiostat for lactate concentration determination. The data from each sensor was collected by the CC2541 and transmitted to a Bluetooth 4.0-enabled receiver. A graphical interface was developed using Python to demonstrate measurement results on a PC. A Johanson Technology 2.45 GHz chip antenna (2450AT42A100) and impedance-matched balun (2450BM15A0002) were employed for wireless transmission. A CR2032 button cell lithium battery (3 V, 220 mAh) was utilized as a power source, regulated for the electronics via a TPS61220 boost converter. In the "active mode", the board consumed, on average, 5 mA from a 3 V supply during (15 mW).

The printed circuit board was assembled and tested in-vitro to validate the functionality and performance. The potentiostat circuit was verified together with the lactate biosensor through an in-vitro amperometric experiment. The ECG AFE was characterized using a CONTEC MS400 Multi-parameter Patient Simulator (ECG simulator). The

output signal of the ECG simulator was read using ADS1293 analog front end chip, and transferred through BLE link to a BLE-enabled device.

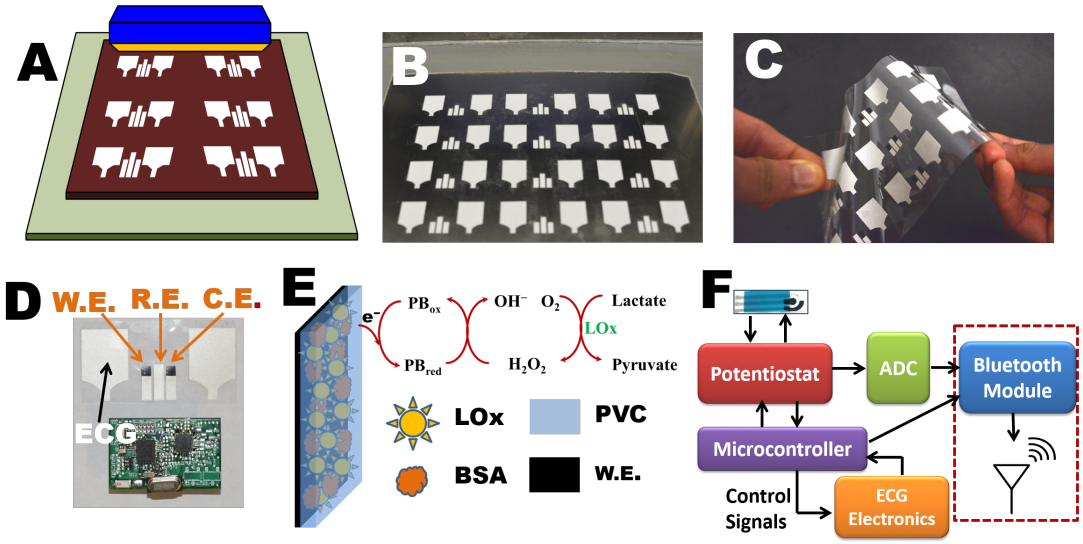

Figure 4.1: Fabrication and function of the Chem–Phys hybrid sensor patch. (a) Schematic showing the screen-printing process. (b) Image of the Chem–Phys printing stencil. (c) An array of printed Chem–Phys flexible patches. (d) Image of a Chem–Phys patch along with the wireless electronics. (e) Schematic showing the LOx-based lactate biosensor along with the enzymatic and detection reactions. (f) Block diagram of the wireless readout circuit.

The Chem-Phys hybrid multi-sensor system must be compact and easy to wear in a location that offers adequate access to both ECG signals and perspiration for lactate measurements. The design must also minimize sensor-body motion, must minimize co-interference between the sensing modalities, and be low-cost. These requirements motivate a flexible epidermal electronic design that can be worn on the chest and fabricated using screen printing technology. The design of the sensing system is shown in Fig4.1. The biosensors were fabricated via conventional low-cost screen printing

technique (conceptually illustrated in Fig4.1A) utilizing custom-designed stencils (photograph in Fig4.1B). The biosensing patches were printed onto a highly flexible, thin polyester sheet (50 μm thickness) for realizing highly conformable sensor patch that adheres well to the human skin without causing any discomfort. An array of fabricated sensors is shown in Fig4.1C. The total patch size was dictated by the bipolar ECG electrodes, which must be separated by a minimum distance in order to attain a high quality signal. Typically, single-lead monitoring systems such as the present design are used for basic heart monitoring, arrhythmias diagnosis, or studying the effect of exercise on the heart, and are placed in the vicinity of the conventional V1-V6 chest lead locations. Electrode size, separation, and placement parameters were determined through a series of experiments involving placement of Ag/AgCl-based ECG electrodes of various sizes (1 x1 cm2, 1.5 x 1.5 cm2, 1.5 x 1 cm2 and 2 x 2 cm2) and separation distances (1 to 6 cm) on subjects with different chest sizes, and observing the resulting ECG waveforms. The study revealed that a compact patch that provides favorable ECG signal could be realized by placing 1.5 x 1.5 cm2 ECG electrodes across the V1 and V2 lead sites with an inter-electrode distance of 4 cm, thereby measuring from the vantage point of the septal surface of the heart as suitable for diagnostics of arrhythmias and the effects of exercise on the heart. This sets an upper-end size of the patch to be 7 x 2 cm2. The chest region is not only convenient for measurement of ECG, but also has a high sweat rate during

physical excursion, and can thus serve as an appropriate location to also measure lactate levels in human perspiration. Additionally, the epidermis and muscle tissues over these locations do not experience complex three dimensional strains and remain fairly stable even during intense physical activities, making measurements here especially convenient. Since the performance of amperometric lactate electrodes is not compromised by reducing their dimension, they were fabricated between the two ECG electrodes, as shown in Fig. 1D. Each of the three electrodes have an active area of 3 x 2.5 mm2. The working electrodes were printed using Prussian Blue ink due to the high selectivity of Prussian Blue towards hydrogen peroxide, a byproduct of the enzymatic oxidation of lactate (Fig4.1E). The reference electrode was printed using Ag/AgCl. Since sweat can provide an alternate electrically-conductive pathway between the ECG electrodes and also between the ECG and amperometric electrodes, thus leading to potential distortion of the recorded ECG signal, a printed hydrophobic layer of Ecoflex® was used to separate the amperometric biosensor from the ECG electrodes to obviate direct electrical contact between the ECG and amperometric electrodes via sweat, thus minimizing the cross-talk between the two sensors. The entire Chem-Phys patch is highly flexible and can be smoothly mated on curved surfaces. Such flexibility is crucial for achieving unobtrusive wearable devices that cause no hindrance or irritation to the wearer. The Chem-Phys patch was interfaced to a custom printed circuit board (PCB) featuring a

potentiostat and analog-to-digital converter (ADC) for amperometric data acquisition, an analog front-end (AFE) for ECG data acquisition, and a Bluetooth Low Energy chip for wireless transmission (Figs4.1D and 4.1F).

Lactate concentration in human sweat depends on a person's metabolism and level of exertion, and typically ranges from 0 to 25 mM. A wide linear detection range coupled with a fast response time is thus essential for continuous epidermal monitoring of lactate. The operating potential of -0.1V (vs to Ag/AgCl) was selected based on the onset potential for electro-oxidation of lactate by the fabricated biosensor, obtained during cyclic voltammetry studies. When the biosensor comes in contact with lactate, the immobilized LOx enzyme catalyzes the oxidation of lactate to generate pyruvate and H2O2. The Prussian Blue transducer, then selectively reduces the H2O2 to generate electrons to quantify the lactate concentration (Fig4.1E).

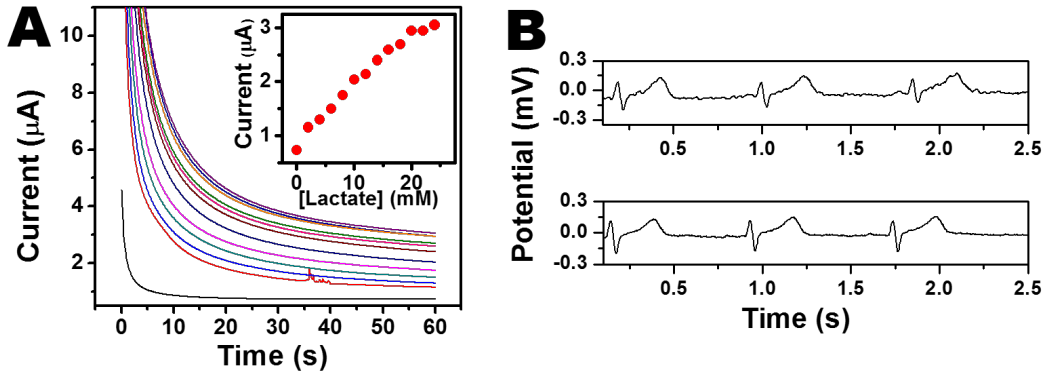

Figure 4.2: In-vitro characterization of Chem-Phys hybrid patch. (A) Amperometric response to increasing lactate concentration from 0 to 28 mM with 2mM additions in phosphate buffer (pH 7.0). Applied voltage = -0.1V vs Ag/AgCl. (B) ECG signals using 3M Red Dot electrodes (top), and printed ECG sensor (bottom).

Fig4.2 shows the amperometric response of the lactate biosensor to increasing lactate concentrations in the physiological range of 0-28 mM. It is evidenced from this figure that the biosensor responds linearly to the lactate concentrations in this range with a sensitivity of 96nA/mM.

The ability of the printed ECG electrodes to record ECG signals was validated by comparing recordings from the fabricated electrodes to commercially-available 3MTM Red DotTM ECG electrodes. As illustrated in Fig4.2, ECG signals recorded for the same subject using commercial and fabricated electrodes at the same location have similar morphologies when acquired using the same AFE circuitry.

The Chem-Phys hybrid patch (Fig4.3A) was fabricated and applied to three healthy male subjects on the fourth intercostal space of the chest (Fig4.3B). Dynamic changes in sweat lactate levels and ECG signals were measured continuously during a bout of intense cycling. In order to ensure that the anaerobic metabolism was invoked, subjects were asked to mount a stationary cycle and maintain a steady cycling cadence while the cycling resistance increased periodically as illustrated in Fig4.3C.

Since ECG measurements were made via bipolar high-impedance electrodes, and lactate measurements were made by applying a constant potential via a low-impedance potentiostat output and measuring current, there is a possibility that a change in the applied potentiostat voltage (for example during start-up) could interfere with ECG mea-

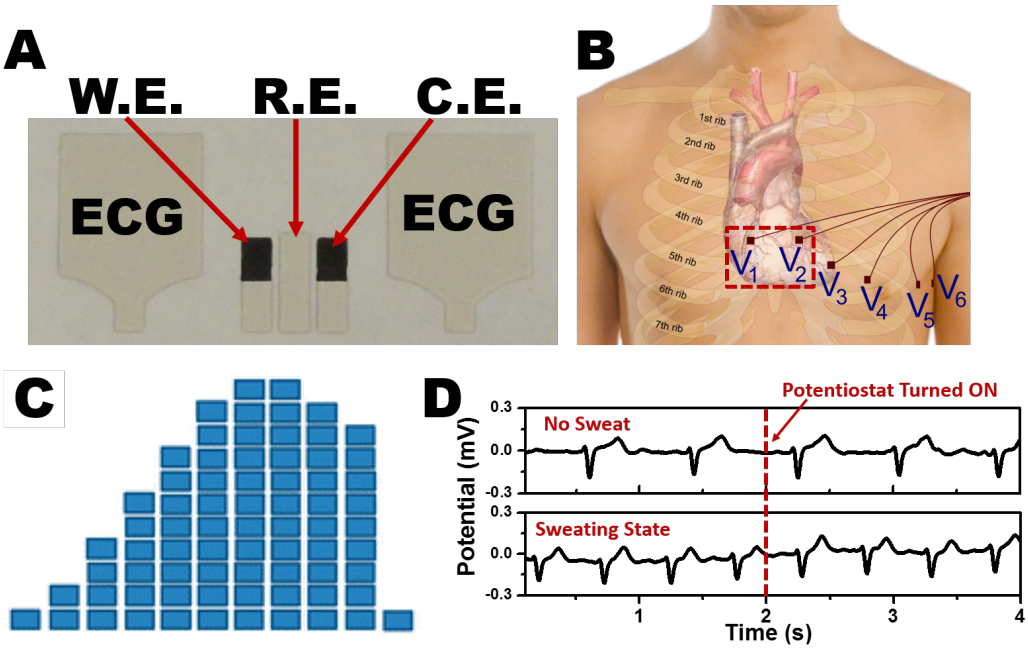

Figure 4.3: On-body test configuration
(A) A photograph of Chem-Phys hybrid patch. (B) Location of the Chem-Phys patch for mounting on the human body; fourth intercostal space of the chest. (C) Cycling resistance for on-body tests. (D) Effect of amperometric measurement on the ECG signal before cycling (no sweat state) and during cycling (sweating state).

surements during the settling time of the potentiostat. At the same time, sweat consists of many ions and could thus acts as an electrically conductive medium that can shunt the lactate and ECG sensors, or the two ECG electrodes together. Co-sensor interference and shunting effects were mitigated by geometrically separating the lactate and ECG electrodes and printing two vertically-oriented hydrophobic layers were next to the lactate biosensor, thereby facilitating flux of new perspiration across the biosensor itself, while minimizing shunting between the lactate and ECG sensors. To validate performance under concurrent hybrid sensing scenarios, the Chem-Phys sensor was mounted on a human subject and set to continuously record ECG prior to, during, and immedi-

ately after turning on the -0.1 V potentiostat output. Experimental results, obtained via a wireless Bluetooth link as shown in Fig4.3D, reveal that the potentiostat has a negligible effect on the morphology of the ECG signals, irrespective of whether the subject was in a resting or cycling state.

To validate performance under realistic conditions, the Chem-Phys patch was tested on three subjects during 15-30 minutes of intense cycling activity; continuous time-series results during each experiment are shown in Fig4.4. At the commencement of the cycling activity, each subject's heart rate, extracted from ECG data, was within the normal resting range of 60 to 120 beat per minute (BPM). At the same time, a negligible current response was measured by the lactate biosensor due to the lack of perspiration. With time, the resistance for cycling was increased, causing the subjects to exert increasing levels of effort to maintain constant cycling speed. This resulted in increasing heart rate and generation of sweat. At the onset of perspiration, lactate is released from the epidermis, and is selectively detected by the LOx-based biosensor. As the resistance increases, the sweat lactate concentration too increases, as illustrated in Figs. 4A-C, showing a correlation between physical exertion, heart rate, and lactate generation. As the cycling continued, the sweat rate for each subject increased, leading to the well-documented phenomenon of dilution factor that causes decrease in the lactate concentration. The final stage of the cycling bout involved a 3 minute cool down period.

During this phase, as expected, the heart rate normalized back near to the normal resting heart rate. At the same time, the lactate concentration measured by the lactate biosensor continued to decrease.

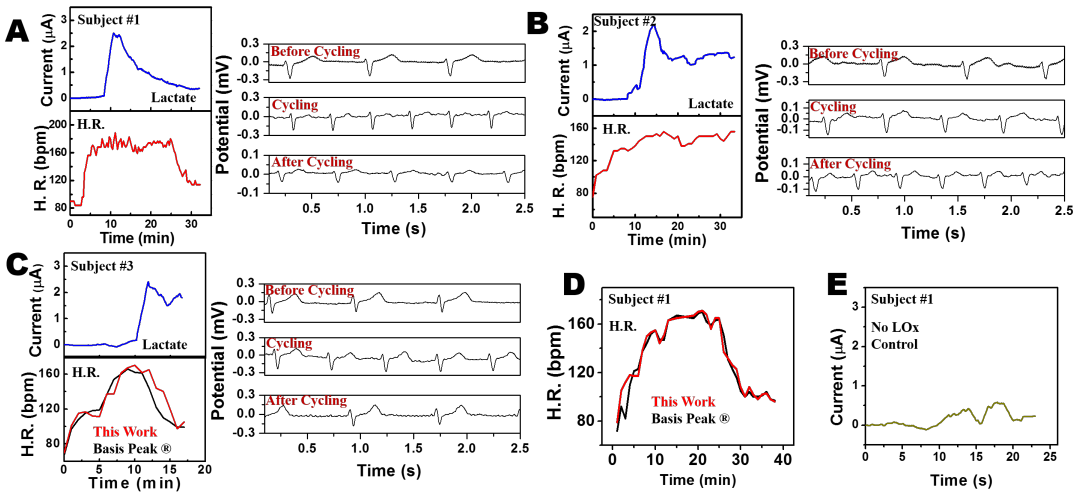

Figure 4.4: Real-time on-body evaluation of the Chem-Phys hybrid patch showing the lactate levels and H.R. for three human subjects.
The corresponding 'blue plots' represent the real-time lactate concentration profiles for each subject, while, the 'red plots' depict the H.R. data obtained by the ECG electrodes of the Chem-Phys patch. The 'black plots' correspond to the H.R. data recorded by the Basis Peak® heart rate monitor. Typical real-time ECG data obtained before, during and after the cycling bout for each subject is also shown in A, B and C. Panel D provides more data for H.R. verifications. Panel E demonstrates response of the control amperometric sensor (without Lox enzyme) for subject #1.

The lactate biosensor data for each subject resembles the expected sweat lactate profile for increasing intensity workouts. To validate that lactate, not other sweat constituents, was specifically measured, a control experiment in which an unmodified (Lox-free) amperometric biosensor was used under the same experimental conditions as above to subject #1. As shown in Fig4.4F, the control biosensor leads to a negligible

current response without the presence of LOx, confirming the high selectivity of the lactate biosensor. To validate ECG data over long time series, even under the presence of experimentally-induced motion, heart rate as extracted from the ECG data is benchmarked against a commercial wristband heat rate monitor (BASIS®) for subjects 1 and 3. Extracted heart rate data matched the wrist-worn device with a Pearson correlation coefficient of r = 0.975.

The Chem-Phys sensor patch described in this study represents the first system that fuses the monitoring of vital signs with on-body chemical sensing into single fully printable wearable platform. On-body epidermal testing in a realistic fitness environment revealed that ECG sensing is in-line with existing wearable devices, and is not adversely affected by simultaneous measurement of lactate via constant-potential amperometry. The lactate control study using an enzyme-free amperometric sensor and correlation of the heart rate data of the hybrid patch to that recorded by a commercial heart rate monitor underscore the promise of the Chem-Phys patch to monitor simultaneously ECG signals and sweat lactate levels for tracking the wearer's physicochemical and electrophysiological status. This device represents an important first step in the research and development of multi-modal wearable sensors that fuse chemical, electrophysiological, and physical sensors for more comprehensive monitoring of human physiology.

4.2 Simultaneous Monitoring of Sweat and Interstitial Fluid Using a Single Wearable Biosensor Platform

The development of wearable biosensors for continuous noninvasive monitoring of target biomarkers is limited to assays of a single sampled biofluid. An example of simultaneous noninvasive sampling and analysis of two different biofluids using a single wearable epidermal platform is demonstrated here [51]. The concept is successfully realized through sweat stimulation (via transdermal pilocarpine delivery) at an anode, alongside extraction of interstitial fluid (ISF) at a cathode. The system thus allows on-demand, controlled sampling of the two epidermal biofluids at the same time, at two physically separate locations (on the same flexible platform) containing different electrochemical biosensors for monitoring the corresponding biomarkers. Such a dual biofluid sampling and analysis concept is implemented using a cost-effective screen-printing technique with body-compliant temporary tattoo materials and conformal wireless readout circuits to enable real-time measurement of biomarkers in the sampled epidermal biofluids. The performance of the developed wearable device is demonstrated by measuring sweat-alcohol and ISF-glucose in human subjects consuming food and alcoholic drinks. The different compositions of sweat and ISF with good correlations of

their chemical constituents to their blood levels make the developed platform extremely attractive for enhancing the power and scope of next-generation noninvasive epidermal biosensing systems.

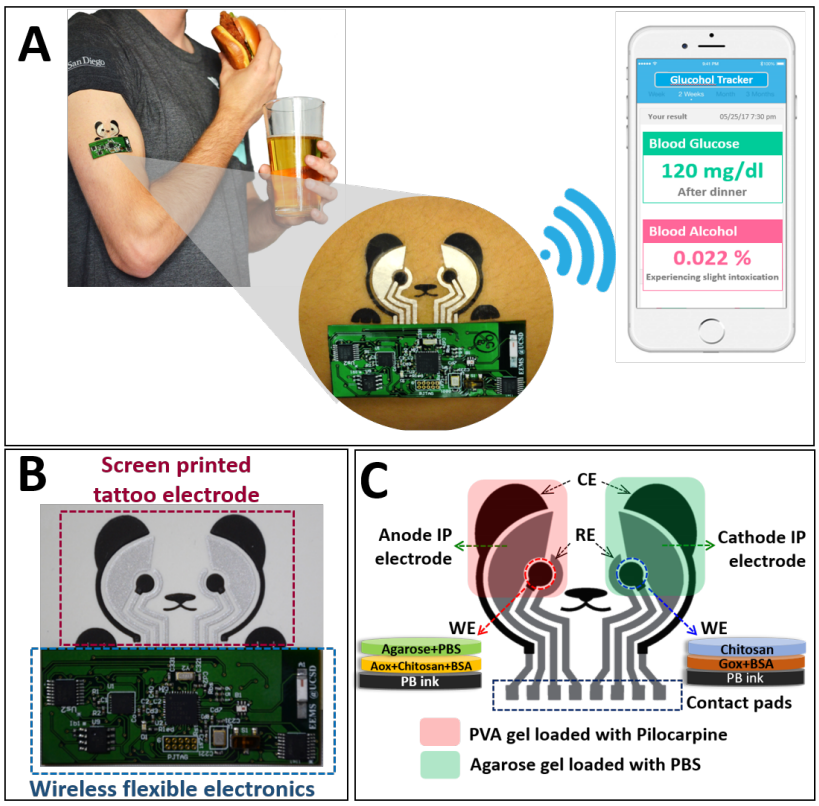

Figure 4.5: The concept of simultaneous noninvasive sampling and monitoring of ISF and sweat. A) Depiction of wearable iontophoretic biosensor device on a printed tattoo platform for glucohol (glucose + alcohol) sensing on a human subject, along with wireless real-time transmission B) Image of the screen-printed glucohol biosensor coupled with wireless flexible printed circuit board. C) Schematic representation of iontophoretic operation. D) Schematic representation of glucohol biosensor. E) Schematic representation of biosensing operation. Amperometric detection of alcohol in the generated sweat and of glucose in the extracted ISF.

Herein, we report on the development of a new class of wearable biomonitoring device that enables, for the first time, simultaneous and yet independent sampling and

analysis of two epidermal biofluids (ISF and sweat) in a single device (Fig4.5A). This dual sampling and detection epidermal system has been realized through the parallel operation of reverse ion- tophoretic ISF extraction across the skin and iontophoretic delivery of a sweat-inducing drug (pilocarpine) into the skin at separate locations. The printed, tattoo-like flexible iontophoretic system has been integrated with electrochemical biosensors to enable simultaneous real-time analysis of the different sampled biofluids. These biosensors were designed to electrochemically measure ISF glucose at the cathode side (using a glucose oxidase (GOx)-based biosensor) and sweat alcohol at the anode side (using an alcohol oxidase (AOx)-based biosensor) as model analytes, yielding a glucohol (glucose + alcohol) wearable epidermal platform. Such wearable system has been fabricated on epidermal temporary tattoo platform through cost-effective screen-printing technique for disposable single use. The developed simultaneous detection of glucose and alcohol offers consider- able promise for a variety of practical applications. A flexible circuit board was magnetically attached to the glucohol tattoo to drive the iontophoretic electrodes, control the biosensors, and wirelessly transmit the sensed information to a smartphone for practical self-monitoring applications (Fig4.5B). The inte- grated wireless electronics were programmed to perform the sequential operations of IP and amperometric measurements with no-apparent cross-talk between these functional sampling and detection steps. Furthermore, the attractive performance and

practicality of the new epidermal tattoo iontophoretic sensor was demonstrated with human subjects consuming glucose and alcohol. Such successful simultaneous on-demand sampling (at rest) and analysis of ISF and sweat on a single wearable device hold considerable promise for enhancing the capabilities and scope of noninvasive epidermal biomarker detection platforms.

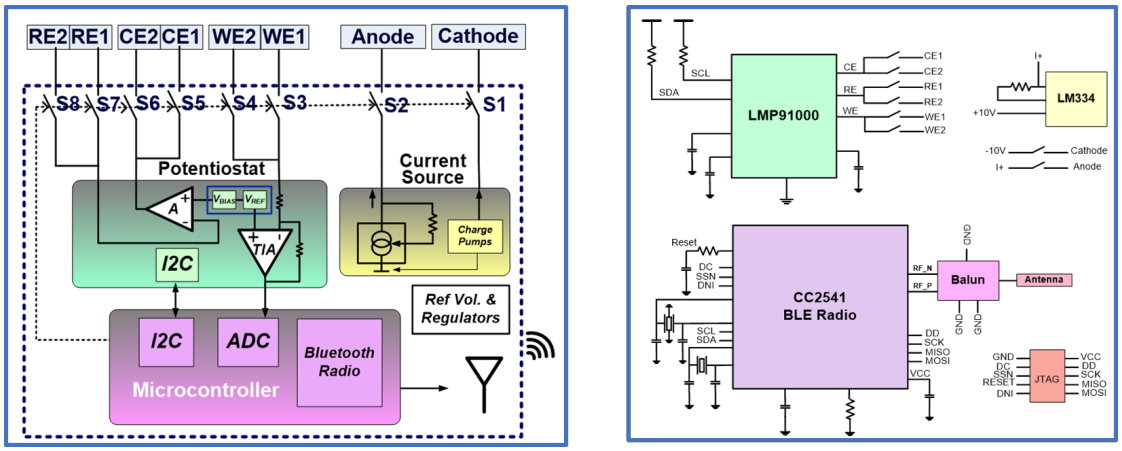

Figure 4.6: Wireless instrumentation electronic board. (A) Simplified schematic of the circuit. (B) A simple block diagram of the instrumentation electronic board.

The wireless electronic instrumentation circuit which was developed to apply the iontophoretic current to the biosensor patch, noninvasively extracts glucose and alcohol molecules, to measure the resulting concentrations via constant-potential amperometry, and wirelessly deliver measured results to a smartphone or laptop for further processing and/or analysis.

The PCB was designed on a 177μm polyimide flexible substrate to conform to

the shape of the body. The board included a Texas Instrument CC2541 2.4-GHz BLE and Proprietary System-on-Chip device, a Texas Instruments LMP91000 Configurable AFE Potentiostat, and several DC-DC converters for voltage supply regulations to generate reference potentials (Fig4.6A).

Additionally, a 3-Terminal Adjustable Current Source (LM334) was selected to provide the required iontophoretic current of 0.8 mA. The iontophoretic current and constant-potential amperometry measurements needed to be completely isolated to avoid unintended current loops in the electrode area. Therefore, an appropriate switching mechanism should be used to provide this isolation. To keep the board area small, a single potentiostat was used. Thus, a set of high- voltage switches were needed to switch between the glucose and alcohol sensing electrodes during amperometry, as well as to enter a high-impedance state during iontophoretic processing. Two Analog Device ADG452BRUZ chips were used to provide eight SPST CMOS switches for eight pins: three glucose amperometric pins, three alcohol amperometric pins, and two iontophoretic pins. In each mode (IP, glucose sensing, alcohol sensing), the BLE microcontroller set the switching modes accordingly (Fig4.6B). The power consumption of the board was provided using a CR2032 Lithium coin battery (Fig4.6). These power levels were measured to be 30 and 6 mW in iontophoretic and amperometric phases, respectively.

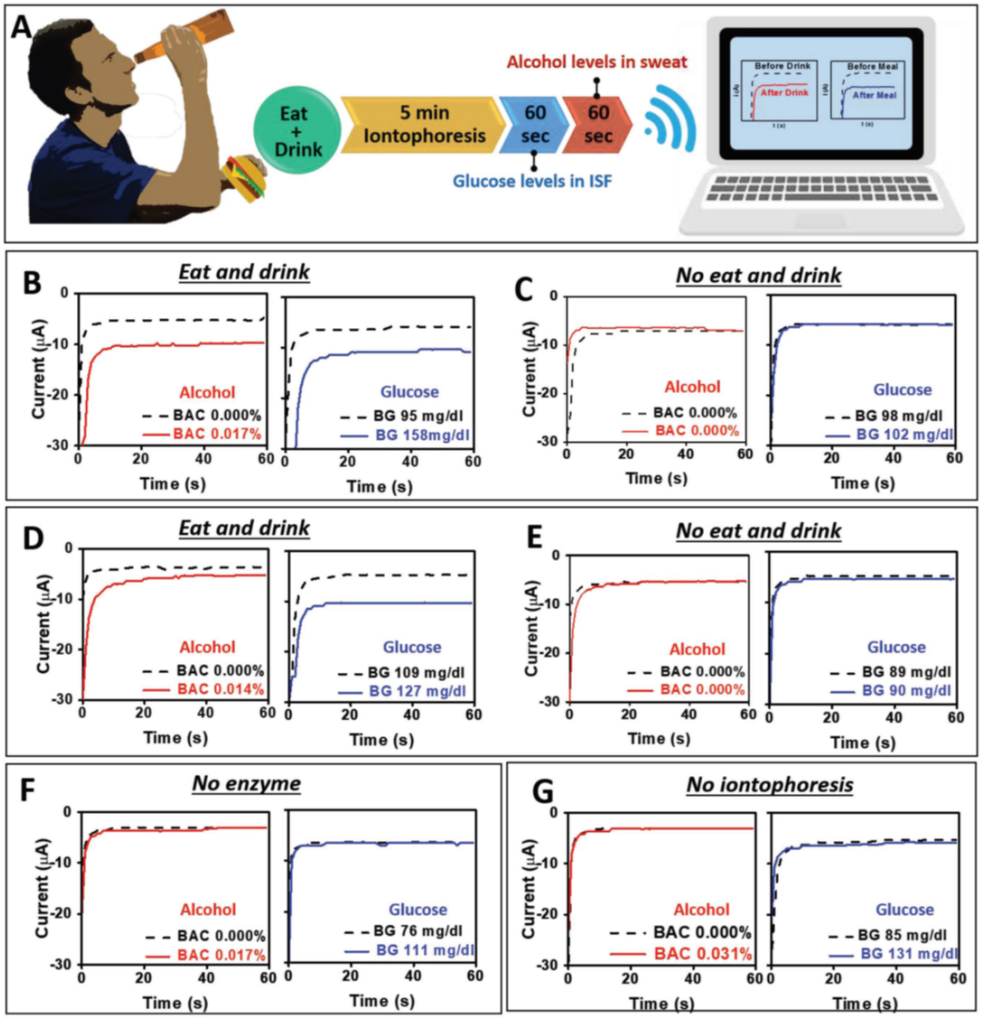

Figure 4.7: Electrochemical characterization of glucohol sensors for on-body operation. A) The time course for operation of an iontophoretic-sensing tattoo device B,D) Amperometric response measured before and after consumption of alcohol and meal. C,E) Amperometric response in control experiments without consumption of alcohol and meal for two human subjects. Amperometric response of the glucohol biosensor without F) the enzyme immobilization or G) iontophoresis.

Based on the selective and sensitive response of the glucohol tattoo toward the target glucose and alcohol biomarkers, we proceeded with on-body testing using hu-

man subjects (Fig4.7). The epidermal demonstrations were conducted with recruited healthy volunteers under their informed written consent. These on-body tests involved the consumption of food and alcoholic beverages to induce spikes in blood glucose and alcohol levels, respectively, expected in real-life scenarios (Fig4.7A). The results shown in Fig4.7B,D were obtained using two healthy male subjects (subject 1 and 2) with the consumption of a meal and alcoholic beverage. Control evaluations carried out without such meal or alcohol uptakes (keeping fasting state), are shown in Fig4.7C,E. Subjects 1 and 2 showed steep rise in their blood glucose and alcohol levels after the ingestion of food and drinks (as measured by commercial glucometer and breath analyzer). The epidermal glucohol sensor displayed a similar trend of increased ISF glucose and sweat alcohol signals. In contrast, no change in the signal of either sweat alcohol or ISF glucose was observed when food and alcohol were not ingested, reflecting a continued fasting state. Additional control experiments were carried out without the enzyme immobilization and without IP, as shown in Fig4.7F,G, respectively. As expected, these control tests displayed consistent negligible current signals, despite the elevated blood glucose and alcohol levels by consumption of food and alcohol. These control experiments indicated that IP played a critical role in sampling the noninvasive biofluids (ISF, sweat) and that the presence of enzyme was required for biosensing the collected analyte. Clearly, the measured glucose and alcohol signals originated from the extracted ISF and stimulated

sweat samples. The immobilized enzymes (GOx, AOx) ensured a selective response for detection of glucose and alcohol in the extracted ISF and generated sweat, respectively.

Finally, it should be noted that the glucohol tattoo was readily transferred onto the upper arm with ease of use as shown in Fig4.8A, and various deformation tests were subsequently carried out in order to investigate the mechanical stability of the device under mechanical strains expected during on-body operation. Upon application to the arm, the wearable device underwent bending, twisting, and stretching to examine its resistance to such strains and for the presence of possible cracks or breaks in the electrode surface (Fig4.8B).

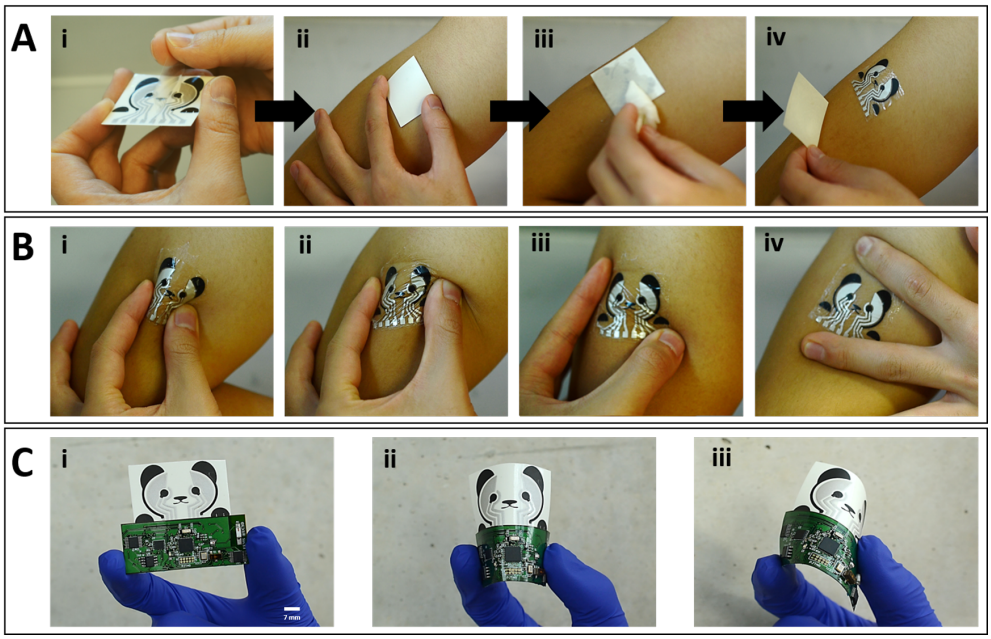

Figure 4.8: Skin conformability and mechanical integrity of glucohol biosensor. A) Tattoo application process B) Mechanical deformation tests of transferred tattoo C) (i) Tattoo integrated with wireless flexible PCB followed by additional strain tests, (ii) 180° inward bend, and (iii) rotational bend. Scale bar: 7 mm.

This examination indicated no apparent cracks following these deformations and that the tattoo remained in good contact with the skin throughout the test. For practical applications, the tattoo sensor was combined with flexible electronics board and similar (twisting and bending) strains were applied (Fig4.8C). These strains caused no apparent structure damage reflecting the conformal character and flexible properties of the entire integrated tattoo device.

We have reported the first example of a dual epidermal fluids sampling and detection system, fully integrated onto a single conformal wearable platform. The design and operation of the new printed flexible device were optimized to ensure reliable and efficient iontophoretically stimulated simultaneous collection of the individual biofluids at the corresponding biosensor sites with no intersample mixing. Such rational design thus allows parallel sampling of the ISF and sweat biofluids toward noninvasive detection of different biomarkers. The dual fluid sampling and analysis concept was implemented using cost-effective screen-printing of body-compliant, disposable temporary tattoo platform along with conformal wireless electronics. The new concept was illustrated for noninvasive glucose and alcohol analysis in healthy human subjects following meal and drink consumptions, with good correlations to commercial blood glucometer and breath-analyzer devices. Future efforts will focus on large population studies for monitoring glucose and related alcohol effects in diabetes and prediabetes subjects.

The new wearable sampling/sensing concept can be readily expanded to the monitoring of different biomarkers in the ISF and sweat fluids in connection to variety of health-care and wellness applications. The simultaneous sampling and analysis of different noninvasive biofluids could thus pave the way for improved biomarker monitoring and enhanced assessment of a wearer's physiological status.

Chapter 4 is based on and mostly a reprint of the following publications:

- Imani, Somayeh[1]; Bandodkar, Amay J.[1]; Muhan, AM Vinu; Kumar, Rajan; Yu, Shengfei; Wang, Joseph; Mercier, Patrick P., "A Wearable Chemical - Electrophysiological Hybrid Biosensing System for Real-Time Health and Fitness Monitoring", Nature Communications, vol. 7, May 2016. ([1]: equally contributed).

- Kim, Jayoung; Sempionatto, Juliane R.; Imani, Somayeh; Hartel, Martin C.; Barfidokht, Abbas; Tang, Guangda; Campbell, Alan S; Mercier, Patrick P.; Wang, Joseph, "Simultaneous Monitoring of Sweat and Interstitial Fluid Using a Single Wearable Biosensor Platform," Advanced Science, Vol. 5, 2018.

The dissertation author was the primary investigator and author of these papers.

Chapter 5

Energy Harvesting from Biofuel Cells

An ideal wearable device is a thin, lightweight, compact, soft, and stretchable one which possesses the extended battery life. While many flexible and stretchable materials have been introduced for fabricating stretchable and novel shapes of sensors and circuits, the stretchable energy source still remains a challenge. Stretchable batteries and super capacitors have been developed to address the issue. These efforts, however, have not succeeded to completely resolve the issue because of their limited energy storage capacity which necessitates frequent recharging. Wireless power transmission has been used as an alternative approach to power the wearables; the typical method can be implemented via near-field communication (NFC) chipsets; Nevertheless, this method requires a large, proximal power source and can tether the user to a fixed location which making the device less user-friendly and not very convenient for many applications. A promising alternative approach is to develop a wearable energy harvester that scavenges energy from body motion, the sun, body heat, and biofluids. Researchers have already

implemented systems to harvest these energies using piezoelectric nanogenerators [52], wearable solar cells [53] [8], and endocochlear potential-based bio-batteries [54]. Of these, utilizing biofluids for generation of electricity by biofuel cells is an appealing avenue since these systems rely only on the body of the user for energy conversion. However, most of the reported on-body BFCs which present high-power density rely on blood glucose as a fuel and hence require implantation within the wearer. This restricts the utilization of these types of biofuel cells for externally-worn devices. On the other hand, sweat as a biofuel can be employed to feature an easy-to-wear non-invasive BFC. Biomedical research shows that the human sweat is rich with several metabolites and electrolytes such as lactate, glucose, pyruvate, or ethanol. Lactate is particularly attractive since its concentration in the human sweat can rise high enough to be exploited by wearable biofuel cells to power wearable electronics.

In 1839, Grove invented a novel economical constant battery, later named fuel cell, by recombining hydrogen and oxygen to produce water and electrical current; the reversed reaction for electrolyzing of water [55].

Conventionally, a fuel cell is an electrochemical cell that converts the chemical energy of a fuel (a hydrogen-rich fuel) and an oxidizing agent (often oxygen) into electricity. This process is performed through a pair of redox reactions which are the reverse reactions for electrolyzing of water. In fact, fuel cells have been known since 1839 when

Sir William Grove successfully reversed the action of the electrolysis of water by recombining hydrogen and oxygen to generate water and electrical current. A fuel cell system consists of a negative and a positive electrode that is separated by an electrolyte(Fig5.1). Biofuel cells, specifically, are devices that use living organisms as fuel to produce electricity. We accomplish this by creating a layer of enzymes specifically designed to react with the underlying biofuel and convert it into electrical energy.

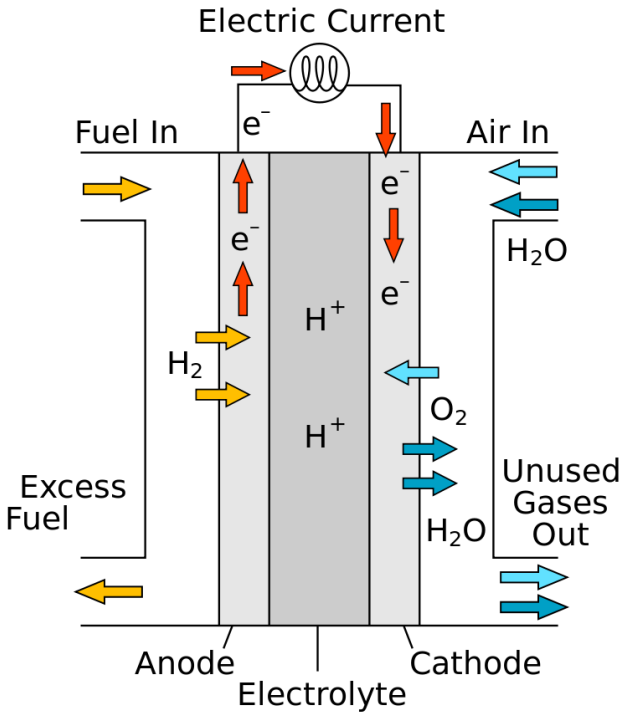

Figure 5.1: Schematic of a fuel cell
A fuel cell is an electrochemical cell that converts the chemical energy of a fuel (a hydrogen-rich fuel) and an oxidizing agent (often oxygen) into electricity.

The electricity production from living creatures, for the first time, was observed in microorganisms by M.C. Potter, a professor of Botany at the University of Durham

[56]. The interest in fuel cells later triggered during the USA space program, in the late 1950s and early 1960s; microbial biofuel cells developed as a possible technology that would generate power from waste disposal in space flights [57]. The enzymatic biofuel cell (EBFC) systems were introduced in the same period with the early goal of a power supply for a permanently implantable artificial heart. The first EBFC employed a bioanode immobilized with glucose oxidase and a platinum (Pt) cathode in 1963 [58]. By 1980s, it was realized that the metallic-catalyst method was not going to be able to deliver the qualities desired in a biofuel cell, and since then researchers focused on working on enzymatic biofuel cells and resolving their issues.

The idea of using BFCs for self-powered biosensors first reported in 2001 by Katz et. al. [59]. Following this idea, many researchers have performed experiments towards implanting BFCs in living creatures such as rats, snails, lobster, insect and so on [57, 60]. This increasing trend for in-vivo studies, though, has been hindered due to low power density, low output voltage level and the lack of ultra-low power electronic circuits for those applications. Nevertheless, recently BFCs have been employed for wearable applications and very promising results have been reported.

Lactate, as an effective electron donor, has been widely used as a biofuel of these newly invented energy sources for many decades [57]. Viability of utilizing sweat lactate as fuel for wearable energy harvesting was first verified by Jia et. Al. in 2013

[61, 62]. In this work, Wang group demonstrated the ability to generate substantial levels of electrical power from human perspiration in a non-invasive and continuous fashion through the use of epidermal biofuel cells based on temporary transfer tattoos (tBFCs) [61].

In 2014, Wang group introduced the textile biofuel cell which utilizes sweat lactate as the fuel to generate electrical energy, producing up to 100 μW/cm2 at 0.34 V during in vitro experimentation, even after repeated bending stress. We have investigated, and implemented an integration of the wearable and flexible biofuel cell with an energy harvesting device for on-demand powering of wearable electronics. To validate energy harvesting, the biofuel cell is integrated into a headband and a wristband, and with the help of an on-board DC/DC converter, extracts energy from perspiring human subjects for direct powering of an LED or a digital watch. Convenient incorporation and removal from a variety of garments are achieved by printing the biofuel cell on a detachable care label. Such textile-based non-invasive biofuel cells can be expected to serve in the future as the power unit for wearable electronics and biomedical devices [63]. Section 5.1 will review some of the details regarding this work.

Flexibility of the lactate biofuel cells is an important feature which needed to be addressed more accurately. The first example of an all-printed, inexpensive, highly stretchable CNT-based electrochemical sensor and biofuel cell array was presented in

[64]. Such combination of intrinsically stretchable printed nanomaterial-based electrodes and strain-enduring design patterns holds considerable promise for creating an attractive class of inexpensive multifunctional, highly stretchable printed devices that satisfy the requirements of diverse healthcare and energy fields wherein resilience toward extreme mechanical deformations is mandatory. In another work, A sheet-type, stretchable biofuel cell was developed by laminating different components by [65]. Highly stretchable textile-based biofuel cells (BFCs), acting as effective self-powered sensors, have been fabricated using screen-printing of customized stress-enduring inks in [66]. These new textile-based stretchable devices thus hold considerable promise for next-generation of smart clothes for monitoring personal health and performance. However, all these designs rely on random composite-based stretchable systems where the underlying electrodes are stretchable, but the overlaying active layers are non-stretchable. The mismatch between the mechanical properties can strain the active layers, leading to gradual delamination and leaching, thus decreasing the performance. Moreover, the low power density of prior-art wearable biofuel cells limits their ability to power useful electronic loads in practice. Bandodkar et. al. has addressed these two issues by introducing a soft, stretchable electronic-skin-based biofuel cell (E-BFC) via a unique combination of lithographically-patterned stretchable electronic framework together with screen-printed, densely-packed three-dimensional carbon-nanotube-based bioanode and

cathode array arranged in a stretchable "island-bridge" configuration [67]. In this work, thanks to the state of art power generated density for the lactate biofuel cells [68], we for the first time were able to power a BLE radio by a wearable biofuel cell; this is an important step towards powering wearables by biofuel cells. We will go through the details of this work in section 5.2.

Our recent research has also demonstrated a practical implementation of sweat lactate biofuel cells for self-powered biosensors in wearable applications [69, 70]. The self-powered biosensor in [69] employs either lactate or glucose biofuel cell to readout and transmit the concentration of the analyte thanks to the ultra-low power and low voltage integrated circuit implementation. Section 5.3 of this dissertation will present some details regarding this work.

In another related work, a self-powered biosensing system with the capability of proximity inductive-coupling communication for supply sensing and temperature monitoring was presented [71]. Also, recently, a battery-less system has been introduced which is capable of simultaneously monitoring sweat rate/loss, pH, lactate, glucose, and chloride. The electronic system on the device is powered by the BFC and the NFC device can readout the measurement results [72].

Researchers have also utilized BFCs for other applications. For example, they have been employed for power supply monitoring in Internet of Things (IOT) applica-

tions [73]. They have also used a self-powered system for building sports big data [74]. In 2018, a hybrid system including biofuel cells and super capacitors (SC) has been implemented to harvest and store the BFC energy in SC [75]. This can be considered as another step towards the smart textiles and developing textile wearable devices.

Finally, while we currently have fairly well-designed biofuel cell systems, the BFC powered wearables require extensive exploration for effective voltage/power management and interfacing to microelectronics to implement new generation of self-powered wearables. This chapter presents three examples of energy harvesting designs towards this goal.

5.1 Wearable textile biofuel cells for powering electronics

In this section, we describe the development and performance of a textile BFC, integrated with a printed-circuit board (PCB)-based wearable energy storage device, to power electronic devices. Thick-film printing technology, offering large-scale low-cost mass production of high-fidelity electrodes, is employed to fabricate the textile BFCs. The versatility of screen-printing offers facile and modular integration of the BFCs in various series/parallel combinations to tailor output voltages and currents to the desired

values. The new textile BFCs have been screen-printed on a detachable care label and hence can be readily incorporated into various garments. The resulting flexible textile-based BFCs consume sweat lactate and dissolved oxygen to produce electrical energy. Upon integrating with an energy-processing PCB, the textile BFC was able to power LED or a wrist watch under in vitro conditions. Real-time on-body powering of these electronic loads have also been demonstrated when using the textile BFCs in a parallel conguration. The attractive performance and real-life application of the textile BFC thus clearly demonstrate its promise as a viable wearable power source. Such characteristics and applications are reported in the following sections.

Due to their ubiquitous daily use, textiles have been recently utilized for supporting various devices, such as batteries and sensors. However, textile-based BFCs integrated within garments to harvest energy directly from an individual to power wearable electronics have not yet been demonstrated. Absorption of the fuel by the underlying textile substrate can greatly hamper the performance of the printed BFC. Hence, a non- absorbing textile is desired. A hydrophobic coating of Scotchguard® was thus adopted to prevent adsorption of the solution and to ensure proper functioning of the textile BFCs. Several types of textiles were examined to identify the most suitable substrate, including cotton (T-shirt), polyester/cotton (sock), polytetra?uoroethylene (Gore-Tex®), and polyester (care label). Initial characterization of BFC electrodes printed on

these substrates revealed that the care label offers the best print quality as well as BFC operation due to its smooth and densely woven texture. Additionally, care labels are widely used in clothing apparels and hence care label-based BFC can be easily incorporated into (and removed from) different types of garments using detachable fastener tape. Accordingly, care labels were employed throughout this work as the substrate for the fabrication of textile BFCs. Fig5.2A shows an array of textile BFCs, attached to a headband, using Velcro® sticky-back hook and loop fastener tape.

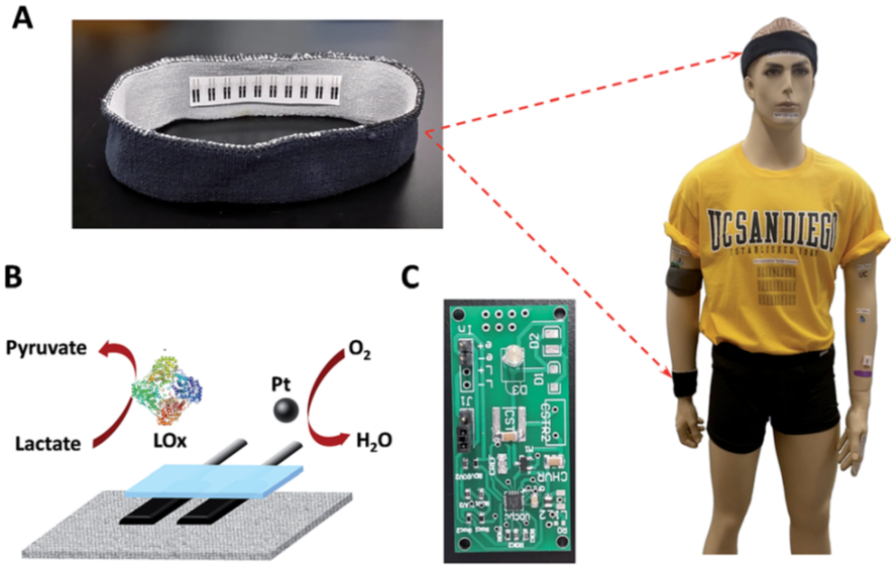

Figure 5.2: Wearable textile BFCs. (A) Textile BFCs integrated in various garments such as headbands or wristbands. (B) A scheme of a textile BFC. (C) A customized printed circuit board prototype for the conversion, conditioning and temporary storage of extracted energy

A continuous and high concentration of fuel supply is desirable for using BFCs to generate energy sufficient for pow- ering electronics. Fortunately, human perspiration contains high levels of lactate fuel. Therefore, the textile BFC was prepared using LOx as the biocatalyst at the bioanode for sweat lactate oxidation and platinum black at the

cathode for oxygen reduction, as shown in Fig5.2B.

From a system perspective, extraction of the maximum possible energy requires co-design between the BFC electrodes and the energy harvesting microelectronics. Specifically, the power generated by the BFC must be conditioned in some manner to match the voltage and current requirements of an electronic load. Unfortunately, only a few emerging implantable BFC studies have discussed this co-design in detail. Since the output voltage and current of a single BFC are rarely perfectly matched to the voltage and current required by electronic loads, energy conditioning thus becomes mandatory and this is typically performed by: (1) arranging individual BFC in series or parallel configurations to stack output voltage (series) or increase the current capability (parallel); and/or (2) employing a DC/DC converter that transforms the voltage and current from the BFC to a different output voltage and current more suited for the electronic load. Since the loaded BFC output voltages are typically lower than required for most electronic devices (which often require voltages greater than 1 V), series stacking of individual BFC elements can be used to increase the effective output voltage. However, as in photovoltaic applica- tions, the overall energy harvesting performance of the series stack is limited by the instantaneous current generation of the weakest BFC in the stack. Thus, while a promising, low-complexity technique for voltage matching between the BFC and the load, series stacking does not offer a means to regulate this voltage, and

is difficult to employ in vivo; as a result, series stacking has primarily been used for in vitro experimentation, or between independent living creatures. Instead, employing a DC/DC converter that boosts the BFC output voltage to a higher level is the generally preferred solution.

As illustrated in Fig5.2C, and Fig5.3, a PCB, featuring a DC/DC boost converter, has been designed in this work, which includes a maximum power point tracking (MPPT) circuit that can dynamically change the input impedance matching conditions to extract the maximum possible energy from the BFC. We employ a BQ25504 boost converter integrated circuit (Texas Instrumental, Dallas, TX) to step-up the voltage to a higher level by charging an energy-buffering capacitor. A schematic of the resulting printed circuit board (PCB), fabricated as a 2-layer board on 1.6 mm FR-4 (Advanced Circuits, Aurora, CO), is shown in Fig5.3. When the energy buffering capacitor reaches a voltage of 3.2 V, the output switch is enabled and power is delivered to the load. Since the instantaneous load power is typically greater than the power coming from the BFC, the capacitor voltage drops during load operation. When the voltage drops to 2.4 V, the output switch is disabled and the load is shut-off. At this point, the capacitor voltage begins to slowly replenish based on incoming energy harvested by the BFC.

To increase the absolute amount of power available under in vivo conditions, four

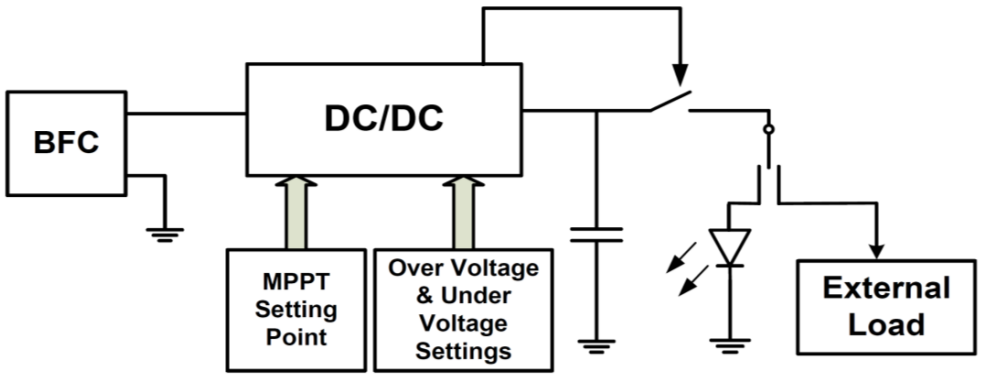

Figure 5.3: Simplified diagram of the energy harvesting PCB board

BFCs were electrically connected in parallel. The board requires an initial power of 10 μW to charge the capacitor, and measures less than 2$\times$5cm2 , which is small enough to be implemented in the headband or wristband. Excluding the test points and different load options on the PCB board can enable a much smaller overall size of 2$\times$2.5cm2.

As mentioned earlier, an energy harvesting demonstration board was designed to prove the performance of the wearable lactate biofuel cell. This design employs BQ25504 boost converter integrated circuit (Texas Instrumental, Dallas, TX) in order to step up the voltage level, and store the energy in a charging capacitor. This capacitor is periodically charged until it contains sufficient energy to power the load for a short period of time by connecting to the load through a switch. Due to the initial power consumption of the chip (10μW @ 300mV), we employed few biofuel cells in parallel combinations. Note that there are some challenging issues in this design. First of all, the TI chip was not designed for electrochemical applications. The maximum power

point tracker employed in this chip is based on the open circuit voltage of the energy source (which is measured every 16s). However, it is not appropriate to measure the open circuit voltage, right after loading the biofuel cell. Therefore, in our application, the operating input voltage gradually was dropping, and after a few minutes the energy harvester did not work properly. In order to mitigate the problem, we added a control switch to disconnect the input while the load is on. This approach lets the biofuel cells relax and avoid the voltage and power degradation of the energy source.

In order to increase the total power produced by the textile BFC to levels sufficient for operating typical electronics, multiple BFCs were connected in a parallel configuration. For example, two BFCs were able to generate 6 mW at 0.376 V, as opposed to 3 mW at 0.358 V for a single BFC. Since 0.376 V is insufficient to directly power most electronic devices, we employed a BQ25504 boost converter integrated circuit to stepup the voltage to upwards of 3.2 V. Specifically, the boost converter is used in an energy-buffering topology [54], where an energy-storing capacitor is periodically charged until it stores sufficient energy to briefly power a load that has a higher instantaneous power requirement than is available directly from the BFC. To verify system functionality, a blue LED requiring 2.5 V and 0.5 mA, was periodically illuminated by the converter output after sufficient energy was buffered. During in vitro experiments the blue LED flashes upwards of 5 times when powered from two parallel textile BFCs

operating with a 14 mM lactate fuel solution (Fig5.4A). To further study the long term operation of the textile BFC, two BFCs were connected in series and five such pairs were connected in parallel to power the LED. When exposed to a 14 mM lactate solution, the LED flashed 9 times initially when the energy buffering capacitor reached a voltage of 3.2 V. Subsequently, the LED turned off for 1.5 min, restricted by the large instantaneous load power requirements, limited converter efficiency at low input voltage, and slow diffusion of the fuel towards the electrode surface. When the capacitor voltage dropped to 2.4 V, the output switch was disabled, and the load was shut-off. At this point, the capacitor voltage began to slowly replenish based on incoming energy harvested by the BFCs, and then the LED flashed again. This ON–OFF cycle lasted for 46 min. At the end, the LED was turned off, most likely due to depletion of the lactate fuel. When replaced with new lactate solution, the LED began flashing again.

To demonstrate system functionality under a realistic environment, a consented subject was asked to perform a stationary bike exercise while wearing a headband integrated with four BFCs connected in parallel. As shown in Fig5.4B, the integrated device was able to ash the LED seven times shortly after the subject started perspiring. This result demonstrated the ability of the integrated device to scavenge energy directly from the wearer and convert the biochemical energy to electricity. The enhanced power generation of the textile BFC enables it to power wearable electronic devices. To further

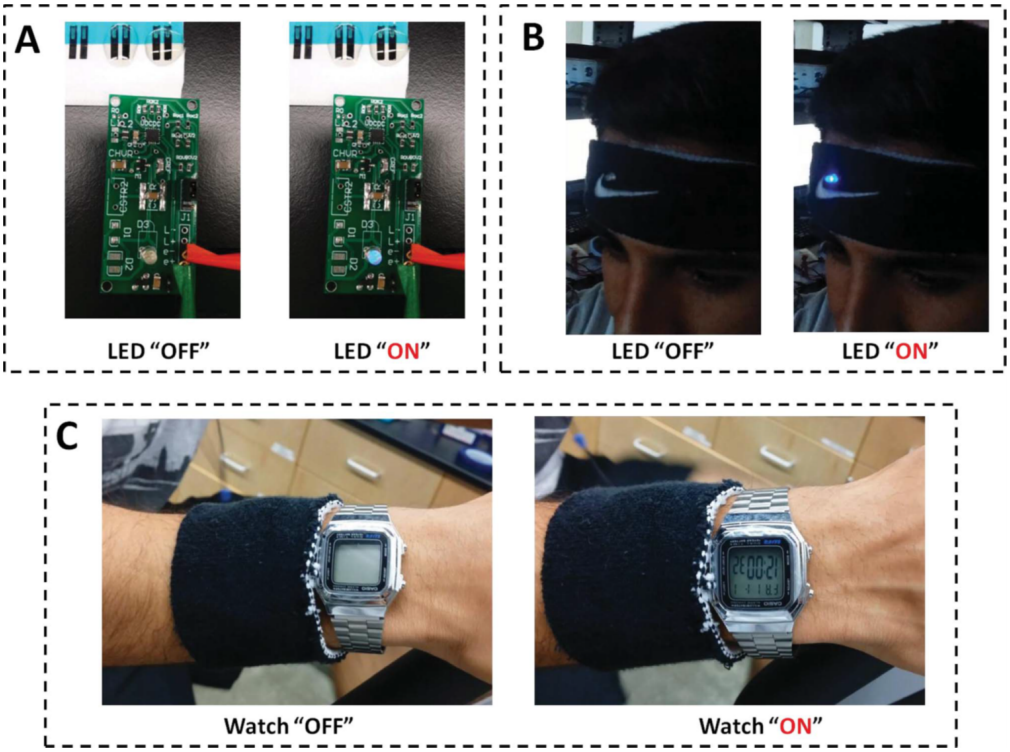

Figure 5.4: (A) Photographs demonstrating operation of an LED powered by two textile BFCs connected in parallel (B) Photographs of LED operation powered by four parallel BFCs, before and after a stationary bicycle exercise; (C) Photographs of a watch powered by four parallel BFCs before and after exercise.

demonstrate this on-body capability, the textile BFCs were incorporated into a wristband garment and used to power a digital watch. The watch, which requires a minimum of 10 mW from a 3 V supply, was powered from four parallel-configured textile BFCs connected with the PCB. During both the experiments the PCB was housed between the two layers of the underlying garment. Fig5.4C displays the watch – mounted with wristband – before and after it was turned ON by the energy harvested from the wearer's sweat by the textile BFCs. The watch remained ON for up to 50 seconds. Limited converter efficiency at low input voltage and slow diffusion of the fuel towards the electrodes may

be the limiting factors for the intermittent operation of the devices.

The present work describes textile BFC harvesting energy directly from human sweat by using lactate as the fuel. In most of the reported BFCs, a constant flow of the fuel supply (commonly glucose) of fixed and higher concentration is provided, leading to continuous high power densities. However, in our case, the fuel (lactate) concentration in sweat changes dynamically. A major factor affecting the lactate concentration is the dilution effect occurring due to increasing sweat rate with time. The sweat rate also affects the convection of both lactate and oxygen to the respective electrode surface, and thus the overall power output. Despite of these unfavorable physiological conditions, the new textile BFC was shown useful in powering commonly used devices. The energy-buffering architecture, coupled with MPPT algorithm enabled sufficient collection of energy during concentration peaks to sustain operation for a longer time than normally possible. Future work will focus on the improvement of the working time of the system. Further improvement of the textile BFC can be achieved by using the biscrolled carbon nanotube yarns as shown very recently upon the completion of present work. Optimizing the relative areas of the two electrodes for maximizing power output, and building a lower power boost converter further optimized to operate under varying input power conditions.

In conclusion, we have described a wearable textile BFC based on direct screen

printing of BFC electrodes onto fabrics, and realized its integration with a PCB to power electronic devices. The textile BFC, which relies on the oxidation of sweat lactate at the bioanode and oxygen reduction at the cathode, can harvest energy directly from the wearer's to generate electricity. The generated power of the parallel BFCs, in connection to the PCB, was able to light a blue LED when integrated in a headband, and to power a watch integrated in a wristband. The favorable behavior of such fabric-based flexible BFC and the new integrated customized electronic device holds considerable promise as a power source for wearable electronics.

5.2 Soft, stretchable, high power density electronic skin-based biofuel cells for scavenging energy from human sweat

This section describes the characterization, and real-life application of a soft, stretchable electronic-skin-based biofuel cell (E-BFC) that exhibits an open circuit voltage of 0.5 V and a power density of nearly 1.2 mW/cm^2 at 0.2 V, representing the highest power density recorded by a wearable biofuel cell to date. High power density is achieved via a unique combination of lithographically- patterned stretchable electronic framework together with screen- printed, densely-packed three-dimensional carbon-

nanotube-based bioanode and cathode array arranged in a stretchable "island-bridge" configuration, which was desined in Wang's group. The E-BFC maintains its performance even under repeated strains of 50%, and is stable for two days. When applied directly to the skin of human subjects, the E-BFC generates $\sim$1mW during exercise. The E-BFC is able to power conventional electronic devices, such as a light emitting diode and a Bluetooth Low Energy (BLE) radio. This is the first example of powering a BLE radio by a wearable biofuel cell. Successful generation of high power density under practical conditions and powering of conventional energy- intense electronic devices represents a major step forward in the field of soft, stretchable, wearable energy harvesting devices.

A custom-made DC-DC converter designed to show the ability of the E-BFC to power a LED and similar electronics. As demonstrated in Fig5.5B,C, the LED continues to light even when the E-BFC is stretched repeatedly by 50%. In addition, a separate study was also conducted to measure the effect of strain (e = 50%) on the short-circuit current and open circuit voltage of the E-BFC (Fig5.5). The data plotted in Fig5.5, clearly demonstrate the negligible impact of such repeated strains on the E-BFC performance.

The ability of the E-BFC to power a BLE device under in-vitro conditions was demonstrated. Circuit diagrams for the DC-DC converter and the BLE device is shown

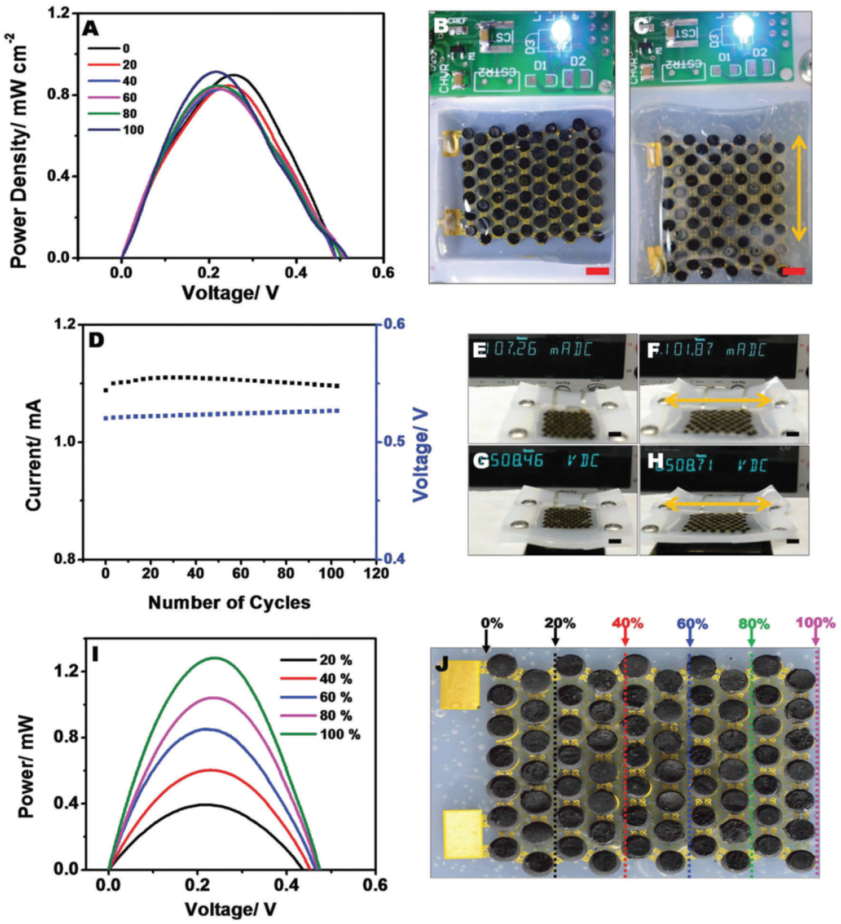

Figure 5.5: Functionality, mechanical resiliency and fuel coverage effect on the E-BFC. (A) Power density versus voltage curves for repeated stretching iterations. Powering LED with a strain of (B) e = 0% and (C) e = 50%. (D) Effect of repeated strains. (E-H) Effect of strain on the short circuit current and open-circuit voltage. (I) The areal coverage effect (J) The extent of spatial coverage by fuel during study conducted in (I).

in Fig5.6.

To demonstrate that the proposed BFC can power a practical wearable device, a custom circuit board featuring a Texas Instruments CC2451 Bluetooth Low Energy (BLE) radio and microcontroller System-on-Chip (SoC) was developed. Since the voltage of the BFC was lower than what was required to power the BLE SoC, the circuit board also featured a Texas Instruments BQ25504 boost converter to step-up the BFC

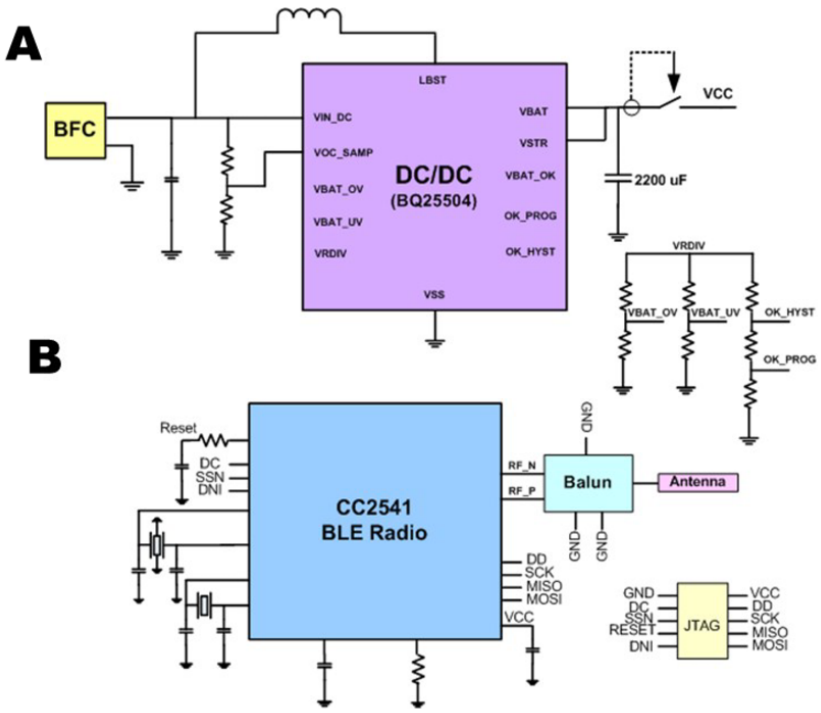

Figure 5.6: Circuit diagrams for the (A) DC-DC converter and the (B) BLE device.

voltage to a higher value. Due to the high peak-toaverage power draw of the BLE SoC (in operation, peak power exceeded 10 mW), the output of the boost converter was decoupled by a 2.2 mF energy-buffering capacitor, selected as a trade-off between size, buffering capacity, and standby current leakage. During system start-up, the BLE radio was disconnected until the capacitor voltage exceeded 3.5 V. When first connected, the radio underwent an initialization routine, and was then programmed to transmit a beacon once per 5 second at an average power consumption of 0.4 mW. Transmitted data was received and demodulated by a computer equipped with a Texas Instruments BLE to serial dongle, and displayed via a custom MATLAB script.

As shown in Fig5.7, the BFC was able to charge the 2.2 mF capacitor to 3.5 V in ∼53 s, indicating an average generated power of approximately 0.5 mW during this experiment. Due to the large current draw of the BLE System-on-Chip (SoC) during its initialization routine, the capacitor output voltage temporarily dropped until the initialization routine completed. After initialization, the BFC was demonstrated to deliver sufficient power to power the BLE SoC at a stabilized voltage of 3.5 V for ∼10 min. The drop in the voltage can be attributed to consumption of the fuel. Without the E-BFC input power, the 2.2 mF decoupling capacitor would only be able to power the load for less than 45 s before its voltage dropped to below 2 V, thereby indicating that the E-BFC is sustaining the load throughout the experiment. This represents the first example of a wearable BFC capable of powering a BLE device.

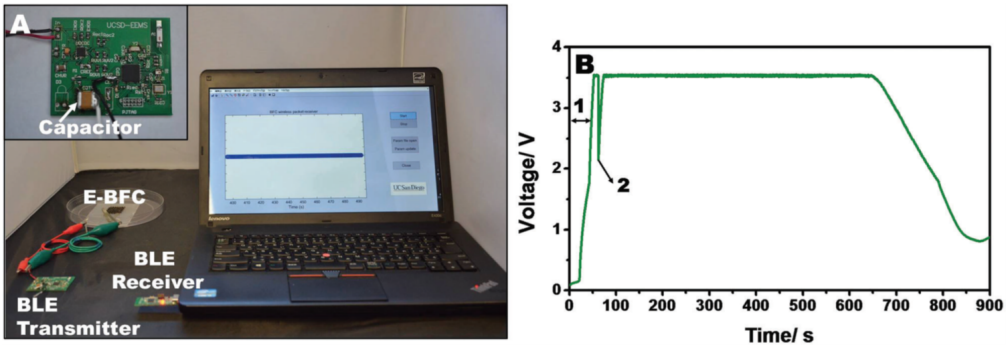

Figure 5.7: Powering of a BLE device by E-BFC. (A) Photograph illustrating data transmission from an E-BFC powered BLE to a laptop. (B) Plot showing voltage variations of the energy-buffering capacitor during the experiment. (1) Charging of the capacitor; (2) connecting the BLE microcontroller

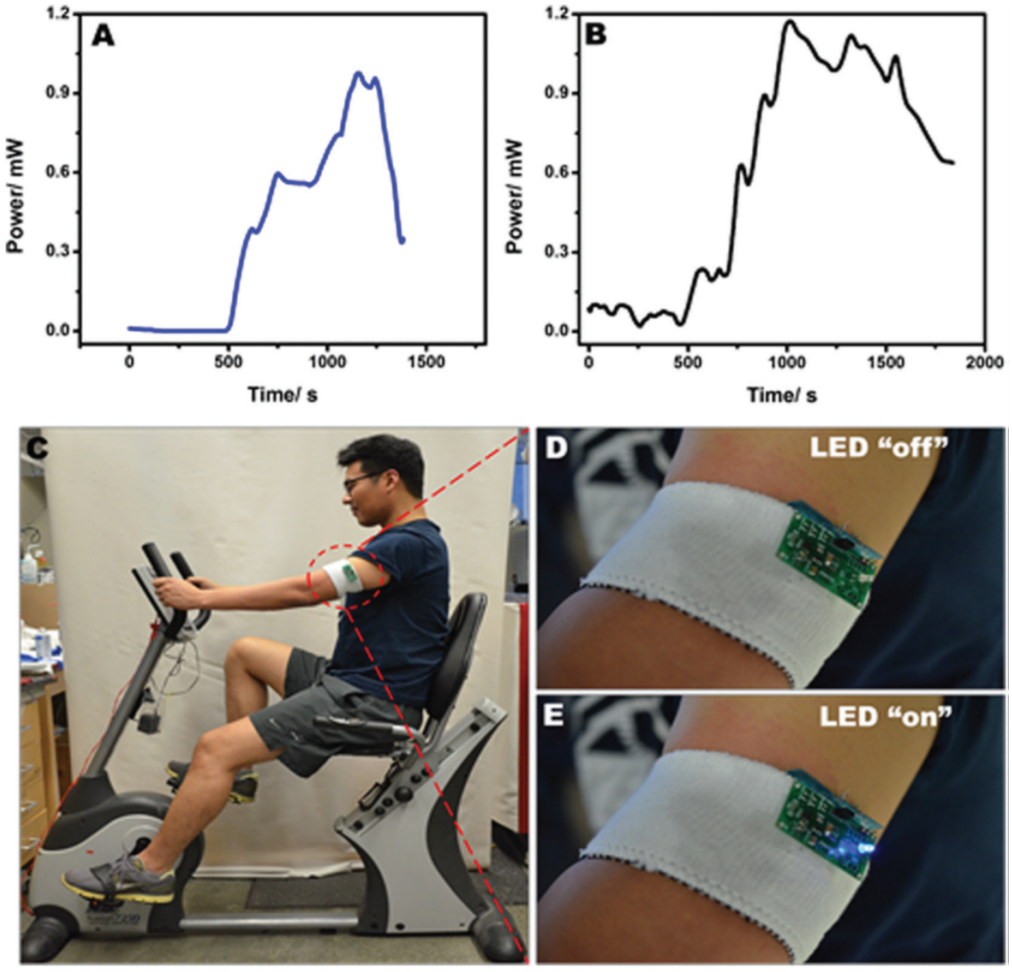

Figure 5.8: Real-time scavenging of energy for two different human subjects(A and B). (C) Image of a perspiring subject adorning the E-BFC, interfaced with the energy harvesting circuit. An image of the LED in (D) 'off' state in absence of sweat and (E) 'on' state in presence of lactate in sweat

The ability of the E-BFC to power common electronics was also demonstrated. Almost all commercially available electronic devices require an operating voltage that is much higher than the voltage at which BFCs produce the highest power. Thus, in order to exploit BFCs to power commercially available electronics, the custom DC-DC converter circuit board was coupled to the E-BFC. This setup was mounted on a

human subject and the sweat generated by the subject was harvested to power a blue LED (Fig5.8C–E). Initially, the LED remained off but started blinking within two mins after the subject started sweating. The LED continued to blink for $\sim$4 min and then the frequency of blinking gradually decreased. This could be due to the consumption of lactate present in the sweat by the E-BFC and decrease in lactate concentration with increased sweat rate. The performance of the E-BFC was several orders better than that of previously reported wearable BFC, which could power a LED for only a few seconds.45 When the LED stopped blinking, the E-BFC was disconnected while the subject continued cycling, leading to the generation of fresh lactate. After a couple of minutes, the E-BFC was reconnected and the LED started blinking again. Such a demonstration reveals the ability of the E-BFC as a potential power source for wearable applications.

5.3 A 0.3-V CMOS Biofuel-Cell-Powered Wireless Glucose/Lactate Biosensing System

This section presents a self-powered wireless physiochemical sensing system for monitoring of glucose or lactate in bodily fluids. The biosensor chip consists of a duty-cycled biofuel cell (BFC) maximum power point tracker analog front end, a passive

$\Delta\Sigma$ analog-to-digital converter (ADC), an RF power oscillator transmitter using a 1-cm external loop antenna, digital data storage, and timing and clock generation circuitries, all designed to operate from the dynamic 0.3V BFC output voltage. The biosensor chip, implemented in 65-nm CMOS and exclusively powered via an enzymatic BFC, can successfully detect changes in glucose/lactate concentration between 2.5 and 15 mM, for the first demonstration of an integrated self-powered chemical biosensing system with digital wireless readout. The biosensor consumes an average power of 1.15 μW.

Enzymatic BFCs are an evolving technology that can produce electrical power from renewable biocatalytic enzymes and metabolytes (e.g., glucose and lactate) operating as fuels. The electrons harvested from such metabolytes can then be delivered into an electronic circuit as a source of power. In 2001, Katz et al. [59] pioneered a BFC as a self-powered biosensor converting a fuel to power that was related to the analyte fuel concentration.

A BFC can be modeled as a voltage source, VBFC, with a series source resistance, RBFC, creating an input voltage to the energy harvester, VIN, as illustrated in Fig5.9(a). According to this model and experimental results [66, 76], the polarization curves of a typical BFC look like Fig5.9(b).

When attempting to power a high-current load, the BFC is overloaded and drops

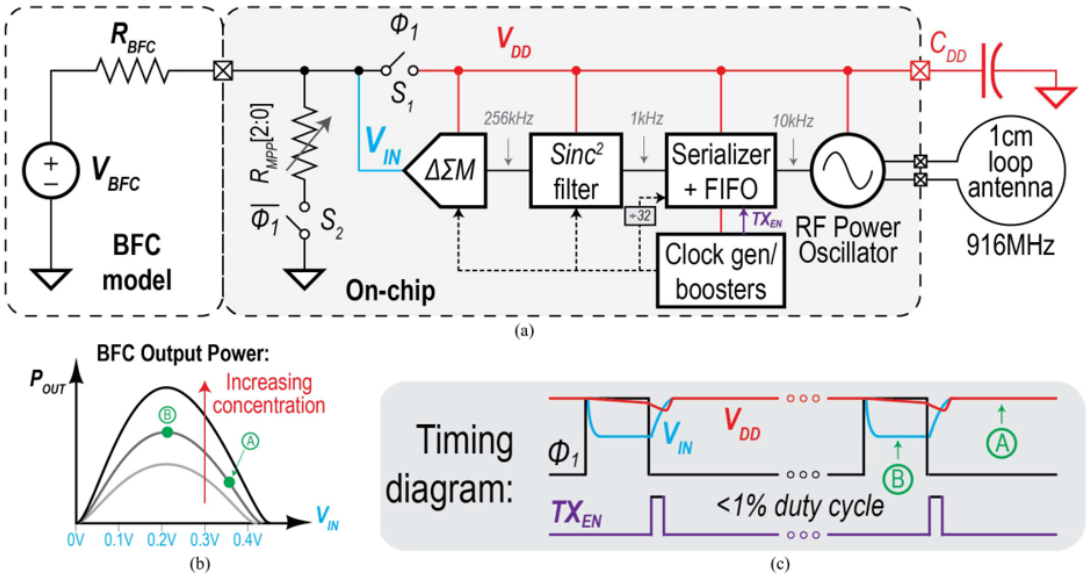

Figure 5.9: (a) System architecture of a dc–dc-converter-free BFC-powered wireless glucose/lactate biosensor system. (b) Representative BFC polarization curves. (c) System functional timing diagram.

most of the current across RBFC and thus, VIN is low; when attempting to power a low-current load, very little voltage is dropped across RBFC, and thus, VIN≅ VBFC, or the BFC's open-circuit voltage [point A in Fig5.9(b)]. In between these two extremes is the Maximum Power Point (MPP), where, when the BFC is presented with a matched load, its output power is maximized [point B in Fig5.9(b)]. As the fuel concentration increases, the output power at the MPP increases linearly. Outside of the MPP, the concentration to output power relationship is not necessarily linear. Thus, a self-powered biosensor should, during readout, operate at the MPP.

There are multiple ways to perform maximum power point tracking (MPPT), including presenting the BFC with a resistance matched to RBFC, or by building a

dc–dc boost converter that achieves this effective impedance through input regulation, all while boosting VIN to a more CMOS-compatible voltage [77, 78]. The latter is generally the preferred strategy, as then the system can utilize the maximum amount of energy available from the harvesting source for other purposes (e.g., powering a radio transmitter). However, BFCs do not operate perfectly analogous to conventional energy harvesters such as photovoltaics (PVs) or thermoelectric generators (TEGs). With PVs and TEGs, it makes sense to always operate at the MPP if possible: the rate of energy extraction does not affect the ability to extract more energy. BFCs, on the other hand, can be thought of as kind of a hybrid battery/energy harvesters, there is an MPP, but continuously harvesting at the MPP will deplete the underlying fuel at the maximum possible rate. If there is a continuous replacement of this fuel, for example, during the periods of high sweating, then this may not be a problem. However, it is difficult to guarantee that fuel replacement will occur at the same rate as energy extraction, and thus, operational longevity is not guaranteed. Thus, with BFCs, it is generally best to not always operate at the MPP, but rather, only operate at the minimum rate of energy extraction needed to continuously sustain the system.

The analysis above suggests that a self-powered BFC based biosensing detection should only operate at the MPP at a low duty ratio, with the majority of the time spent operating in a lower-power mode [point A in Fig5.9(b)]. Since the open-circuit voltage

of BFCs is on the order of 0.3–0.5 V, here, we propose to forgo a dc–dc boost converter (and its bulky inductor), and instead directly power the system from VIN. Since a dc–dc converter is no longer used, a matched resistor is periodically deployed for MPPT purposes.

The overall system architecture is shown in Fig5.9(a). At steady state, the BFC passes current through switch S1 during phase Ø1 to establish VDD, which is near the opencircuit voltage of the BFC, as the circuit is in a low-power sleep state for the majority of phase Ø1. Since continuously presenting a matched load at the MPP depletes fuel at the maximum possible rate, limiting longevity, the system instead only presents a matched load, RMPP, at a 1% duty ratio via periodic activation of switch S2 during phase Ø1. A timing diagram is shown in Fig5.9(c). During phase Ø1, the system is sustained by a 1 μF 1 $\times$ 0.5 mm2 ceramic decoupling capacitor, CDD. The matched resistor, RMPP, is implemented on-chip as a 3-bit binary weighted resistance, with resistance ranging from 30 to 200Ω, a suitable range for the BFCs tested in this paper. During phase Ø1, a passive $\Delta\Sigma$ samples and digitizes VIN, which drops according to the MPP and applied resistance. Digitized data are then serialized, buffered, and delivered to an integrated wireless transmitter.

The rest of this section describes circuit design challenges and solutions toward operating precision mixed-signal circuits, and the experimental results.

Since the energy available from the glucose/lactate BFC harvester is limited and its open-circuit voltage is very low (0.3–0.5 V), the target analog-to-digital converter (ADC) must operate under as low as 0.3 V and consume ultra-low power. Among various ADC architectures, the successive approximation register (SAR) ADC has been demonstrated to be highly efficient and its VDD can readily be scaled down to very low voltages as it mostly consists of digital circuits. Compared to oversampled $\Delta\Sigma$ ADCs, the SAR ADCs are opamp-free architecture, and thus, do not require high-gain and high bandwidth opamps, which consume significant static power. However, the achievable effective number of bit (ENOB) in SAR ADCs is low (8–9 bits) [79–81].

To increase ENOB beyond 10 bits, digital-to-analog converter (DAC) calibration technique [82], noise-shaping architectures [83], or datadriven noise-reduction methods [84] are required to overcome DAC capacitive array mismatch and comparator noise, which demand exponentially growing capacitive DAC size, circuit overhead, and large power. Thus, SAR ADCs are not necessarily the best choice for this application. In turn, $\Delta\Sigma$ ADCs exploit oversampling and noise-shaping advantages to reduce noise. However, $\Delta\Sigma$ ADCs largely depend on power-expensive op-amps, and thus, traditional $\Delta\Sigma$ Modulator ($\Delta\Sigma$M) circuits are not practical at 0.3 V. Inverter-based $\Delta\Sigma$Ms [85] and bulk-driven techniques [86] are among possible ultra-low-voltage $\Delta\Sigma$M designs previously reported. In all cases, the power consumption constraint limits their use in

self-powered applications. Since designing amplifiers to attain low noise and large gain at low supply voltages is difficult without consuming microwatts of power, an energy-efficient passive discrete time (DT) $\Delta\Sigma$M is employed here. Unlike the active integrator shown in Fig5.10(a), the passive integrator, depicted in Fig5.10(b), draws no direct current from VDD, therefore reducing the $\Delta\Sigma$M power. Also, VDD can readily be scaled down to 0.3 V, assuming the gate of switching transistors is adequately driven Utilizing a charge pump to increase system VDD to more robustly operate an op-amp would require even more power than the low-voltage designs in [85], and would also introduce additional inefficiencies in the charge pump itself, which is generally limited to $\sim 85\%$ efficiency using on-chip capacitors [87].

The passive integrator [88] has several advantages over its active counterpart: it is 1/ f -noise free, critical for low signal bandwidths, and more linear. The operational transconductance amplifier (OTA) of the active integrator operating from a 0.3-V VDD suffers from low-voltage headroom, and thus, suffers from nonlinearity. However, the passive integrator approach does have several shortcomings: with the same oversampling ratio (OSR), a passive modulator requires larger capacitors to maintain the same thermal noise level and lowpass filtering corner frequency as an active integrator. Also, passive integrators suffer from lack of dc gain —they are known as leaky

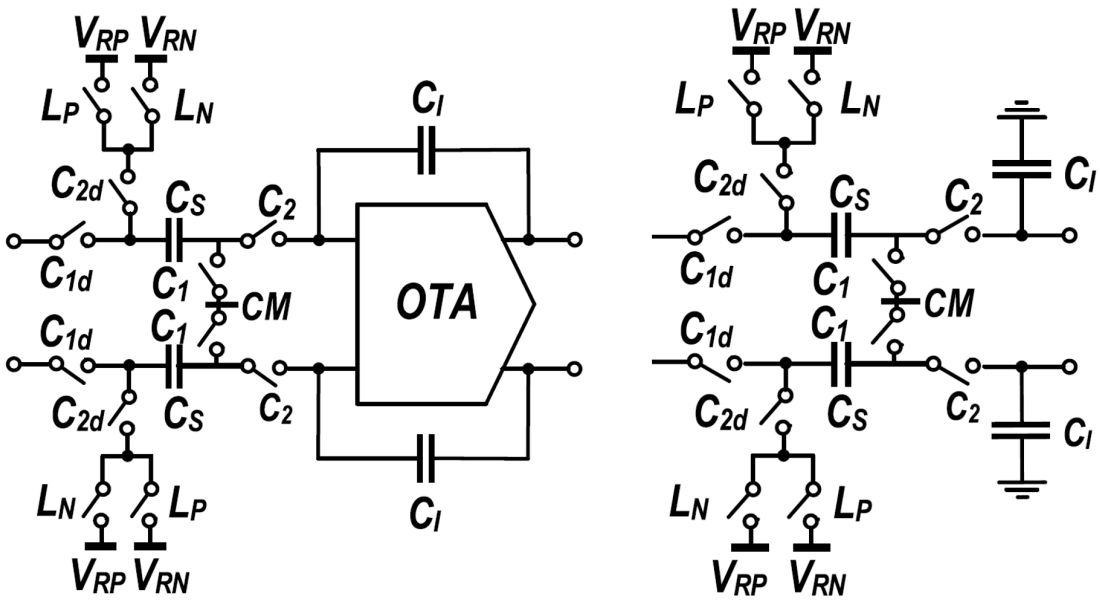

Figure 5.10: (a) Traditional active integrator using power-consuming OTA. (b) Power-efficient passive integrator

integrators—which makes the modulator more prone to coupling noise, and thus, its signal-to-noise ratio (SNR) is typically lower than the standard active $\Delta\Sigma$M. Here, we knowingly trade low SNR for lower power consumption at low voltage in this application.

Fig5.11 shows the $\Delta\Sigma$M circuit implementation, which utilizes a basic passive integrator in the 1st stage and a gain-boosting passive integrator in the 2nd stage [88,89], as an alternative to power hungry active integrators. The gain boosting scheme can potentially be used at the 1st stage to achieve a higher SNR, but due to nonlinear OFF currents of parallel sampling switches, the modulator signal to noise and distortion ratio (SNDR) degrades significantly.

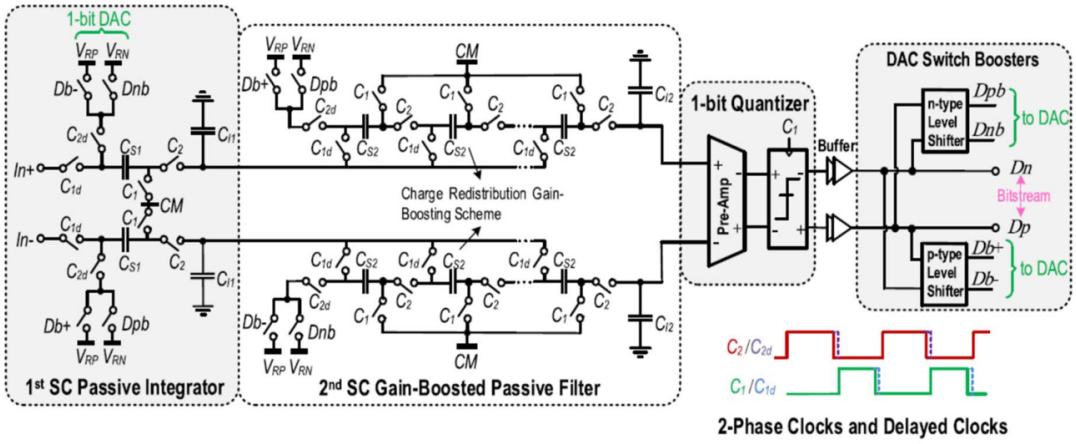

Figure 5.11: Complete circuit schematic of the 2nd-order passive 1-bit DT $\Delta\Sigma$ modulator

Due to the internal signal attenuation at the 1st stage output, the 2nd stage has relaxed linearity requirement, and therefore utilizes a gain-boosting integrator to reduce in-band noise with minimal power penalty. Specifically, a charge redistribution scheme was employed, where the 1st integrator's output is sampled onto capacitors CS2 in phase C1 (all in parallel), and then, the precharged CS2s are positioned in series to charge share with the integrating capacitor CI2 in phase C2.

Taking advantage of low bandwidth voltage/current content of glucose/lactate BFCs, $\Delta\Sigma$M can use a relatively large OSR, which reduces in-band kT/C noise of the switching transistors, thereby decreasing capacitor size and the chip area. The sampling and integrating capacitor sizes are 1 and 32 pF, respectively. The latter is determined from the filter 3dB bandwidth, while the former is determined from the kT/C noise

requirement. At 0.3-V supply, it is very challenging to realize a good sampling switch due to significant degradation of the ratio of ON conductance and OFF current even when using low- Vth transistors. The sampling switch needs a sufficiently high ON conductance to minimize nonlinear distortions, and the leakage current (OFF current) should be very low such that it does not result in signal-dependent ADC errors.

To increase the ratio of ON conductance and OFF current, numerous circuit techniques were employed in the sampling switch. The gate of NMOS transistors is driven by a $3\times$voltage boosting circuit that improves ION/IOFF by 92%, and the gate of PMOS transistors is activated by a negative clock level shifter; this brings the PMOS gate voltage down to a $-200mV$, resulting in an 8 dB SNDR improvement. Meanwhile, cascaded transmission gates help reduce OFF current, and the employed OFF-current-limiting feedback amplifier including a PMOS source follower and a leakage current-biased NMOS further decreases the switch nonlinear leakage current, simply by pushing the internal nodes to the same voltage as the sampling capacitors, and thus reducing Vds and Ids , respectively. All other switches in $\Delta\Sigma$M shown in Fig5.11 are designed using NMOS or PMOS transistors and are activated by a $3\times$clock booster (for NMOS), or a $200mV$ charge pump (for PMOS).

The 1-bit quantizer is realized via a dynamic comparator followed by an SR latch. To mitigate comparator non-idealities (e.g., kick-back noise and offset) and relax

comparator sensitivity, a preamplifier circuit is employed. For robust operation at 0.3 V in the subthreshold regime, low-threshold transistors are used and only two transistors are stacked to mitigate the low-voltage headroom. To boost the gain up to 25 dB without consuming significant power, a cross-coupled load was employed, while diode-connected PMOSs maintain the output common-mode voltage at the supply mid-level.

The single-bit DAC is realized by using basic NMOS or PMOS switches connected to reference voltages VRP and VRN (Fig5.11). At 0.3-V supply, even when using low-Vth transistors, it is not possible to turn on the DAC switches sufficiently. The output digital bits [Dn and Dp] of the single-bit quantizer are thus buffered and level shifted by the n-type and p-type voltage level shifters to drive the gate of switches. The gate of NMOS switch is activated by a $2\times$ clock booster, and the gate of PMOS switch is driven by a $200mV$ charge pump circuit.

As shown in Fig5.9(a), the ADC samples the BFC data in phase Ø1. However, during phase Ø1, the $\Delta\Sigma$M's clocks are gated, and large, low-dropout NMOS switch placed between input transistors and ground of the preamp and comparator circuits separate them from VDD to save system power. The clock signals for $\Delta\Sigma$M (256 kHz), $Sinc^2$ decimating filter (1 kHz), Serializer (10 kHz), and the TX (1.024 MHz) are all generated from a 1.024 MHz master clock, generated either from an integrated ring oscillator or from an off-chip source.

The 1.024 MHz clock is divided by 4 digitally to create a 256 kHz signal for ΔΣM, and it is used as a reference to generate two non-overlapping clocks (C1 and C2) and delays (C1d and C2d) to eliminate charge injection between sampling and integrating phases of the ΔΣM. The modulator VRP/VRN is near-VDD and ground, respectively, implemented by using an ultra-low voltage biasing circuitry operating in subthreshold regime.

The presented self-powered wireless biosensing chip implemented in a 65-nm LP CMOS technology, and measured using Glucose and Lactate biofuel cells.

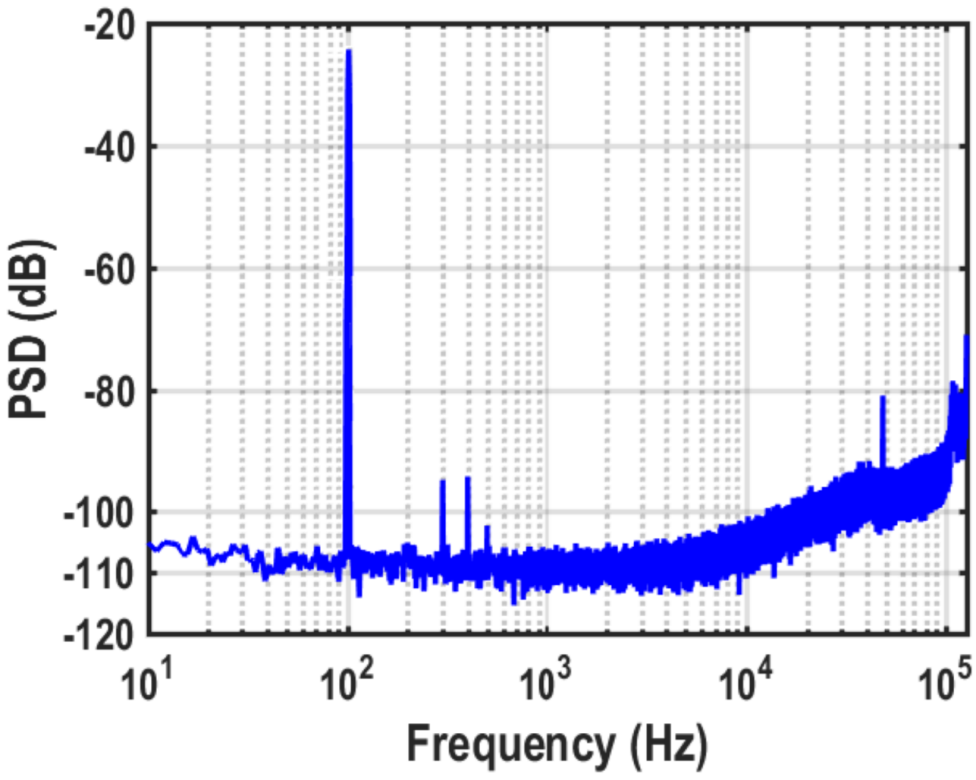

Figure 5.12: Measured power spectral density for a 100-Hz sinusoidal input

The output spectrum of the $\Delta\Sigma$M, sampled at a 256 kHz clock frequency during active mode, is shown in Fig5.12, indicating 64 dB SNR, 60 dB SNDR, and 65 dB dynamic range (DR), respectively, for a 3 kHz signal bandwidth. The ADC including digital decimation filter consumes 180 nW power at 0.3 V. The estimated DR is 65 dB from a 300-mV supply voltage.

A 10-bit ADC is designed for possible operation of $\Delta\Sigma$ ADC at lower supply voltages as SNR degrades significantly at 0.23–0.25 V. Also, 10-bit ADC enables possible extension of the application to a wider DR for sensing metabolite concentrations much smaller than 2 mM. Implemented fully differentially in a $30\mu m \times 650\mu m$ of core area, the $\Delta\Sigma$ ADC achieves a figure-of-merit (FoM) of 37 fJ/conv.-step at 0.3 V. During inactive mode, the ADC consumes only 2 nW.

In vitro testing of the system was performed, where the glucose or lactate BFC was used as the sole source of power for the system. As shown in Fig5.13, the system can operate from the BFC power source, and can successfully detect changes in lactate (glucose) concentration between 2.5 and 15 mM (5–15 mM). The correlation between analyte concentration and the MPP in both sets of experiments was high (R2 = 0.984 and 0.961 for lactate and glucose, respectively). The power output begins to saturate at high-concentration levels due to increased enzymatic kinetics, which would require careful characterization and calibration in eventual clinical use.

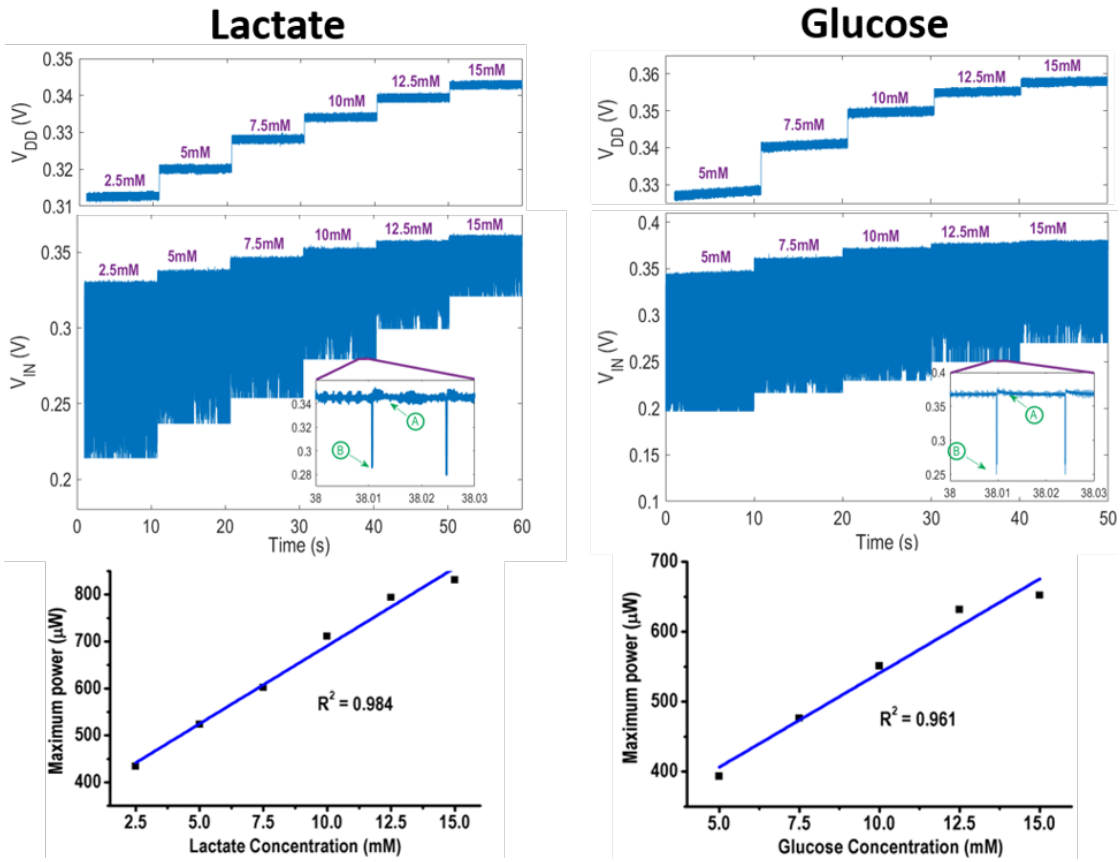

Figure 5.13: Measured dynamic VDD variation and BFC output power during in vitro experiments for lactate (left) and glucose (right). Calibration curves from these measurements (bottom).

This section has demonstrated a self-powered wireless biosensing system capable of utilizing glucose or lactate as an energy source while simultaneously measuring their concentrations.

The self-powered sensing paradigm eliminated the need for a battery, and since the open-circuit voltage of the BFCs was sufficiently large, a dc–dc converter was also eliminated. To enable robust functionality at down to 0.3 V, a passive $\Delta\Sigma$M was implemented to digitize glucose/lactate concentration, and a bootstrapped and clamped direct-

RF power oscillator was used to wirelessly transmit sensed data. The 65-nm test chip consumed an average of 1.15 μW, and was demonstrated to operate as a self-powered glucose or lactate biosensor during in vitro experiments. Future work will involve the study of long-term bioactivity of renewable immobilized enzymes in different environments expected in more realistic scenarios, which can affect BFC resistance, power extraction capabilities, and longevity.

Chapter 5 is based on and mostly a reprint of the following publications:

- Jia, Wenzhao; Wang, Xuan; Imani, Somayeh; Bandodkar, Amay J; Ramírez, Julian; Mercier, Patrick P; Wang, Joseph, "Wearable textiles biofuel cells for powering electronics," Journal of Materials Chemistry A, Vol. 2, 2014.

- Bandodkar, Amay. J; You, Jung-Min; Kim, Nam-Heon; Gu, Yue; Kumar, Rajan; Mohan, AM Vinu; Kurniawan, Jonas; Imani, Somayeh; Nakagawa, Tatsuo; Parish, Brianna; Parthasarathy, Mukunth; Mercier, Patrick P; Xu, Sheng; Wang, Joseph, "Soft, stretchable, high power density electronic skin-based biofuel cells for scavenging energy from human sweat," Energy and Environmental Science, Vol. 10, pp. 1581-1589, 2017.

- Fazli Yeknami, Ali; Wang, Xiaoyang; Imani, Somayeh; Nikoofard, Ali; Jeerapan, Itthipon; Wang, Joseph; Mercier, Patrick P, "A 0.3V Biofuel-Cell-Powered

Glucose/Lactate Biosensing System Employing a 180nW 64dB SNR Passive $\Delta\Sigma$ ADC and a 920MHz Wire-less Transmitter," in Proc. IEEE International Solid-State Circuits Conference (ISSCC), Feb. 2018.

- Fazli Yeknami, Ali; Wang, Xiaoyang; Jeerapan, Itthipon; Imani, Somayeh; Nikoofard, Ali; Wang, Joseph; Mercier, Patrick P, "A 0.3V Biofuel-Cell-Powered Glucose/Lactate Biosensing System," IEEE Journal of Solid-State Circuits, vol. 53, no. 11, Nov. 2018.

The dissertation author was the primary investigator and author of these papers.

Chapter 6

Conclusion

Wearable devices offer the exciting ability to monitor the physiologic state of humans in a real-time manner. To be practical, wearable sensors must be comfortable, unobtrusive, and compliant with the soft features of the human body. Significant recent efforts have thus been made toward the development of soft, epidermally mounted systems. At the same time, wearable devices should monitor interesting and/or actionable parameters, and thus, significant research activity has augmented the measurement of vital signs and motion with the monitoring of biochemical markers.

This dissertation has discussed state-of-the-art technologies, techniques, and challenges in translating electrochemical biosensors from the bench to the body. Some biosensing system capable of monitoring different analytes such as lactate, glucose, uric acid, and alcohol presented to elucidate the fabrication procedure, electronic design, and integration challenges of wearable chemical devices. Some system-level and circuit level strategies have been utilized for implementing low power instrumentation circuits.

Together with the novel low power circuitry, we have also utilized novel electrochemical biosensors to introduce completely new biosystems that provide information to improve future health monitoring and activity tracking applications. For example, we introduced the first instance of multimodal sensing of both electrophysiological signals and electrochemical signals.

In order to introduce new power efficient wearable devices, utilizing biofuel cells as energy sources have been also investigated. Two energy harvesting circuits have been implemented for demonstration of scavenging energy from lactae of sweat. Finally, a self-powered sensor has been introduced for the first demonstration of an integrated self-powered chemical biosensing system with digital wireless readout.

To enable the next-generation of wearable products, wearable chemical biosensing systems must present higher stability at lower power. Further research should be devoted to develop algorithms and data management procedures to calibrate and analyze the generated sensor data.

References

[1] D.-H. Kim, R. Ghaffari, N. Lu, and J. a. Rogers, "Flexible and Stretchable Electronics for Biointegrated Devices," *Annual Review of Biomedical Engineering*, vol. 14, no. 1, pp. 113–128, 2012.

[2] G. Matzeu, L. Florea, and D. Diamond, "Advances in wearable chemical sensor design for monitoring biological fluids," *Sensors and Actuators B: Chemical*, vol. 211, pp. 403–418, 5 2015.

[3] A. J. Bandodkar, W. Jia, and J. Wang, "Tattoo-Based Wearable Electrochemical Devices: A Review," *Electroanalysis*, vol. 27, no. 3, pp. 562–572, 3 2015.

[4] S. Imani, P. P. Mercier, A. J. Bandodkar, J. Kim, and J. Wang, "Wearable chemical sensors: Opportunities and challenges," in *IEEE Int. Symp. Circuits Syst.*, vol. 2016-July, 2016, pp. 1122–1125.

[5] A. J. Bandodkar, R. Nuñez-Flores, W. Jia, and J. Wang, "All-Printed Stretchable Electrochemical Devices," *Advanced Materials*, vol. 27, no. 19, pp. 3060–3065, 2015.

[6] A. J. Bandodkar, C. S. López, A. Mohanan, V. Mohan, L. Yin, R. Kumar, and J. Wang, "All-printed magnetically self-healing electrochemical devices," *Science Advances*, 2016.

[7] D. P. Rose, M. Ratterman, D. K. Griffin, L. Hou, N. Kelley-Loughnane, R. K. Naik, J. A. Hagen, I. Papautsky, and J. Heikenfeld, "System-level design of an RFID sweat electrolyte sensor patch," in *2014 36th Annual International Conference of the IEEE Engineering in Medicine and Biology Society*, 2014, pp. 4038–4041.

[8] B. J. Kim, D. H. Kim, Y.-Y. Lee, H.-W. Shin, G. S. Han, J. S. Hong, K. Mahmood, T. K. Ahn, Y.-C. Joo, K. S. Hong, N.-G. Park, S. Lee, and H. S. Jung, "Highly efficient and bending durable perovskite solar cells: toward a wearable power source," *Energy & Environmental Science*, vol. 8, no. March, pp. 916–921, 2015.

[9] A. J. Bandodkar, S. Imani, R. Nuñez-flores, R. Kumar, C. Wang, A. M. V. Mohan, J. Wang, and P. P. Mercier, "Re-usable electrochemical glucose sensors integrated into a smartphone platform," *Biosensors and Bioelectronic*, vol. 101, pp. 181–187, 2018.

[10] J. R. Windmiller and J. Wang, "Wearable Electrochemical Sensors and Biosensors: A Review," *Electroanalysis*, vol. 25, no. 1, pp. 29–46, 2013.

[11] A. J. Bandodkar, D. Molinnus, O. Mirza, T. Guinovart, J. R. Windmiller, G. Valdés-Ramírez, F. J. Andrade, M. J. Schöning, and J. Wang, "Epidermal tattoo potentiometric sodium sensors with wireless signal transduction for continuous non-invasive sweat monitoring," *Biosensors and Bioelectronics*, vol. 54, pp. 603–609, 4 2014.

[12] H. Graf and H. R. Muhlemann, "Telemetry of plaque pH from interdental area." *Helvetica odontologica acta*, vol. 10, no. 2, pp. 94–101, 10 1966.

[13] ——, "Oral telemetry of fluoride ion activity." *Archives of oral biology*, vol. 14, no. 3, pp. 259–263, 3 1969.

[14] C. Zuliani, G. Matzeu, and D. Diamond, "A potentiometric disposable sensor strip for measuring pH in saliva," *Electrochimica Acta*, vol. 132, pp. 292–296, 6 2014.

[15] J. Kim, G. Valdés-Ramírez, A. J. Bandodkar, W. Jia, A. G. Martinez, J. Ramírez, P. Mercier, and J. Wang, "Non-invasive mouthguard biosensor for continuous salivary monitoring of metabolites." *The Analyst*, vol. 139, no. 7, pp. 1632–6, 4 2014.

[16] D. Diamond, K. T. Lau, S. Brady, and J. Cleary, "Integration of analytical measurements and wireless communications–current issues and future strategies." *Talanta*, vol. 75, no. 3, pp. 606–612, 5 2008.

[17] M. S. Mannoor, H. Tao, J. D. Clayton, A. Sengupta, D. L. Kaplan, R. R. Naik, N. Verma, F. G. Omenetto, and M. C. McAlpine, "Graphene-based wireless bacteria detection on tooth enamel." *Nature communications*, vol. 3, p. 763, 3 2012.

[18] P. Kassal, I. M. Steinberg, and M. D. Steinberg, "Wireless smart tag with potentiometric input for ultra low-power chemical sensing," *Sensors and Actuators B: Chemical*, vol. 184, pp. 254–259, 7 2013.

[19] P. Kassal, J. Kim, R. Kumar, W. R. de Araujo, I. M. Steinberg, M. D. Steinberg, and J. Wang, "Smart bandage with wireless connectivity for uric acid biosensing as an indicator of wound status," *Electrochemistry Communications*, vol. 56, pp. 6–10, 7 2015.

[20] H. Endo, Y. Yonemori, K. Hibi, H. Ren, T. Hayashi, W. Tsugawa, and K. Sode, "Wireless enzyme sensor system for real-time monitoring of blood glucose levels in fish," *Biosensors and Bioelectronics*, vol. 24, no. 5, pp. 1417–1423, 1 2009.

[21] K. Hibi, K. Hatanaka, M. Takase, H. Ren, and H. Endo, "Wireless biosensor system for real-time L-lactic acid monitoring in fish." *Sensors (Basel, Switzerland)*, vol. 12, no. 5, pp. 6269–6281, 2012.

[22] A. Depari, A. Flammini, S. Rinaldi, and A. Vezzoli, "Multi-sensor system with Bluetooth connectivity for non-invasive measurements of human body physical parameters," *Sensors and Actuators A: Physical*, vol. 202, pp. 147–154, 11 2013.

[23] D. Zhang, J. Jiang, J. Chen, Q. Zhang, Y. Lu, Y. Yao, S. Li, G. Logan Liu, and Q. Liu, "Smartphone-based portable biosensing system using impedance measurement with printed electrodes for 2,4,6-trinitrotoluene (TNT) detection," *Biosensors and Bioelectronics*, vol. 70, pp. 81–88, 8 2015.

[24] T. R. Merriman and N. Dalbeth, "The genetic basis of hyperuricaemia and gout," *Joint Bone Spine*, vol. 78, no. 1, pp. 35–40, 1 2011.

[25] V. Bhole, J. W. J. Choi, S. Woo Kim, M. de Vera, and H. Choi, "Serum Uric Acid Levels and the Risk of Type 2 Diabetes: A Prospective Study," *The American Journal of Medicine*, vol. 123, no. 10, pp. 957–961, 10 2010.

[26] Y. Hellsten, P. C. Tullson, E. A. Richter, and J. Bangsbo, "Oxidation of urate in human skeletal muscle during exercise," *Free Radical Biology and Medicine*, vol. 22, no. 1-2, pp. 169–174, 1 1997.

[27] K. Shibasaki, M. Kimura, R. Ikarashi, A. Yamaguchi, and T. Watanabe, "Uric acid concentration in saliva and its changes with the patients receiving treatment for hyperuricemia," *Metabolomics*, vol. 8, no. 3, pp. 484–491, 2012.

[28] M. Soukup, I. Biesiada, A. Henderson, B. Idowu, D. Rodeback, L. Ridpath, E. G. Bridges, A. M. Nazar, and K. G. Bridges, "Salivary uric acid as a noninvasive biomarker of metabolic syndrome," *Diabetology & Metabolic Syndrome*, vol. 4, no. 1, p. 14, 2012.

[29] International Diabetes Foundation, "IDF Diabetes Atlas Seventh Edition," International Diabetes Foundation, Tech. Rep., 2015. [Online]. Available: http://www.diabetesatlas.org

[30] L. Guariguata, D. Whiting, C. Weil, and N. Unwin, "The International Diabetes Federation diabetes atlas methodology for estimating global and national prevalence of diabetes in adults," *Diabetes Research and Clinical Practice*, vol. 94, no. 3, pp. 322–332, 12 2011.

[31] J. L. Dieleman, R. Baral, M. Birger, A. L. Bui, A. Bulchis, A. Chapin, H. Hamavid, C. Horst, E. K. Johnson, J. Joseph, R. Lavado, L. Lomsadze, A. Reynolds, E. Squires, M. Campbell, B. DeCenso, D. Dicker, A. D. Flaxman, R. Gabert, T. Highfill, M. Naghavi, N. Nightingale, T. Templin, M. I. Tobias, T. Vos, and

C. J. L. Murray, "US Spending on Personal Health Care and Public Health, 1996-2013," *JAMA*, vol. 316, no. 24, pp. 2627–2646, 2016.

[32] G. Valdés-Ramírez, Y.-C. Li, J. Kim, W. Jia, A. J. Bandodkar, R. Nuñez-Flores, P. R. Miller, S.-Y. Wu, R. Narayan, J. R. Windmiller, R. Polsky, and J. Wang, "Microneedle-based self-powered glucose sensor," *Electrochemistry Communications*, vol. 47, pp. 58–62, 10 2014.

[33] S. K. Vashist, "Non-invasive glucose monitoring technology in diabetes management: A review," *Analytica Chimica Acta*, vol. 750, pp. 16–27, 10 2012.

[34] A. Abellán-Llobregat, I. Jeerapan, A. Bandodkar, L. Vidal, A. Canals, J. Wang, and E. Morallón, "A stretchable and screen-printed electrochemical sensor for glucose determination in human perspiration," *Biosensors and Bioelectronics*, vol. 91, pp. 885–891, 5 2017.

[35] S. R. Patton, "Adherence to Glycemic Monitoring in Diabetes," *Journal of Diabetes Science and Technology*, vol. 9, no. 3, pp. 668–675, 2015.

[36] V. Dantu, J. Vempati, and S. Srivilliputhur, "Non-invasive blood glucose monitor based on spectroscopy using a smartphone." *Conference proceedings : ... Annual International Conference of the IEEE Engineering in Medicine and Biology Society. IEEE Engineering in Medicine and Biology Society. Annual Conference*, vol. 2014, pp. 3695–3698, 2014.

[37] N. Jendrike, A. Baumstark, S. Pleus, C. Liebing, A. Beer, F. Flacke, C. Haug, and G. Freckmann, "Evaluation of Four Blood Glucose Monitoring Systems for Self-Testing with Built-in Insulin Dose Advisor Based on ISO 15197:2013: System Accuracy and Hematocrit Influence," *Diabetes Technology & Therapeutics*, vol. 20, no. 4, pp. 303–313, 2018.

[38] Y. Wu, A. Boonloed, N. Sleszynski, M. Koesdjojo, C. Armstrong, S. Bracha, and V. T. Remcho, "Clinical chemistry measurements with commercially available test slides on a smartphone platform: Colorimetric determination of glucose and urea," *Clinica Chimica Acta*, vol. 448, pp. 133–138, 8 2015.

[39] A. C. Sun, C. Yao, V. A.G., and D. A. Hall, "An efficient power harvesting mobile phone-based electrochemical biosensor for point-of-care health monitoring," *Sensors and Actuators B: Chemical*, vol. 235, pp. 126–135, 11 2016.

[40] A. J. Bandodkar, W. Jia, J. Ramírez, and J. Wang, "Biocompatible Enzymatic Roller Pens for Direct Writing of Biocatalytic Materials: "Do-it-Yourself" Electrochemical Biosensors," *Advanced Healthcare Materials*, vol. 4, no. 8, pp. 1215–1224, 2015.

[41] J. Kim, I. Jeerapan, S. Imani, T. N. Cho, A. Bandodkar, S. Cinti, P. P. Mercier, and J. Wang, "Noninvasive Alcohol Monitoring Using a Wearable Tattoo-Based Iontophoretic-Biosensing System," *ACS Sensors*, 2016.

[42] G. Simpson, "Accuracy and precision of breath-alcohol measurements for a random subject in the postabsorptive state." *Clinical chemistry*, vol. 33, no. 2 Pt 1, pp. 261–268, 2 1987.

[43] M. Dumett, G. Rosen, J. Sabat, A. Shaman, L. Tempelman, C. Wang, and R. Swift, "Deconvolving an Estimate of Breath Measured Blood Alcohol Concentration from Biosensor Collected Transdermal Ethanol Data." *Applied mathematics and computation*, vol. 196, no. 2, pp. 724–743, 3 2008.

[44] T. M. Worner and J. Prabakaran, "The accuracy of breath alcohol analysis using the breathalyzer." pp. 349–350, 1985.

[45] R. Swift, "Transdermal alcohol measurement for estimation of blood alcohol concentration." *Alcoholism, clinical and experimental research*, vol. 24, no. 4, pp. 422–423, 4 2000.

[46] R. M. Swift, C. S. Martin, L. Swette, A. LaConti, and N. Kackley, "Studies on a wearable, electronic, transdermal alcohol sensor." *Alcoholism, clinical and experimental research*, vol. 16, no. 4, pp. 721–725, 8 1992.

[47] T. R. Leffingwell, N. J. Cooney, J. G. Murphy, S. Luczak, G. Rosen, D. M. Dougherty, and N. P. Barnett, "Continuous objective monitoring of alcohol use: twenty-first century measurement using transdermal sensors." *Alcoholism, clinical and experimental research*, vol. 37, no. 1, pp. 16–22, 1 2013.

[48] M. Gamella, S. Campuzano, J. Manso, G. G. d. Rivera, F. López-Colino, A. Reviejo, and J. Pingarrón, "A novel non-invasive electrochemical biosensing device for in situ determination of the alcohol content in blood by monitoring ethanol in sweat," *Analytica Chimica Acta*, vol. 806, pp. 1–7, 1 2014.

[49] S. Imani, A. Bandodkar, A. Mohan, R. Kumar, S. Yu, J. Wang, and P. Mercier, "A wearable chemical-electrophysiological hybrid biosensing system for real-time health and fitness monitoring," *Nature Communications*, vol. 7, 2016.

[50] A. J. Bandodkar and J. Wang, "Non-invasive wearable electrochemical sensors: a review," *Trends in Biotechnology*, vol. 32, no. 7, pp. 363–371, 7 2014.

[51] J. Kim, J. R. Sempionatto, S. Imani, M. C. Hartel, A. Barfidokht, G. Tang, A. S. Campbell, P. P. Mercier, and J. Wang, "Simultaneous Monitoring of Sweat and Interstitial Fluid Using a Single Wearable Biosensor Platform," *Advanced Science*, 2018.

[52] H. Wu, Y. Huang, F. Xu, Y. Duan, and Z. Yin, "Energy Harvesters for Wearable and Stretchable Electronics : From Flexibility to Stretchability," *Advanced Materials*, vol. 28, pp. 9881–9919, 2016.

[53] L. Zhang, E. Shi, C. Ji, Z. Li, P. Li, Y. Shang, Y. Li, J. Wei, K. Wang, H. Zhu, D. Wu, and A. Cao, "Nanoscale Fiber and fabric solar cells by directly weaving carbon nanotube yarns with," *Nanoscale*, vol. 4, pp. 4954–4959, 2012.

[54] P. P. Mercier, A. C. Lysaght, S. Bandyopadhyay, A. P. Chandrakasan, and K. M. Stankovic, "Energy extraction from the biologic battery in the inner ear," *Nature Biotechnology*, vol. 30, no. 12, pp. 1240–1243, 2012.

[55] W. R. Grove, "On Voltaic Series and the Combination of Gases by Platinum," *Philosophical Magazine and Journal of Science*, vol. 14, no. 86-87, pp. 127–130, 1839.

[56] M. C. Potter, "On the difference of potential due to the vital activity of microorganisms," *Proc. Univ. Durham Phil. Soc.*, vol. 3, pp. 245–249, 1950.

[57] R. A. Bullen, T. C. Arnot, J. B. Lakeman, and F. C. Walsh, "Biofuel cells and their development," *Biosensors & Bioelectronics*, vol. 21, pp. 2015–2045, 2006.

[58] A. T. Yahiro, S. M. Lee, and D. O. Kimble, "enzyme utilizing bio-fuel cell studies," *Biochimica et Biophysica ACTA*, vol. 88, pp. 375–383, 1963.

[59] E. Katz, A. F. Buckmann, and I. Willner, "Self-Powered Enzyme-Based Biosensors," *J. Am. Chem. Soc.*, vol. 123, pp. 10 752–10 753, 2001.

[60] E. Katz and K. Macvittie, "Implanted biofuel cells operating in vivi – applications and perspectives – feature article," *Energy & Environmental Science*, vol. 6, pp. 2791–2803, 2013.

[61] W. Jia, G. Valdés-Ramírez, A. J. Bandodkar, J. R. Windmiller, and J. Wang, "Epidermal biofuel cells: energy harvesting from human perspiration," *Angewandte Chemie (International ed. in English)*, vol. 52, no. 28, pp. 7233–7236, 7 2013. [Online]. Available: http://www.ncbi.nlm.nih.gov/pubmed/23729381

[62] A. J. Bandodkar and J. Wang, "Wearable Biofuel Cells : A Review," *Electroanalysis*, vol. 1, no. 858, pp. 1188–1200, 2016.

[63] W. Jia, X. Wang, S. Imani, A. J. Bandodkar, J. Ramirez, P. P. Mercier, and J. Wang, "Wearable textile biofuel cells for powering electronics," *Journal of Materials Chemistry A*, vol. 2, no. 43, pp. 18 184–18 189, 2014. [Online]. Available: http://dx.doi.org/10.1039/C4TA04796F

[64] A. J. Bandodkar, I. Jeerapan, J.-m. You, and J. Wang, "Highly Stretchable Fully-Printed CNT-Based Electrochemical Sensors and Biofuel Cells: Combining Intrinsic and Design-Induced Stretchability," *Nano Letters*, 2016.

[65] Y. Ogawa, Y. Takai, Y. Kato, H. Kai, T. Miyake, and M. Nishizawa, "Stretchable biofuel cell with enzyme-modi fi ed conductive textiles," *Biosensors and Bioelectronic*, vol. 74, pp. 947–952, 2015. [Online]. Available: http://dx.doi.org/10.1016/j.bios.2015.07.063

[66] I. Jeerapan, J. R. Sempionatto, A. Pavinatto, J.-m. You, and J. Wang, "Stretchable biofuel cells as wearable textile-based self-powered sensors," *Journal of Materials Chemistry A*, pp. 18 342–18 353, 2016.

[67] A. J. Bandodkar, J.-m. You, N.-h. Kim, Y. Gu, R. Kumar, A. M. V. Mohan, J. Kurniawan, S. Imani, T. Nakagawa, B. Parish, M. Parthasarathy, P. P. Mercier, S. Xu, and J. Wang, "Soft, stretchable, high power density electronic skin-based biofuel cells for scavenging energy from human sweat," *Energy & Environmental Science*, pp. 1581–1589, 2017.

[68] X. Huang, L. Zhang, Z. Zhang, S. Guo, H. Shang, Y. Li, and J. Liu, "Biosensors and Bioelectronics Wearable biofuel cells based on the classification of enzyme for high power outputs and lifetimes," *Biosensors and Bioelectronic*, vol. 124-125, pp. 40–52, 2019. [Online]. Available: https://doi.org/10.1016/j.bios.2018.09.086

[69] A. F. Yeknami, X. Wang, S. Member, I. Jeerapan, S. Imani, S. Member, A. Nikoofard, S. Member, J. Wang, P. P. Mercier, and S. Member, "A 0 . 3-V CMOS Biofuel-Cell-Powered Wireless Glucose / Lactate Biosensing System," *IEEE Journal of Solid-State Circuits*, vol. 53, no. 11, pp. 3126–3139, 2018.

[70] A. F. Yeknami, X. Wang, S. Imani, A. Nikoofard, I. Jeerapan, J. Wang, and P. P. Mercier, "A 0.3V biofuel-cell-powered glucose/lactate biosensing system employing a 180nW 64dB SNR passive δ ADC and a 920MHz wireless transmitter," *Digest of Technical Papers - IEEE International Solid-State Circuits Conference*, vol. 61, pp. 284–286, 2018.

[71] A. Kobayashi, K. Ikeda, Y. Ogawa, M. Nishizawa, K. Nakazato, and K. Niitsu, "Design and Experimental Verification of a 0.19 V 53 W 65 nm CMOS Integrated Supply-Sensing Sensor With a Supply-Insensitive Temperature Sensor and an Inductive-Coupling Transmitter for a Self-Powered Bio-sensing System Using a Biofuel Cell," *IEEE Transactions on Biomedical Circuits and Systems*, vol. 11, no. 6, pp. 1313–1323, 2017.

[72] A. J. Bandodkar, P. Gutruf, J. Choi, K. Lee, Y. Sekine, J. T. Reeder, W. J. Jeang, A. J. Aranyosi, S. P. Lee, J. B. Model, R. Ghaffari, C.-j. Su, J. P. Leshock, T. Ray,

A. Verrillo, K. Thomas, V. Krishnamurthi, S. Han, and J. Kim, "Battery-free, skin-interfaced microfluidic/electronic systems for simultaneous electrochemical , colorimetric , and volumetric analysis of sweat," *Science Advances*, no. January, pp. 1–16, 2019.

[73] A. Kobayashi, K. Hayashi, S. Arata, S. Murakami, G. Xu, and K. Niitsu, "Dual-Oscillator-Based Supply Voltage Monitor for Biofuel-Cell-Combined Biosensing Systems," in *ISCAS*, no. c, 2019, pp. 6–10.

[74] H. Guan, T. Zhong, H. He, T. Zhao, and L. Xing, "A self-powered wearable sweat-evaporation-biosensing analyzer for building sports big data," *Nano Energy*, vol. 59, no. February, pp. 754–761, 2019. [Online]. Available: https://doi.org/10.1016/j.nanoen.2019.03.026

[75] J. Lv, I. Jeerapan, F. Tehrani, and L. Yin, "Sweat-based wearable energy harvesting-storage hybrid textile devices," *Energy & Environmental Science*, vol. 11, pp. 3431–3442, 2018.

[76] A. J. Bandodkar, "Review—Wearable Biofuel Cells: Past, Present and Future," *Journal of The Electrochemical Society*, vol. 164, no. 3, pp. H3007–H3014, 2017. [Online]. Available: http://jes.ecsdl.org/lookup/doi/10.1149/2.0031703jes

[77] S. Bandyopadhyay and A. P. Chandrakasan, "Platform Architecture for Solar, Thermal, and Vibration Energy Combining With MPPT and Single Inductor," *IEEE Journal of Solid-State Circuits*, vol. 47, no. 9, pp. 2199–2215, 2012.

[78] S. S. Amin and P. P. Mercier, "MISIMO: A multi-input single-inductor multi-output energy harvester employing event-driven MPPT control to achieve 89% peak efficiency and a 60,000x dynamic range in 28nm FDSOI," in *2018 IEEE International Solid - State Circuits Conference - (ISSCC)*. IEEE, 2018, pp. 144–146.

[79] P. Harpe, E. Cantatore, and A. v. Roermund, "A 10b/12b 40 kS/s SAR ADC With Data-Driven Noise Reduction Achieving up to 10.1b ENOB at 2.2 fJ/Conversion-Step," *IEEE Journal of Solid-State Circuits*, vol. 48, no. 12, pp. 3011–3018, 2013.

[80] H. Tai, Y. Hu, H. Chen, and H. Chen, "11.2 A 0.85fJ/conversion-step 10b 200kS/s subranging SAR ADC in 40nm CMOS," in *2014 IEEE International Solid-State Circuits Conference Digest of Technical Papers (ISSCC)*, 2014, pp. 196–197.

[81] J. Lin and C. Hsieh, "A 0.3 V 10-bit 1.17 f SAR ADC With Merge and Split Switching in 90 nm CMOS," *IEEE Transactions on Circuits and Systems I: Regular Papers*, vol. 62, no. 1, pp. 70–79, 2015.

[82] X. Wang, H. Huang, and Q. Li, "Design Considerations of Ultralow-Voltage Self-Calibrated SAR ADC," *IEEE Transactions on Circuits and Systems II: Express Briefs*, vol. 62, no. 4, pp. 337–341, 2015.

[83] H. Garvik, C. Wulff, and T. Ytterdal, "An 11.0 bit ENOB, 9.8 fJ/conv.-step noise-shaping SAR ADC calibrated by least squares estimation," in *2017 IEEE Custom Integrated Circuits Conference (CICC)*, 2017, pp. 1–4.

[84] L. Chen, X. Tang, A. Sanyal, Y. Yoon, J. Cong, and N. Sun, "A 0.7-V 0.6- μW 100-kS/s Low-Power SAR ADC With Statistical Estimation-Based Noise Reduction," *IEEE Journal of Solid-State Circuits*, vol. 52, no. 5, pp. 1388–1398, 2017.

[85] F. Michel and M. S. J. Steyaert, "A 250 mV 7.5 μW 61 dB SNDR SC $\Delta\Sigma$ Modulator Using Near-Threshold-Voltage-Biased Inverter Amplifiers in 130 nm CMOS," *IEEE Journal of Solid-State Circuits*, vol. 47, no. 3, pp. 709–721, 2012.

[86] L. H. C. Ferreira and S. R. Sonkusale, "A 0.25-V 28-nW 58-dB Dynamic Range Asynchronous Delta Sigma Modulator in 130-nm Digital CMOS Process," *IEEE Transactions on Very Large Scale Integration (VLSI) Systems*, vol. 23, no. 5, pp. 926–934, 2015.

[87] L. G. Salem and P. P. Mercier, "A Recursive Switched-Capacitor DC-DC Converter Achieving $2^{N}-1$ Ratios With High Efficiency Over a Wide Output Voltage Range," *IEEE Journal of Solid-State Circuits*, vol. 49, no. 12, pp. 2773–2787, 2014.

[88] A. Fazli Yeknami and A. Alvandpour, "A 0.5-V 250-nW 65-dB SNDR Passive $\Delta\Sigma$ Modulator for Medical Implant Devices," Electronic Devices, Department of Electrical Engineering, Linköping University, pp. 2010–2013, 2013.

[89] A. F. Yeknami, F. Qazi, and A. Alvandpour, "Low-Power DT $\Delta\Sigma$ Modulators Using SC Passive Filters in 65 nm CMOS," *IEEE Transactions on Circuits and Systems I: Regular Papers*, vol. 61, no. 2, pp. 358–370, 2014.